N 71-16887

MATHEMATICAL MODELING OF CRYOGENIC HEAT PIPES

By

S. W. Chi

Final Report to Goddard Space Flight Center, NASA

Grant No. NGR09-005-071

September 1970

Department of Space Science and Applied Physics

The Catholic University of America

Washington, D.C.

MATHEMATICAL MODELING OF CRYOGENIC HEAT PIPES

By

S. W. Chi*

Final Report to Goddard Space Flight Center, NASA

Grant No. NGR09-005-071

September 1970

Department of Space Science and Applied Physics

The Catholic University of America

Washington D. C.

*Present Address: Department of Civil, Mechanical and Environmental Engineering, The George Washington University, Washington D.C. 20006.

ABSTRACT

A qualitative investigation of performance of heat pipes using different working fluids is first made; significance of liquid property variations on the performance of cryogenic heat pipe is observed. A theory for the cryogenic heat pipe, which takes into account the liquid property variations, is then developed. Predictions by the present theory compare favorably with Haskin's experiments.

A computer program in Fortran IV language is written for the theory. Physical properties of cryogenic fluids, which are required as program input data are collected. For convenience of the user of the theory, a complete listing of the program with user's instructions and collected properties of cryogens are appended to the report.

A performance chart is developed for presentation of complete performance of cryogenic heat pipes. A procedure for computer aided design of cryogenic heat pipe is also described. The procedure consists of the following steps: (i) choice of fluid and wick structure, (ii) determination of wick dimensions, and (iii) generation of performance chart for the designed heat pipe.

CONTENTS

1.	INTRODUCTION	1
2.	PRELIMINARY INVESTIGATION	2
3.	MATHEMATICAL MODEL FOR A CRYOGENIC HEAT PIPE	5
	3.1 LIQUID TEMPERATURE DISTRIBUTION	6
	3.2 TOTAL TEMPERATURE DROP	8
	3.3 MAXIMUM HEAT TRANSFER CAPABILITY	9
	3.4 COMPUTER PROGRAM AND FLUID PROPERTIES	11
4.	PERFORMANCE CHART AND DESIGN PROCEDURE	11
	4.1 PERFORMANCE CHART	11
	4.2 DESIGN PROCEDURE	12
5.	CONCLUSIONS AND RECOMMENDATIONS	13
	5.1 CONCLUSIONS	13
	5.2 RECOMMENDATIONS	14
6.	REFERENCES	16
FIGURES		18
APPENDIX A:	A COMPUTER PROGRAM FOR HEAT PIPE DESIGN AND PERFORMANCE CALCULATIONS	25
APPENDIX B:	COLLECTED PHYSICAL PROPERTIES OF CRYOGENS	35

Nomenclature

b	permeability factor for capillary structure
c_{pf}	liquid specific heat at constant pressure
h_{fg}	heat of vaporization
K	thermal conductivity
m	mass transfer rate
N_f	liquid transport factor defined as $\rho_f \gamma_f h_{fg}/\mu_f$
p_v	vapor pressure
ΔP_c	maximum capillary pressure defined as $2\gamma_f/r_c$
ΔP_f	liquid pressure drop
ΔP_v	vapor pressure drop
Q	heat transfer rate
r_i	inner radius of container wall
r_o	outer radius of container wall
r_v	radius of vapor flow passage
r_c	effective radius for capillary pressure
r_f	effective capillary radius for liquid flow
R	gas constant
U	Thermal conductance
t	wick thickness
T	temperature
y	distance measured from r_i toward axis of heat pipe
z	axial length
γ_f	surface tension
ε	porosity of capillary structure
μ	dynamic viscosity
ρ	density

Subscripts:

a	adiabatic section
be	bulk average value of liquid at evaporator section
bc	bulk average value of liquid at condenser section
c	condenser section
e	evaporator section
f	liquid phase
i	inner wall of container
m	liquid saturated wick
max	maximum
o	outer wall of container
rad	radiation
ref	refrigeration
s	saturation state
v	vapor phase
w	material of container wall
wk	material of capillary wick

1. INTRODUCTION

There have been a considerable number of investigation[1-12] of high and normal ambient temperature heat pipes in the last few years, both theoretical and experimental; accordingly, the design technique and operating characteristics of these heat pipes are now reasonably well understood. By comparison, the cryogenic heat pipe has not yet been extensively studied. Although feasibility of the cryogenic heat pipe has been demonstrated by the Haskin's experiments and much information is to be found in his paper[13], analytical design and performance prediction procedures for the cryogenic heat pipe are not available in the open literature. The present report describes a theoretical study of the cryogenic heat pipe.

The cryogenic heat pipe has been lagging in development chiefly because of its rather limited application potential. The integrated Cryogenic Cooling Engine (ICICLE) System, under development at NASA, Goddard Space Flight Center, uses a central cryogenic refrigerator for cooling to cryogenic temperatures and thereby increasing the sensitivity and performance of multiple spacecraft experiments, sensors, components, etc. Cryogenic heat pipes are needed to provide effective thermal links between the central refrigerator and one or more remotely located cooling platforms.

The intention of this research was to develop a theoretical procedure for design and performance prediction of cryogenic heat pipes; this development will be described below in three sections. First, a preliminary

investigation of the operating characteristics of the heat pipe will be made and the effect of the temperature-dependent-property variations of the cryogen on the heat pipe performance will be discussed. Then, a mathematical model, which takes the variable properties of the cryogen into account, will be developed. Finally, illustrative performance charts derived from the present theory will be presented, and a procedure for design calculations will be described. As far as possible, the present theory will also be compared with the Haskin's experiments at the crucial points of the argument.

Sections 2 and 3 below are mainly devoted to a development of the argument leading to the present theory, they may be omitted by readers concerned solely with the use of the theory. Such readers should turn to Section 4, which contains a summary of the computer aided design and performance prediction procedures which are recommended for use. A complete listing of computer program for design and performance calculations and a collection of properties of cryogens are given in Appendices.

2. PRELIMINARY INVESTIGATION

A heat pipe is a device whose principle of operation consists of the evaporation of a liquid, the transport of the vapor through a duct, the condensation of the vapor and the subsequent return of the condesate through a wick of capillary structure for re-evaporation. These processes are illustrated in Figure 1. An analytical model for the performance of the heat pipe was first formulated by Cotter[2]; his results are the most widely used.

With some simplification[5], the equation for the maximum heat transfer rate derived by Cotter may be expressed as

$$Q_{max} = N_f t\left(\frac{8\pi r_i r_f^2}{b r_c (z_e + 2z_a + z_c)}\right),^{*} \qquad (1)$$

The liquid transport factor, N_f, is a function of the working fluid while all other terms on the right hand side of the above equation depend on the heat pipe design. Figure 2 shows the values of the liquid transport factor, N_f, for several working fluids suitable for heat pipes.

The temperature gradient of a heat pipe is determined mainly by the heat flux density and the radial thermal conductance of the wick material saturated with the working fluid in the liquid state[8,9,13]. Qualitatively, the conductance of the liquid saturated wick may be assumed to be proportional to the thermal conductivity of the liquid divided by the wick thickness[8,13,14] i.e.,

$$U \propto K/t, \text{ or } T \propto Qt/K. \qquad (2)$$

Now, for a heat pipe of fixed physical dimensions and wick thickness, its approximate operating characteristics with different working fluids may be derived from Equations 1 and 2. These are: (i) the maximum heat transfer capability of the heat pipe is directly proportional to the value of liquid transport factor of the working fluid, and (ii) the temperature drop at equal heat transfer rate is inversely proportional to the liquid thermal conductivity of the working fluid. Figure 3 shows the values of the liquid thermal conductivity for several fluids.

Similarly, the approximate operating characteristics of heat pipes of equal maximum heat transfer capability may also be derived from

---

* Equation 1 is valid for a heat pipe of Figure 1 operating under zero-gravity condition and with vapor flow passage being much larger than wick thickness.

Equations 1 and 2. These are: (i) the wick thickness required is inversely proportional to the value of the liquid transport factor of the working fluid, and (ii) the temperature drop at equal heat transfer rate is inversely proportional to the product of the liquid thermal conductivity and the liquid transport factor. For the convenience of future reference, this product is named as the liquid thermal conductance factor. Its values for several fluids are plotted in Figure 4.

We have derived above the approximate relative operating characteristics of heat pipes in terms of the liquid transport factor, liquid thermal conductivity and liquid thermal conductance factor. The low values for the cryogenic fluids, as can be seen in Figures 2 through 4, indicate small heat transfer capability and large temperature drop for the cryogenic heat pipe. For example, the temperature drop for the Haskin's liquid nitrogen heat pipe[13] is about 20°K at 20 watts. Under this condition, the cryogenic heat pipe may not be considered as an isothermal device.

In addition, the operational temperature range of the heat-pipe working fluid is between the triple point and the critical temperature of the fluid. This temperature range is always small for the cryogenic fluid: e.g., 63°K for liquid nitrogen. As the properties of the fluid within this range changes from one extreme (solid) to the other (gas), the effect of variable properties of the liquid on the performance of the cryogenic heat pipe is expected to be large. The values of γ_f and K for liquid nitrogen, for example, change from 10.53 to 8.27 dynes/cm and 1.52×10^4 to 1.36×10^4 ergs/(cm-°K-sec) respectively when the temperature changes from 70°K to 80°K.

The above consideration shows that the effect of liquid property

variations on the performance of the cryogenic heat pipe is significant. On the other hand, it will be shown below that the effect of vapor property variations on the performance of the cryogenic heat pipe is insignificant.

The vapor pressure drop of a heat pipe is always smaller than the capillary pumping pressure. For simplicity, however, let us assume that the vapor pressure drop is equal to the capillary pumping pressure. Then, the vapor pressure drop may be expressed as

$$\Delta p_v = 2\,\gamma_f/r_c. \tag{3}$$

The corresponding vapor temperature drop can be obtained by substituting Δp_v from Equation 3 into the well-known Clausius-Clapeyron equation. The result is

$$\Delta T_v = \frac{RT_v^2}{p_v h_{fg}} \cdot \frac{2\,\gamma_f}{r_c}. \tag{4}$$

The magnitude of ΔT_v for the cryogen is usually amall because of the small values of T_v and γ_f and large values of p_v and h_{fg}. For example, for saturated nitrogen at atmospheric pressure with r_c being 50 microns, the evaluated ΔT_v is only $0.03^{\circ}K$, which is insignificant in most applications.

3. MATHEMATICAL MODEL FOR A CRYOGENIC HEAT PIPE

Having observed the importance of the liquid property variations and the insignificance of the vapor property variations on the performance of the cryogenic heat pipe, a theory for cryogenic heat pipe performance, which takes account of the liquid property variations is now presented.

The analyses which follow use the heat pipe of Figure 1 with constant vapor-flow-passage and container diameters. In order to account for the liquid-property variation, the liquid temperature distribution

will first be derived. Following this, the operating temperature and heat transfer capability of the heat pipe will be considered.

3.1 Liquid Temperature Distribution

Because of the small thermal conductivity of the cryogen, it is desirable that the wick thickness of the cryogenic heat pipe be made as small as possible for the required heat transfer rate. In the calculation, it will be assumed that the wick thickness is much smaller than the radius of the vapor-flow passage. The mass flux in the capillary wick is approximated by a uniform distribution. Also, the usual channel flow assumptions for heat transfer calculations[15] will be made; these are, the axial conduction is small in comparison with convection, and the property values are evaluated at the liquid bulk average temperature. The derivation for the temperature in the evaporator section is given below in detail. Similar analysis has been used for the condenser section, but for brevity results for the condenser section are stated without details of derivation.

A stationary liquid and wick control volume of thickness dy and boundaries of the evaporator are represented in Figure 5 with terms which appear in the energy conservation equations and the boundary conditions. The principle of conservation of energy requires that

$$\frac{d^2T}{dy^2} = \frac{m_e c_{pf,be} y}{2\pi r_i z_e t K_{m,be}} \cdot \frac{dT}{dy} \; ; \tag{5}$$

and the boundary conditions are

$$\begin{aligned} -2\pi r_i z_e K_{m,be} \frac{dT}{dy} &= Q, \text{ at } y = 0; \\ -2\pi r_i z_e K_{m,be} \frac{dT}{dy} &= m_e h_{fg}, \text{ at } y = t; \\ T &= T_s, \text{ at } y = t. \end{aligned} \tag{6}$$

The solution for the system of Equations 5 and 6 may be obtained by straightforward integration. The results are:

$$T = T_s + \frac{Q}{2\pi r_i z_e K_{m,be}} \int_y^t \exp\left(\frac{m_e c_{pf,be}}{4\pi r_i z_e t K_{m,be}} y^2\right) dy, \tag{7}$$

for the liquid temperature distribution;

$$T_{e,i} - T_s = \frac{Q}{2\pi r_i z_e K_{m,be}} \int_0^t \exp\left(\frac{m_e c_{pf,be}}{4\pi r_i z_e t K_{m,be}} y^2\right) dy, \tag{8}$$

for the radial temperature drop across the wick at the evaporator; and

$$T_{be} = T_s + \frac{Q}{2\pi r_i z_e t K_{m,be}} \int_0^t \left(\int_y^t \exp\left(\frac{m_e c_{pf,be}}{4\pi r_i z_e t K_{m,be}} y^2\right) dy\right) dy, \tag{9}$$

for the bulk average temperature of the liquid at the evaporator. In these Equations 7 through 9, m_e is required to satisfy the equation

$$\frac{m_e h_{fg,s}}{Q} = \exp\left(\frac{m_e c_{pf,be} t}{4\pi r_i z_e K_{m,be}}\right). \tag{10}$$

By a similar procedure, we have obtained the following temperature distribution equations for the condenser:

$$T = T_s - \frac{Q}{2\pi r_i z_c K_{m,bc}} \int_y^t \exp\left(\frac{-m_c c_{pf,bc}}{4\pi r_i z_c t K_{m,bc}} y^2\right) dy \tag{11}$$

for the liquid temperature distribution;

$$T_s - T_{c,i} = \frac{Q}{2\pi r_i z_c K_{m,bc}} \int_0^t \exp\left(\frac{-m_c c_{pf,bc}}{4\pi r_i z_c t K_{m,bc}} y^2\right) dy, \tag{12}$$

for the radial temperature drop across the wick at the consdenser; and

$$T_{bc} = T_s - \frac{Q}{2\pi r_i z_c t K_{m,bc}} \int_0^t \left(\int_t^t \exp\left(\frac{-m_c c_{pf,bc}}{4\pi r_i z_c t K_{m,bc}} y^2\right) dy\right) dy \tag{13}$$

for the bulk average temperature of the liquid at the condenser. The value of m_c in Equations 11 through 13 is required to satisfy the condition,

$$\frac{m_c h_{fg,s}}{Q} = \exp\left(\frac{-m_c c_{pf,bc} t}{4\pi r_i z_c K_{m,bc}}\right). \qquad (14).$$

In the above Equations 5 through 14, the values of the thermal conductivity for the liquid saturated wick, K_m, are dependent upon the wick structure as well as thermal conductivities of the liquid and the wick material at the temperature under consideration. Equations developed by Gorring and Churchill[16] are recommended to be used. For example, for the fibrous or mesh-screen wick the equation recommended is

$$K_m = K_f \cdot \frac{K_f + K_{wk} - (1 - \varepsilon)(K_f - K_{wk})}{K_f + K_{wk} + (1 + \varepsilon)(K_f - K_{wk})} \quad . \qquad (15)$$

The equations governing the liquid bulk average temperature and the radial temperature drop at the evaporator as well as at the condenser have been obtained. The property values in these equations are evaluated at the respective bulk average temperatures for the evaporator and condenser. However, the bulk average temperatures are not known at the beginning of the calculation. Iteration processes have to be used to solve these equations.

3.2 Total Temperature Drop

For heat pipe performance, the temperature difference between the evaporator outer wall and the condenser outer wall and the absolute temperature at the evaporator outer wall (or the condenser outer wall) are important parameters for the designers and the users of the heat pipe. The temperature drops across the evaporator wick and the condenser wick have been discussed above in detail; i.e., they may be calculated by Equations 8 and 12, respectively.

The radial temperature drops across the container walls may be calculated by equations[15],

$$T_{e,o} - T_{e,i} = \frac{Q}{2\pi K_w z_e} \ln(r_o/r_i), \tag{16}$$

and

$$T_{c,i} - T_{c,o} = \frac{Q}{2\pi K_w z_c} \ln(r_o/r_i), \tag{17}$$

for the evaporator and condenser walls, respectively.

Hence, the condenser wall temperature and the total temperature drop for the heat pipe may be calculated by the equations,

$$T_{c,o} = T_s - (T_s - T_{c,i}) - (T_{c,i} - T_{c,o}), \tag{18}$$

and

$$T_{e,o} = (T_{e,o} - T_{e,i}) + (T_{e,i} - T_s) + (T_s - T_{e,i}) + (T_{c,i} - T_{c,o}). \tag{19}$$

In these equations, values of $(T_{e,o}-T_{e,i})$, $(T_{e,i}-T_s)$, $(T_s-T_{c,i})$ and $(T_{c,i}-T_{c,o})$ are calculated by Equations 16, 8, 12 and 17, respectively.

Since a number of simplifying assumptions have been used in the above derivation of the temperature distribution equations, a comparison between theory and available experimental data is made. Figure 6 shows the experimental data for a liquid nitrogen heat pipe from Table 1 of Reference 13, and the present predictions under the same conditions. The agreement between theory and experiments is satisfactory.

3.3 Maximum Heat Transfer Capability

Designers and users of the heat pipe are also interested in the maximum heat transfer capability besides the operating temperatures discussed above. Because of the low surface tension and high pressure of the cryogen, the heat transfer capability for the cryogenic heat pipe is expected to be wick limited[12]. That is, it may be assumed that Q_{max} under zero-

gravity conditions can be obtained by equating the maximum capillary pressure with the sum of the liquid pressure drop and the vapor pressure drop,

$$\Delta p_c = \Delta p_f + \Delta p_v. \tag{20}$$

For the isothermal case, the equations for Δp_c, Δp_f, and Δp_v have been derived by Cotter[2]. They are respectively as follows,

$$\Delta p_c = \frac{2\gamma_f}{r_c}, \tag{21}$$

$$\Delta p_f = \frac{bQ_{max}}{2\pi\varepsilon(r_i^2 - r_v^2)r_f^2} \frac{\mu_f}{\rho_f h_{fg}} (z_e + 2z_a + z_c), \tag{22}$$

and

$$\Delta p_v = \frac{4Q_{max}}{\pi r_v^4} \frac{\mu_v}{\rho_v h_{fg}} (z_e + 2z_a + z_c). \tag{23}$$

where Equation 22 corresponds to Cotter's equation for small maximum heat transfer capability, which may be assumed to be true for the cryogenic heat pipe because of the low values of the liquid transport factor for cryogens (see Section 2).

For cryogenic heat pipes, we are required to introduce appropriate property values into Equations 21 through 23. In view of the success in using the bulk average temperature method for the temperature-drop calculations (see Figure 6), the values of μ_f and ρ_f are evaluated at the bulk average temperatures for the evaporator, adiabatic, and condenser section, respectively. Since evaporation (or condensation) and the capillary pumping are phenomena at the vapor-liquid interface, γ_f and h_{fg} are evaluated at the saturation vapor temperature, which may be assumed uniform ($\Delta T_v \approx 0$) for a heat pipe operating under given conditions.

Introducing the appropriate fluid properties discussed above into Equations 21 through 23 and then substituting them into Equation 20, we obtain the following governing equation for the maximum heat transfer

capability of the cryogenic heat pipe.

$$\frac{2\gamma_{f,s}}{r_c} = \frac{Q_{max}}{h_{fg,s}} \left(\frac{b}{2\pi\varepsilon(r_i^2 - r_v^2)r_f^2} \left(\frac{\mu_{f,be}}{\rho_{f,be}} z_e + 2\frac{\mu_{f,s}}{\rho_{f,s}} z_a + \frac{\mu_{f,bc}}{\rho_{f,bc}} z_c \right) + \frac{4}{\pi r_v^4} \frac{\mu_{v,s}}{\rho_{v,s}} (z_e + 2z_a + z_c) \right). \tag{24}$$

3.4 Computer Program and Fluid Properties

A program for the above theory has been written in Fortran IV language. This program and instructions for its use are given in Appendix A.

Besides the heat-pipe dimensions and wick structures, nine physical properties of heat-pipe working fluids are relevant to performance of the heat pipe. These nine properties are the saturation vapor pressure, saturation vapor density, saturation vapor viscosity, heat of vaporization, saturation liquid surface tension, saturation liquid density, saturation liquid viscosity, saturation liquid specific heat, and saturation liquid thermal conductivity at various temperatures. They have been collected from several References[19-23] for nine fluids, namely: helium, hydrogen, neon, flourine, nitrogen, argon, oxygen, methane and Freon-14. These collected data are presented in Appendix B.

4. PERFORMANCE CHART AND DESIGN PROCEDURE

4.1 Performance Chart

A mathematical model for analyses of the cryogenic heat pipe has been formulated. Unlike the liquid metal heat pipe, which may often be considered as an isothermal device[2], the performance characterization of the cryogenic heat pipe must include not only the maximum heat transfer capability but also the condenser and evaporator wall temperatures. The

evaporator and condenser wall temperatures are determined from Equations 18 and 19 as a function of the heat transfer rate while the maximum heat transfer capability is found from Equation 24.

For complete presentation of performance of a heat pipe in a single chart, constant heat-transfer-rate, Q, curves may be mapped on the coordinates $(T_{e,o}-T_{c,o})$ versus $T_{c,o}$. In addition, the maximum heat transfer capability of the heat pipe may also be traced on the same coordinates. Figure 7 shows an example of such performance charts for a stainless steel 304 heat pipe with r_o, r_i, r_v, z_e, z_a and z_c equal to 0.5, 0.48, 0.42, 6, 48, and 6, cm respectively. Wrapped stainless steel 304 mesh screen is used for the wick with ε=0.5, b=12, r_c=0.01cm and r_f=0.01cm. Liquid nitrogen is chosen as the working fluid.

4.2 Design Procedure

In many cases, the problem of designing a heat pipe is specified as follows:

For a given application of the heat pipe, the range of operating temperature, the required heat transfer rate, the structure of wick meaterial, the physical dimension of the container and the lengths of the evaporator, adiabatic and condenser sections are specified. It is required to find the desired working fluid, the dimensions of capillary wick, and the performance of the designed heat pipe.

The procedure of solving this problem by the present theory is as follows:

1. To design for minimum temperature drop, it is required to choose a working fluid with maximum value of liquid thermal

conductance factor; so the choice of working fluid for the specified range of operation may be made by reference to Figure 4.

2. With the structure of wick material specified, the required wick thickness for the specified heat transfer rate can be calculated by the use of the computer program listed in Appendix A.

3. Following the determination of the wick dimensions and the working fluids as described above, a performance chart for the heat pipe may be generated, again with the aid of the computer program listed in Appendix A.

5. CONCLUSIONS AND RECOMMENDATIONS

5.1 Conclusions

In conclusion the results of this program can be summarized as follows:

1. The significance of the liquid property variations on the performance of cryogenic heat pipe was discovered. A theory taking account of liquid property variations has accordingly been developed for the cryogenic heat pipes. A computer program written in Fortran IV language has been developed for the theory to facilitate design and performance calculations.

2. Property values of cryogens relevant to heat pipe performance have been collected and appended to this report (see Appendix B).

3. The use of charts is suggested to facilitate complete characterization of heat pipe performance. For an example of such charts, see Figure 7.
4. A procedure for the computer aided design of cryogenic heat pipes is developed and described in Sections 4.2.
5. Comparison of the theory with the existing experimental data for a cryogenic heat pipe[13] has been made (see Figure 6). The agreement between them is satisfactory. However, it should be mentioned here that this comparison is only a partial confirmation of the theory. For example, no data are available at the present to check predictions for the maximum heat transfer capability.

5.2 Recommendations

It is recommended that the present theory should be extended and developed in the following ways:

1. There is a need for experimental work of greater range and higher accuracy, so that the theory can be further refined. In particular, endeavour should be made in experiments to obtain the complete performance chart of the heat pipe under test (see Figure 7). Following this, thorough examination of the theoretical implication would be able to be made.
2. It is generally believed that boiling limitation on the operation of cryogenic heat pipe is important. However, at the present time no such data are available. Both theoretical and experimental studies of boiling limitation on cryogenic heat pipes should be made.

3. As for the thermal conductivity of cryogen saturated wick, Gorring and Churchill's correlation appears appropriate, when the liquid is the major phase and the wick material is the minor phase. However, because of the low thermal conductivity of cryogens, there is an advantage in using wick material which has metal as a major phase, such as sintered metal. Thermal conductivity of sintered metal saturated with cryogens should measured and the data be correlated.
4. An extension of the present theory should be made to include its applicability to the heat pipes of composite wick structures and to the ambient and high temperature heat pipes.

6. REFERENCES

1. Grover, G. M., Cotter, T. P., and Erickson, G. F., "Structures of very high thermal conductance," J. Appl. Phys., vol.35, pp.1990-1991, (1964).

2. Cotter, T. P., "Theory of heat pipes," Los Alamos Scientific Laboratory, Report No. La-3246-MS, (1965).

3. Kemme, J. E., "Heat pipe capability experiments," Los Alamos Scientific Laboratory, Report No. LA-3585-MS, (1966).

4. Cosgrove, J. H., Ferrell, J.K., and Carnesale, A., "Operating Characteristics of capillary-limited heat pipes," J. Nuclear Energy, vol. 21, pp.547-558, (1967).

5. Feldman, K. T., Jr., and Whiting, G. H., "The heat pipe," Mech. Eng. Feb., pp.30-33, (1967).

6. Frank, S., Smith, J. T., and Taylow, K. M., "Heat pipe design manual," Martin Marietta, Rept. No. MND-3288, (1967).

7. Levy, K. E., "Theoretical investigation of heat pipes operating at low vapor pressures," J. Eng. Ind., pp.547-552, (1968).

8. Larson, J. W., and Couch, J. P., "Comparison between vapor chamber and conducting fin Brayton radiator," NASA TMX-61163, (1968).

9. Schwartz, J., "Performance map of the water heat pipe and the phenomena of noncondensable gas generation," ASME Paper No. 69-HT-15, (1969).

10. Marto, P. J., and Mosteller, W. L., "Effect of nucleate boiling on on the operation of low temperature heat pipe," ASME Paper No. 69-HT-24, (1969).

11. Chato, J. C., and Streckert, J. H., "Performance of a wick-limited heat pipe," ASME Paper No. 69-HT-20, (1969).

12. Kemme, J. E., "Heat pipe design consideration," Los Alamos Scientific Laboratory, Report No. LA-4221-MS, (1969).

13. Haskin, W. L., "Cryogenic heat pipe," AFFDSOTR-66-228, (1967).

14. Phillips, E. C., and Hinderman, J. D., "Determination of properties of capillary media useful in heat pipe design," ASME Paper No. 69-HT-18, (1969).

15. Rohsenow, W. M., and Choi, H., "Heat, Mass, and Momentum Transfer," pp.98, 136-145, Prentice-Hall, Englewood Cliffs, N.J., (1961).

16. Gorring, R. L., and Churchill, S. W., "Thermal conductivity of heterogeneous material," Chem. Eng. Prog., vol.57, no.7, pp.53-59, (1961).

17. Langston, L. S., and Kunz, H. R., "Liquid transport properties of some heat pipe wicking materials," ASME Paper No. 69-HT-17, (1969).

18. Magee, F. N., and Doering, R. D., "Vuillenmier cycle cryogenic refrigerator developments,: AFFDL-TR-68-67, (1968).

19. Johnson, V. J., "A compendium of the properties of materials (Phase 1) -- Part 1, properties of fluids," WADD TR 60-56, (1960).

20. Hirschfelder, J. O., Curtiss, C. F., and Bird, R. B., " Molecular Theory of Gases and Liquids," John Wiley & Sons, Inc., New York, N.Y., (1965).

21. Anon., "Preliminary thermodynamic properties of Freon-14," E. I. Du Pont de Nemours & Company, Inc., T-14, (1961).

22. Nelson, L. C., and Obert, E. F., "Generalized compressibility Charts," Chem. Eng., July issue, pp.203-208, (1954).

23. Maslan, F. D., and Littman, T. M., "Compressibility chart for hydrogen and inert gases," Ind. Eng. Chem., vol. 45, pp. 1566-1568, (1950).

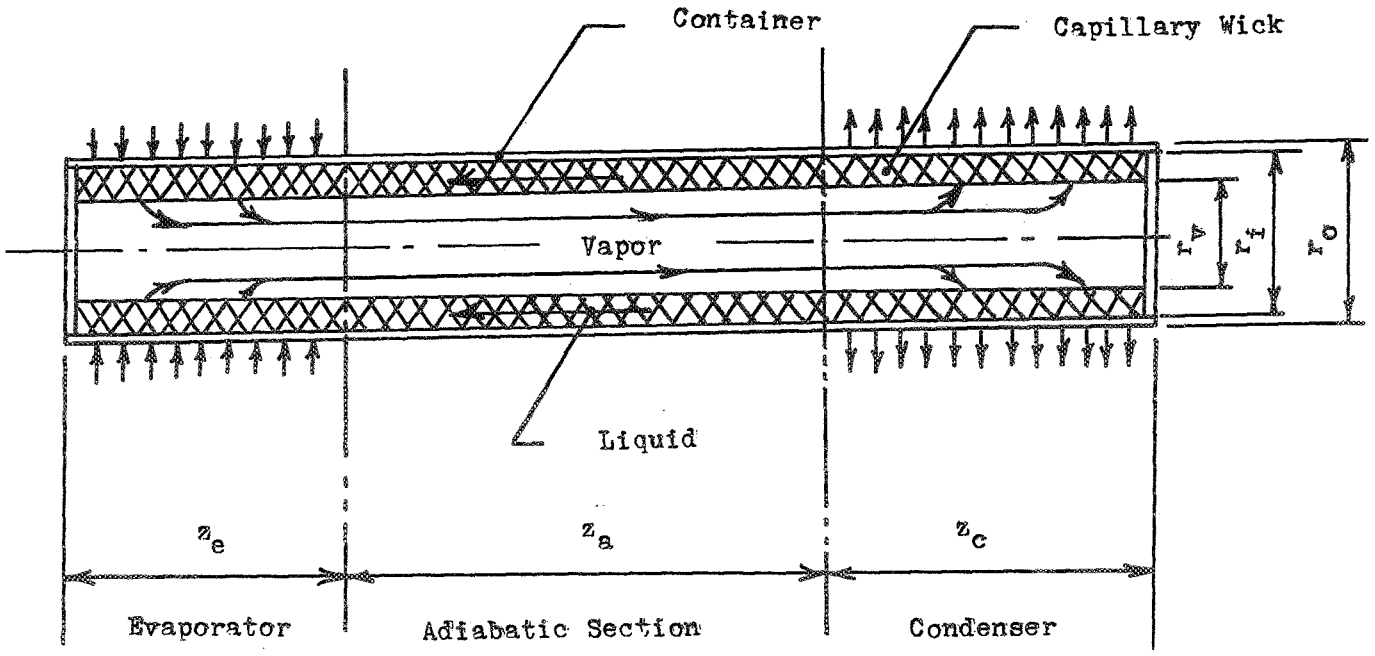

Figure 1 Schematic Representation of a Heat Pipe

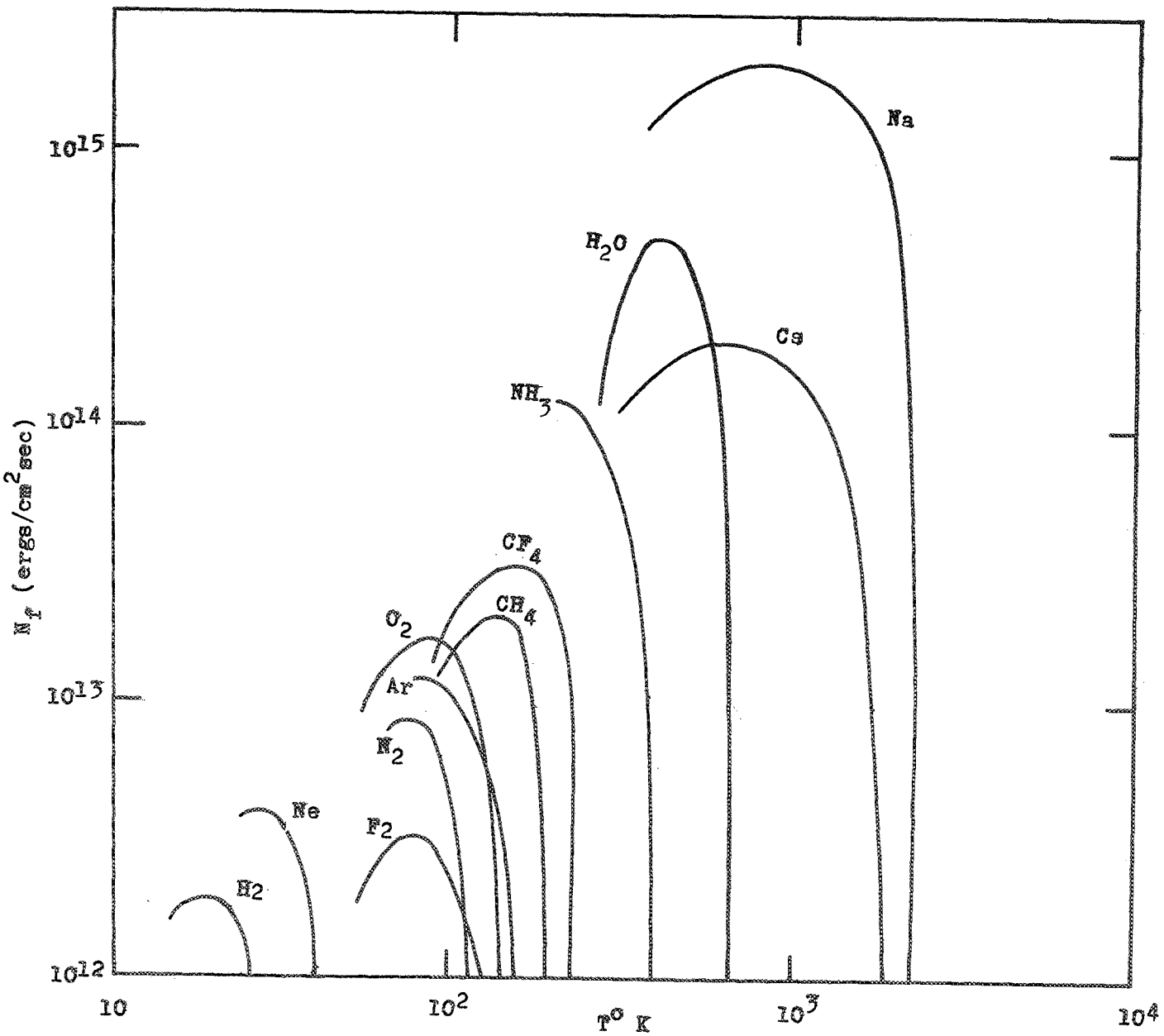

Figure 2 Liquid Transport Factor for Various Fluids

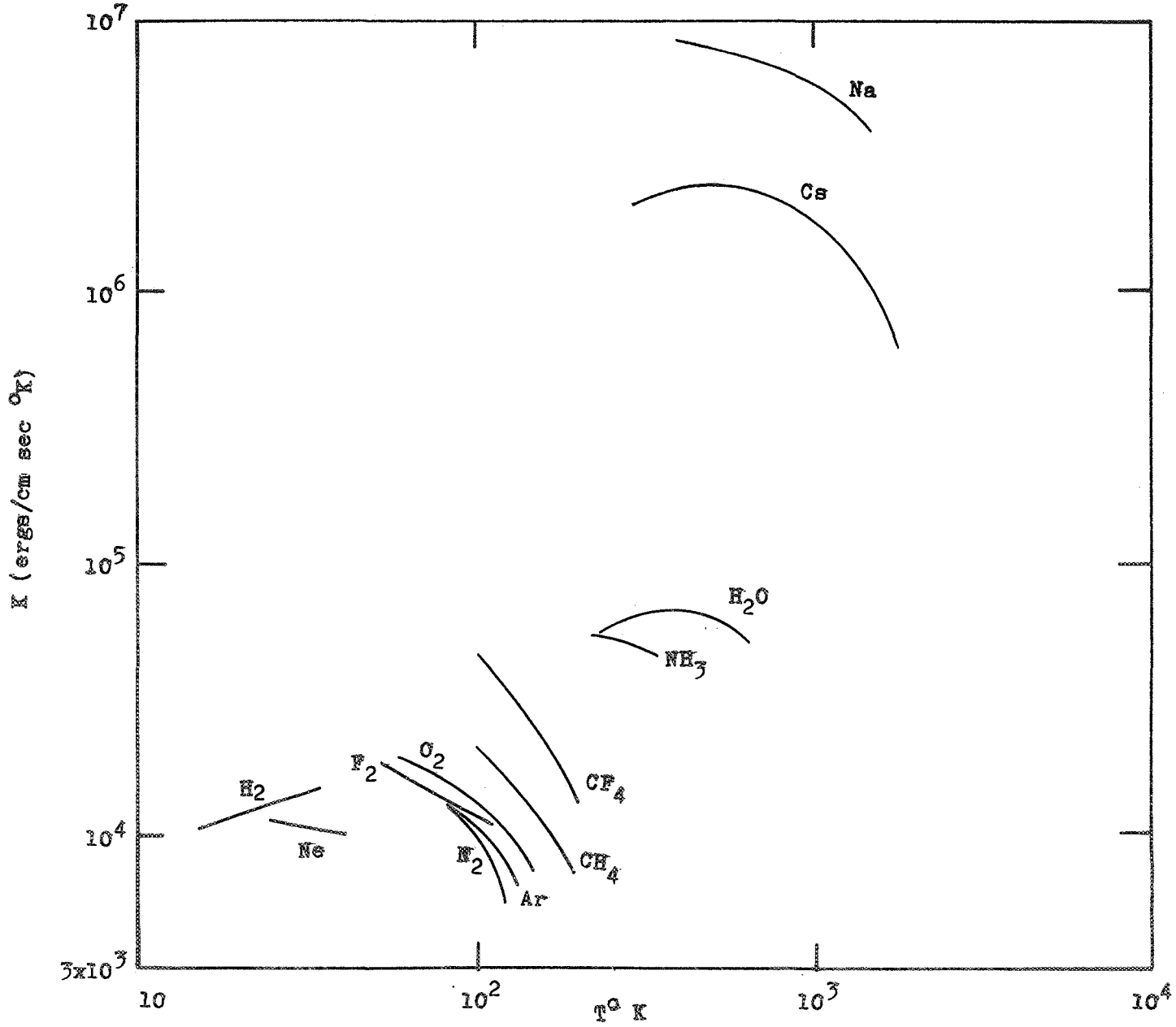

Figure 3 Liquid Thermal Conductivity for Various Fluids

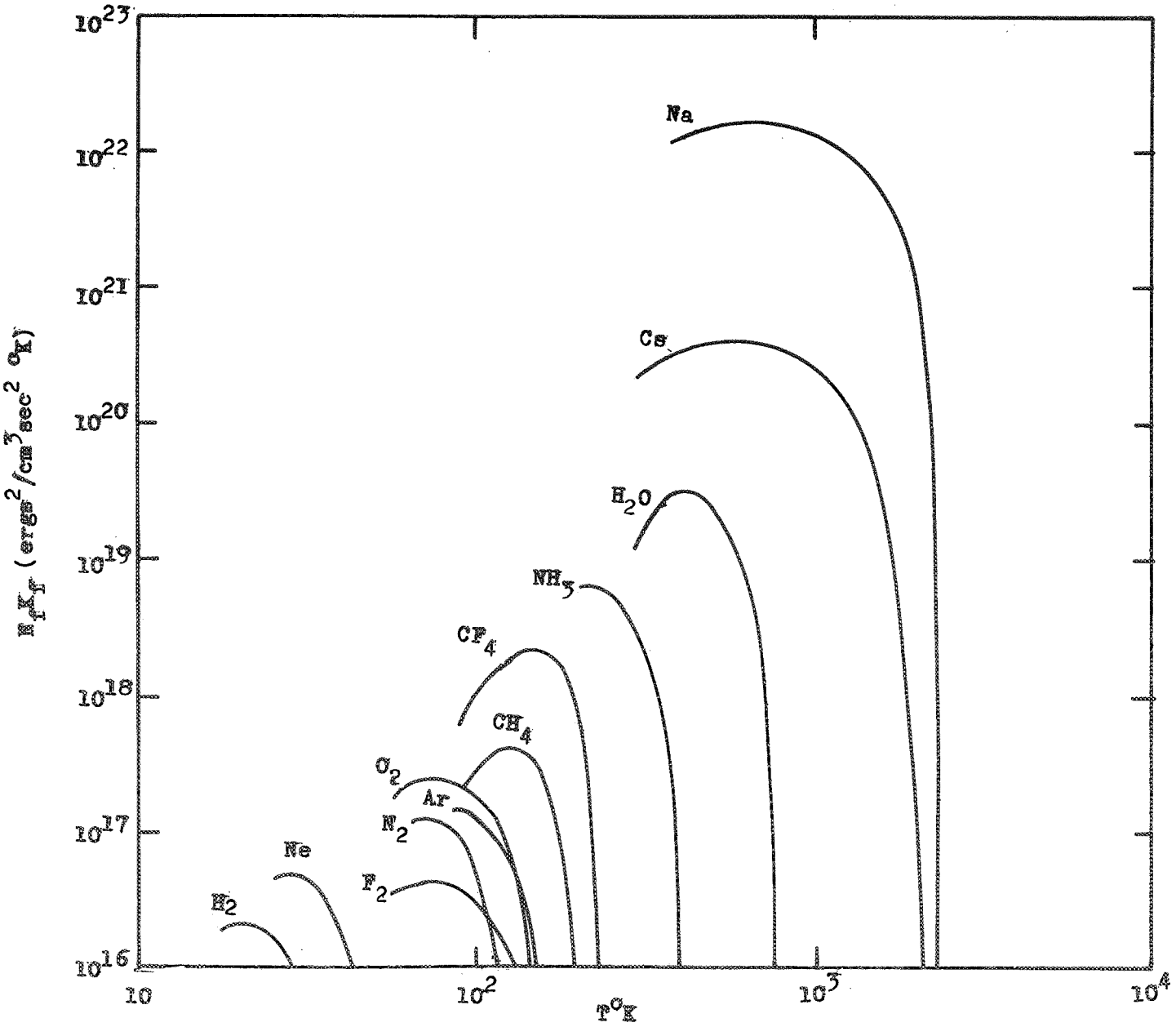

Figure 4 Liquid Thermal Conductance for Various Fluids

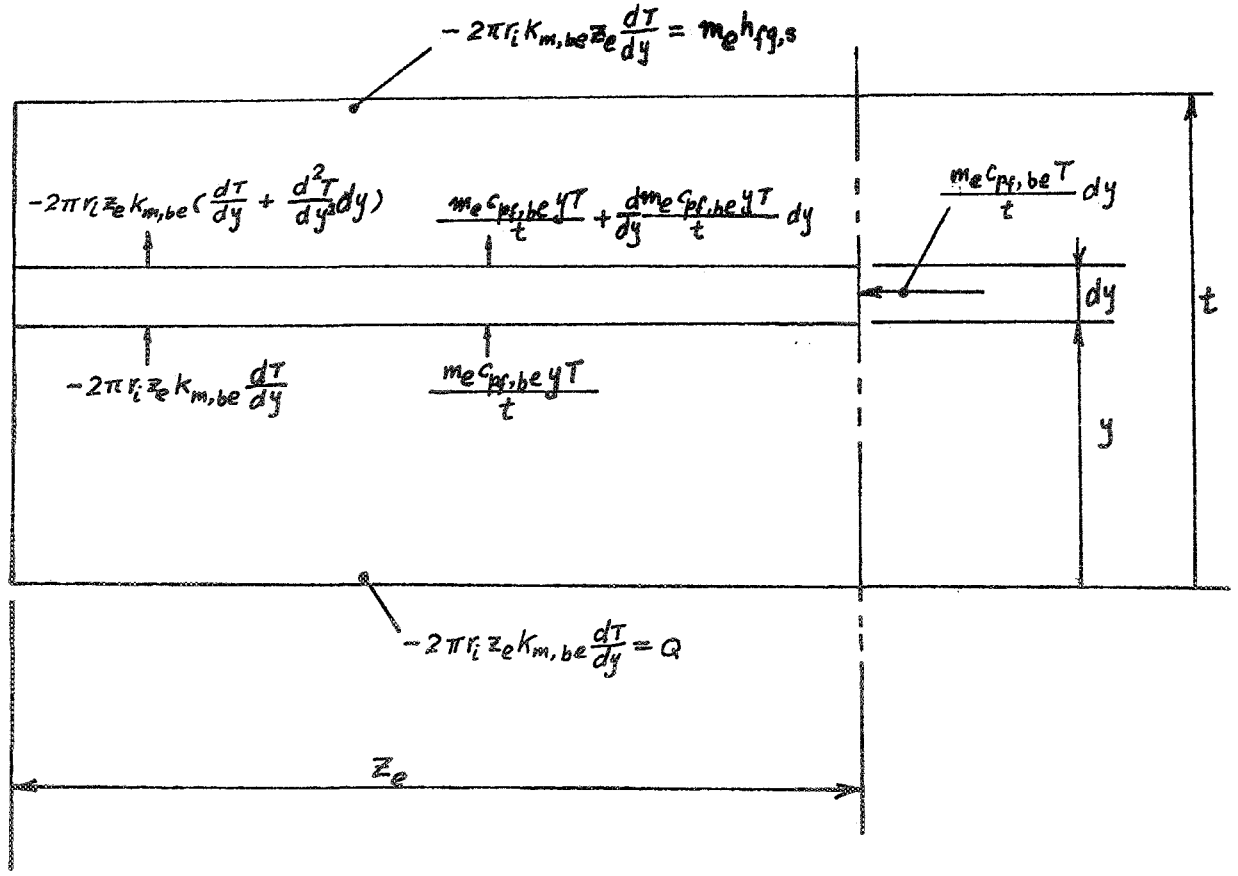

Figure 5 Liquid Control Volume with Energy Terms

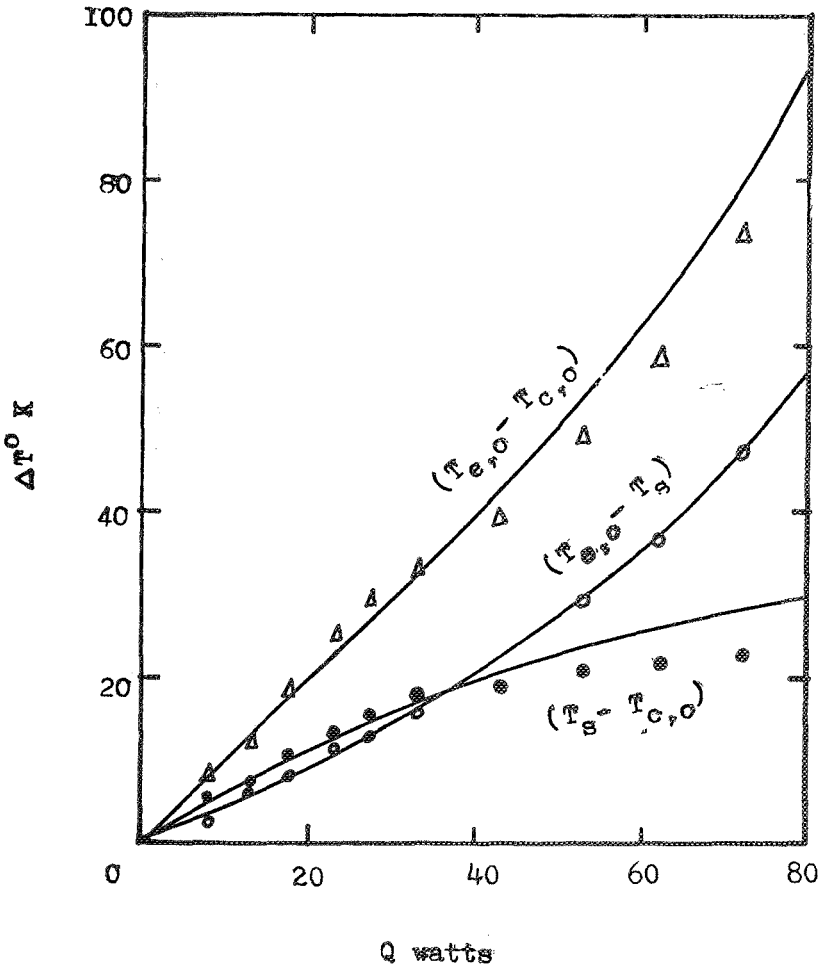

Figure 6 Comparison of Present Theory with Haskin's Experiments

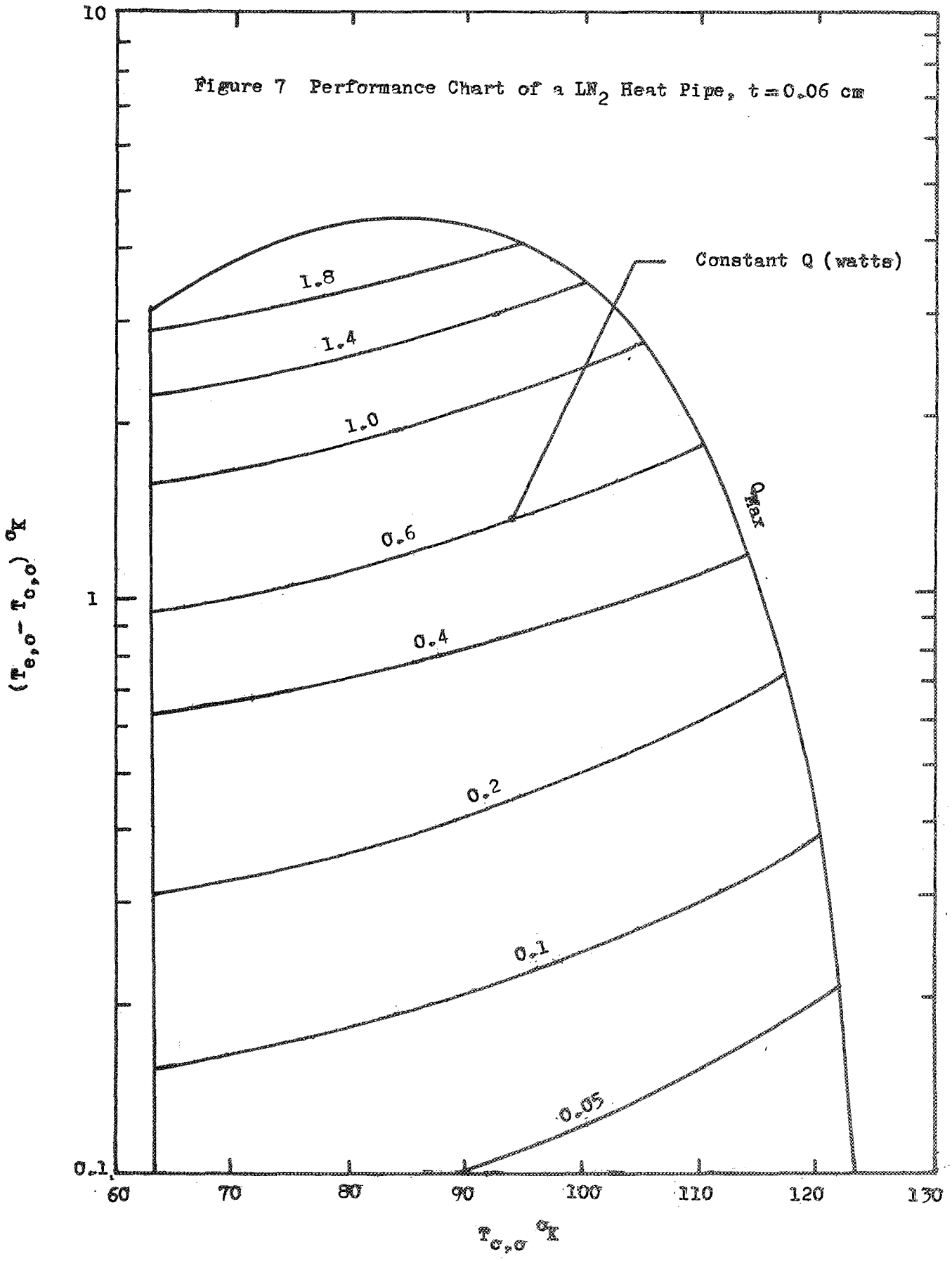

Figure 7 Performance Chart of a LN_2 Heat Pipe, t = 0.06 cm

APPENDIX A

A COMPUTER PROGRAM FOR HEAT PIPE DESIGN AND PERFORMANCE CALCULATIONS

A complete listing of the computer program in Fortran IV language is given below. In addition, Figure 1 shows the flow diagram of the program; and Table A1 shows an input data sheet. All the integers are 5-digit figures (I5); and all constants are 15-digit figures (E15.6). The Fortran Symbols are defined as follows:

IDOP specified 1 for design calculations and specified 2 of performance calculations

QQ the initial heat transfer rate in ergs/sec for performance calculation; arbitrary constant may be assigned for design calculations

DQ stepwise increase in heat transfer rate for performance calculations; arbitrary constant may be assigned for design calculations

KKI number of different heat pipe dimensions under study

KWK specified 1 for simple heat pipe of uniform wick structure; specified 2 for channel or artery heat pipe

NDR number of increments of vapor flow passage

DR stepwise change of radius of vapor flow passage in cm

NITV number of increments of DQ

RO container outer radius in cm

RI container inner radius in cm

RV1 initial radius of vapor flow passage in cm

RF effective hydraulic radius for liquid flow in cm

ZE length of evaporator section in cm

ZA length of adiabatic section in cm

ZC length of condenser section in cm

FEE specified zero for gravity free condition

B permeability factor for capillary structure

EPS porosity of capillary structure

RC effective radius for capillary pressure cm

CTA wetting angle for capillary action

BEC permeability factor for the for the evaporator and condenser, only required to be specified for artery or channel heat pipe

RIEC outer radius in cm for liquid flow for the evaporator and condenser, only required for artery or channel heat pipe

RVEC inner radius in cm for liquid flow for the evaporator and condenser, only required for artery or channel heat pipe

RFEC hydraulic radius in cm for liquid flow in evaporator and condenser, only required for artery or channel heat pipe

EPSEC porosity for evaporator and condenser, only required for artery or channel heat pipe

BA permeability factor for adiabatic section, only required for artery or channel heat pipe

RIA outer radius in cm for liquid flow for the adiabatic section, only required for artery or channel heat pipe

RVA inner radius in cm for liquid flow for the adiabatic section, only required for artery or channel heat pipe

RFA hydraulic radius in cm for liquid flow in the adiabatic section, only required for artery or channel heat pipe

EPSA porosity for the adiabatic section, only required for artery or channel heat pipe

NO number of vapor conditions under study

TSAT saturation vapor temperature in ^{o}K

PSAT saturation vapor pressure in dynes per cm^2

CPF liquid specific heat at saturation temperature in ergs/gm/^{o}K

DENF saturation liquid density in gm/cm^3

VSF saturation liquid viscosity in poises

CDF saturation liquid thermal conductivity in ergs/cm-sec-^{o}K

SFT surface tension in dynes/cm

HFG heat of vaporization in ergs/gm

DENG saturation vapor density in gm/cm^3

VSG saturation vapor viscosity in poises

R gas constant ergs/gm/^{o}K

CDW thermal conductivity of container wall in ergs/cm-sec-^{o}K

CDWK thermal condutivity of wick material in erg./cm-sec-^{o}K

AF change in liquid thermal conductivity per unit change in temperature in erg/cm-sec-^{o}K/^{o}K

AW change in container wall thermal conductivity per unit change in temperature in erg/cm-sec-^{o}K/^{o}K

AWK change in wick thermal conductivity per unit change in temperature in erg/cm-sec-^{o}K/^{o}K

ADENF change in liquid density per unit change in temperature in gm/cm^{3}/^{o}K

ACPF change in liquid specific heat per unit change in temperature in erg/gm-^{o}K/^{o}K

AVSF change in liquid viscosity per unit change in temperature in poises/^{o}K

Listing of computer program

```
F40      V20      13-JUN-70        9:54     PAGE 1

C HEAT PIPE 2 SIMPLIFIED THEORY
      COMMON TSAT,PSAT,CPF,DENF, VSF,CDF,SFT,HFG,DENG,
     1VSG,R,CDW,CDWK,AF,AW,AWK,ADENF,ACPF,AVSF,
     2Q,RI,RV,ZE,ZC,EPS,
     3TVE,TIE,TVC,TIC,TAVE,TAVC,VSAVE,VSAVC,DSAVE,DSAVC
      READ(2,11) IDOP
      READ (2,2) QO,DQ
      READ (2,11) KKI
      DO 400 KY=1,KKI
      READ(2,11) KWK
      READ(2,11) NDR
      READ (2,1) DR
      READ (2,11) NITV
      READ (2,4) RO,RI,RV1,RF
      READ (2,4) ZE,ZA,ZC,FEE
      READ (2,4) B,EPS,RC,CTA
      READ(2,3) BEC,RIEC,RVEC
      READ(2,2) RFEC,EPSEC
      READ(2,3) BA,RIA,RVA
      READ(2,2) RFA,EPSA
      READ (2,11) NO
      DO 100 I=1,NO
      WRITE (3,60) I
      READ (2,3) TSAT,PSAT,CPF
      READ (2,4) DENF,VSF,CDF,SFT
      READ (2,3)      HFG,DENG,VSG
      READ (2,3) R,CDW,CDWK
      READ (2,3) AF,AW,AWK
      READ (2,3) ADENF,ACPF,AVSF
      RV=RV1+DR
      DO 300 IDR=1,NDR
      RV=RV +DR
   11 FORMAT (I5)
    1 FORMAT (E15,6)
    2 FORMAT (2E15,6)
    3 FORMAT (3E15,6)
    4 FORMAT (4E15,6)
   60 FORMAT (///7H CYCLE=,I5)
   61 FORMAT (23H     TSAT              PSAT)
   62 FORMAT (53H       RO                RI                RV
   63 FORMAT (38H       ZE                ZA                ZC)
   65 FORMAT (7H QMAX= ,E15,6)
      ARES = 6,28318*RO*ZE
      ARCS = 6,28318*RO*ZC
      ZV= 0,5*(ZE+ZC)+ZA
      ZF=ZV
      ZT=ZV
      A=2,*SFT*COS(CTA)/RC
      BB=8,*VSG*ZV/(3,14159*DENG*RV**4*HFG)
      VSAVE=VSF
      DSAVE =DENF
      VSAVC=VSF
      DSAVC=DENF
```

```
      IF(KWK-1) 610,611,610
  611 BEC=B
      RIEC=RI
      RVEC=RV
      RFEC=RF
      EPSEC=EPS
      BA=B
      RIA=RI
      RVA=RV
      RFA=RF
      EPSA=EPS
  610 CONTINUE
      DO 120 ITRN=1,4
      CEC=BEC/(3.14159*EPSEC*(RIEC**2-RVEC**2)*RFEC**2*HFG)
      CEC=CEC*(0.5*ZE*VSAVE/DSAVE+0.5*ZC*VSAVC/DSAVC)
      CA=BA/(3.14159*EPSA*(RIA**2-RVA**2)*RFA**2*HFG)
      CA=CA*ZA*VSF/DENF
      C=CEC+CA
      QMAX=A/(BB+C)
      Q=QMAX
      CALL AVPPT
      CONTINUE
  120 CONTINUE
      IF (IDOP-1) 111,110,111
  110 Q=0.0
      DQ=QMAX/NITV
      GO TO 115
  111 Q=QQ
  115 CONTINUE
      WRITE (3,61)
      WRITE (3,2) TSAT,PSAT
      WRITE (3,62)
      WRITE (3,4) RO,RI,RV,RC
      WRITE (3,63)
      WRITE (3,3) ZE,ZA,ZC
      WRITE (3,65) QMAX
      WRITE (3,66)
    7 FORMAT (7E15.6)
   66 FORMAT  (99H       Q                TE                TC
     1            DTTE              DTTC              DTT )
      DO 200 M=1,NITV
      Q=Q+DQ
      DPC=A
      DPV=BB*Q
      DPF=C*Q
      DPG=D
      DTV=R*TSAT**2.0*DPV/(PSAT*HFG)
      TES=Q
      TCS=Q
      TVE=TSAT
      TIE=TSAT
      TOE=TSAT
      TVC=TSAT
```

```
      TIC=TSAT
      TOC=TSAT
      CALL AVPPT
      CONTINUE
      DO 500 K11=1,4
      CDWE=CDW*AW*(0.5*(TIE+TOE)-TSAT)
      CDWC=CDW*AW*(0.5*(TIC+TOC)-TSAT)
      TWES=TES*ALOG(RO/RI)/(6.28318*CDWE*ZE)
      TWCS=TCS*ALOG(RO/RI)/(6.28318*CDWC*ZC)
      TOE=TIE+TWES
      TOC=TIC-TWCS
      DTTE=TOE-TSAT
      DTTC=TSAT-TOC
      DTT=TOE-TOC
      EFCO=Q*ZT/(DTT*3.14159*RO**2)
  500 CONTINUE
      WRITE (3,7) Q,TOE,TOC,EFCO,DTTE,DTTC,DTT
  200 CONTINUE
  300 CONTINUE
  100 CONTINUE
  400 CONTINUE
      CALL EXIT
      END
```

ANTS

```
203622077174    1        202622077174
```

```
/,COMM,/+0      PSAT     /,COMM,/+1      CPF      /,COMM,/+2
/,COMM,/+3      VSF      /,COMM,/+4      CDF      /,COMM,/+5
/,COMM,/+6      HFG      /,COMM,/+7      DENG     /,COMM,/+10
/,COMM,/+11     R        /,COMM,/+12     CDW      /,COMM,/+13
/,COMM,/+14     AF       /,COMM,/+15     AW       /,COMM,/+16
/,COMM,/+17     ADENF    /,COMM,/+20     ACPF     /,COMM,/+21
/,COMM,/+22     Q        /,COMM,/+23     RI       /,COMM,/+24
/,COMM,/+25     ZE       /,COMM,/+26     ZC       /,COMM,/+27
/,COMM,/+30     TVE      /,COMM,/+31     TIE      /,COMM,/+32
/,COMM,/+33     TIC      /,COMM,/+34     TAVE     /,COMM,/+35
/,COMM,/+36     VSAVE    /,COMM,/+37     VSAVC    /,COMM,/+40
/,COMM,/+41     DSAVC    /,COMM,/+42
```

GRAMS

```
JOBFF   INTO,   INTI,   FLOUT,  FLIRT,  COS     AVPPT   FLOAT
ALOG    EXIT
```

S

```
1002            QQ      1003            DD      1004
1005            KY      1006            KWK     1007
1010            DR      1011            VITV    1012
```

```
      SUBROUTINE AVPPT
      COMMON TSAT,PSAT,CPF,DENF, VSF,CDF,SFT,HFG,DENG,
     1VSG,R,CDW,CDWK,AF,AW,AWK,ADENF,ACPF,AVSF,
     2Q,RI,RV,ZE,ZC,EPS,
     3TVE,TIE,TVC,TIC,TAVE,TAVC,VSAVE,VSAVC,DSAVE,DSAVC
      SBAE=3.14159*(RI*RV)
      SBAC=SBAE*ZC
      SBAE=SBAE*ZE
      SBTK=RI-RV
      SBM=Q/HFG
      SBK=(CDF+CDWK-(1.-EPS)*(CDF-CDWK))/
     1(CDF+CDWK+(1.-EPS)*(CDF-CDWK))
      SBK=SBK*CDF
      SBKE=SBK
      SBKC=SBK
      SBCE=CPF
      SBCC=CPF
      DO 210 ISB1=1,4
      SBME=SBM
      SBMC=SBM
      DO 211 ISB2=1,4
      FME =EXP (0.5*SBME*SBCE*SBTK/(SBKE*SBAE))
      DFME=HFG/Q-SBCE*FME*SBTK/(2.*SBKE*SBAE)
      FME=SBME*HFG/Q-FME
      SBME=SBME-FME/DFME
      FMC=EXP(-0.5*SBMC*SBCC*SBTK/(SBKC*SBAC))
      DFMC=HFG/Q+SBCC*FMC*SBTK/(2.*SBKC*SBAC)
      FMC=SBMC*HFG/Q-FMC
      SBMC=SBMC-FMC/DFMC
  211 CONTINUE
      ALFE=0.5*SBME*SBCE/(SBTK*SBKE*SBAE)
      ALFC=0.5*SBMC*SBCC/(SBTK*SBKC*SBAC)
      DY=SBTK/100.
      Y=SBTK
      TVE=TSAT
      TVC=TSAT
      TIE=0.
      TIC=0.
      TAVE=0.
      TAVC=0.
      TIEN=0.
      TICN=0.
      DO 220 ISB3=1,100
      TIE=TIE+0.5*TIEN
      TIC=TIC+0.5*TICN
      Y=Y-DY
      TIEN=DY*EXP(ALFE*Y*Y)
      TICN=DY*EXP(-1.*ALFC*Y*Y)
      TIE=TIE+0.5*TIEN
      TIC=TIC+0.5*TICN
      TAVE=TAVE+TIE
      TAVC=TAVC+TIC
  220 CONTINUE
```

```
      TAVE=0.01*(TAVE-0.5*TIF)
      TAVC=0.01*(TAVC-0.5*TIC)
      TIE=TSAT*Q*TIE/(SBKE*SBAE)
      TIC=TSAT-Q*TIC/(SBKC*SBAC)
      TAVE=TSAT+Q*TAVE/(SBKE*SBAE)
      TAVC=TSAT-Q*TAVC/(SBKC*SBAC)
      SKWKE=CDWK+AWK*(TAVE-TSAT)
      SKWKC=CDWK+AWK*(TAVC-TSAT)
      SKFE=CDF+AF*(TAVE-TSAT)
      SKFC=CDF+AF*(TAVC-TSAT)
      SBKE=(SKFE+SKWKE-(1.-EPS)*(SKFE-SKWKE))/
     1(SKFE+SKWKE+(1.-EPS)*(SKFE-SKWKE))
      SBKE=SKFE*SBKE
      SBKC=(SKFC+SKWKC-(1.-EPS)*(SKFC-SKWKC))/
     1(SKFC+SKWKC+(1.-EPS)*(SKFC-SKWKC))
      SBKC=SKFC*SBKC
      SBCE=CPF+ACPF*(TAVE-TSAT)
      SBCC=CPF+ACPF*(TAVC-TSAT)
  210 CONTINUE
      VSAVE=VSF+AVSF*(TAVE-TSAT)
      VSAVC=VSF+AVSF*(TAVC-TSAT)
      DSAVE=DENF+ADENF*(TAVE-TSAT)
      DSAVC=DENF+ADENF*(TAVC-TSAT)
      RETURN
      END
```

NSTANTS

	202622077174	1	207620000000	2	172507534121

MMON

AT	/,COMM,/+0	PSAT	/,COMM,/+1	CPF	/,COMM,/+2
NF	/,COMM,/+3	VSF	/,COMM,/+4	CDF	/,COMM,/+5
T	/,COMM,/+6	HFG	/,COMM,/+7	DENG	/,COMM,/+10
G	/,COMM,/+11	R	/,COMM,/+12	CDW	/,COMM,/+13
WK	/,COMM,/+14	AF	/,COMM,/+15	AW	/,COMM,/+16
K	/,COMM,/+17	ADENF	/,COMM,/+20	ACPF	/,COMM,/+21
SF	/,COMM,/+22	Q	/,COMM,/+23	RI	/,COMM,/+24
	/,COMM,/+25	ZE	/,COMM,/+26	ZC	/,COMM,/+27
S	/,COMM,/+30	TVE	/,COMM,/+31	TIE	/,COMM,/+32
C	/,COMM,/+33	TIC	/,COMM,/+34	TAVE	/,COMM,/+35
VC	/,COMM,/+36	VSAVE	/,COMM,/+37	VSAVC	/,COMM,/+40
AVE	/,COMM,/+41	DSAVC	/,COMM,/+42		

BPROGRAMS

P

ALARS

PPT	500	SBAE	501	RI	24
	25	SBAC	502	ZC	27

Figure A1 Flow diagram of the computer program

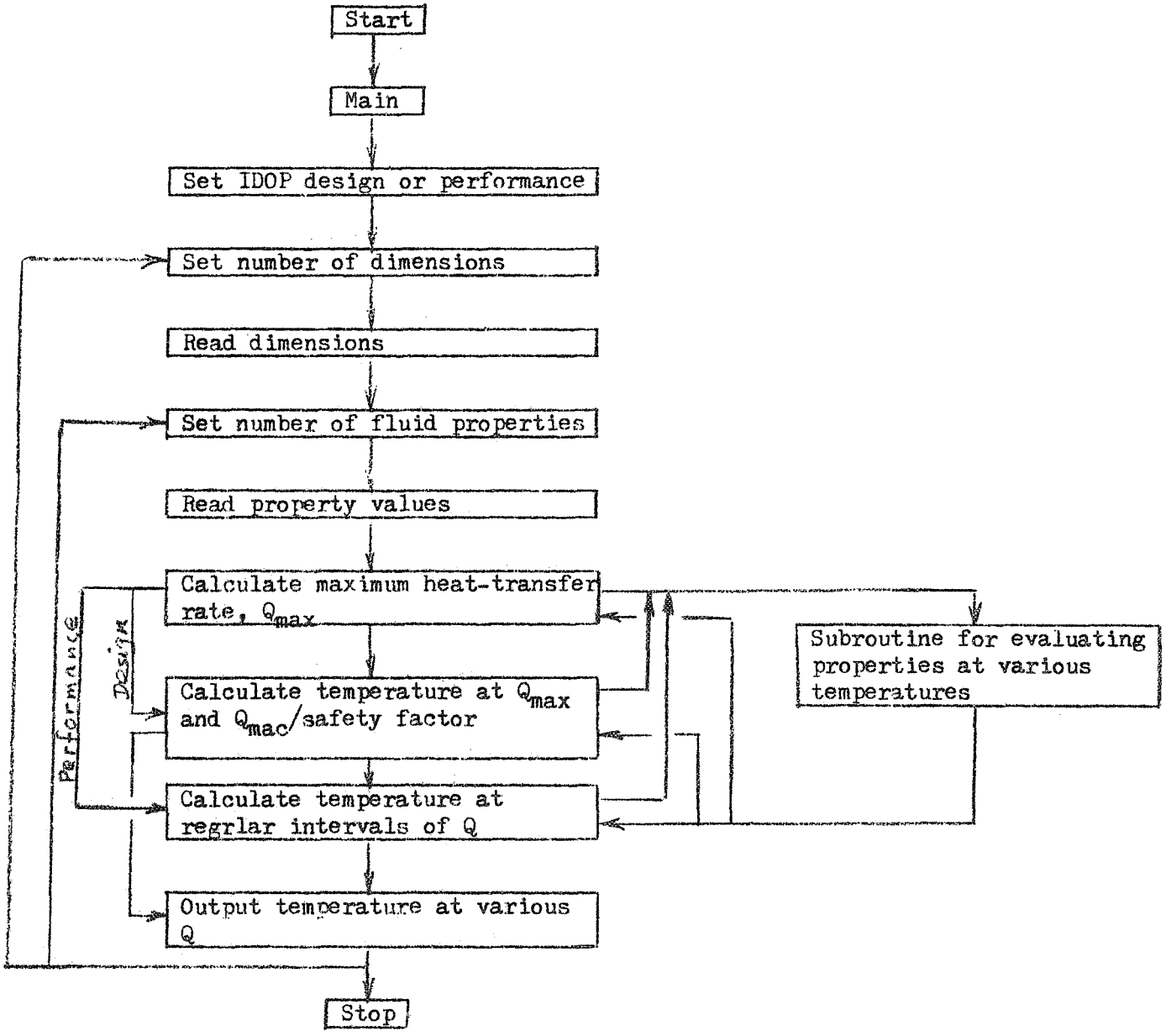

Table A1

Computer program input data

IDOP			
QQ	DQ		
KKI			
KWK			
NDR			
DR			
NITV			
RO	RI	RV1	RF
ZE	ZA	ZC	FEE
B	EPS	RC	CTA
BEC	RIEC	RVEC	
RFEC	EPSEC		
BA	RIA	RVA	
RFA	EPSA		
NO			
TSAT	PSAT	CPF	
DENF	VSF	CDF	SFT
HFG	DENG	VSG	
R	CDW	CDWK	
AF	AW	AWK	
ADENF	ACPF	AVSF	

APPENDIX B

COLLECTED PHYSICAL PROPERTIES OF CRYOGENS

Nine physical properties of cryogens, saturation vapor pressure, saturation vapor density, saturation vapor viscosity, heat of vaporization, saturation liquid surface tension, saturation liquid density, saturation liquid viscosity, saturation liquid specific heat, and saturation liquid thermal conductivity have been collected and plotted versus temperature for each of the nine cryogens, helium, hydrgen, neon, flourine, nitrogen, argon, oxygen, methane and Freon-14. In addition, triple point temperature and critical temperature for each of these nine cryogens are presented in Table B1.

List of Figures for Properties of Cryogens

Figures B1(a to i)* Properties of helium

Figures B2(a to i) Properties of hydrogen

Figures B3(a to i) Properties of neon

Figures B4(a to i) Properties of flourine

Figures B5(a to i) Properties of nitrogen

Figures B6(a to i) Properties of argon

Figures B7(a to i) Properties of oxygen

Figures B8(a to i) Properties of methane

Figures B9(a to i) Properties of Freon-14

(a)* Saturation vapor pressure

(b)* Saturation vapor density

(c)* Saturation vapor viscosity

(d)* Heat of vaporization

(e)* Saturation liquid surface tension

(f)* Saturation liquid density

(g)* Saturation liquid viscosity

(h)* Saturation liquid specific heat

(i)* Saturation liquid thermal conductivity

Table B1 Triple-point and Critical Temperatures for Several Cryogens

Cryogens	Triple-point Temperature, °K	Critical Temperature, °K
Helium	----	5.2
Hydrogen	13.9	33.2
Neon	19.0	44.4
Flourine	53.5	118.2
Nitrogen	63.2	126.2
Argon	83.8	150.7
Oxygen	54.4	154.6
Methane	88.7	190.7
Freon-14	89.5	228.0

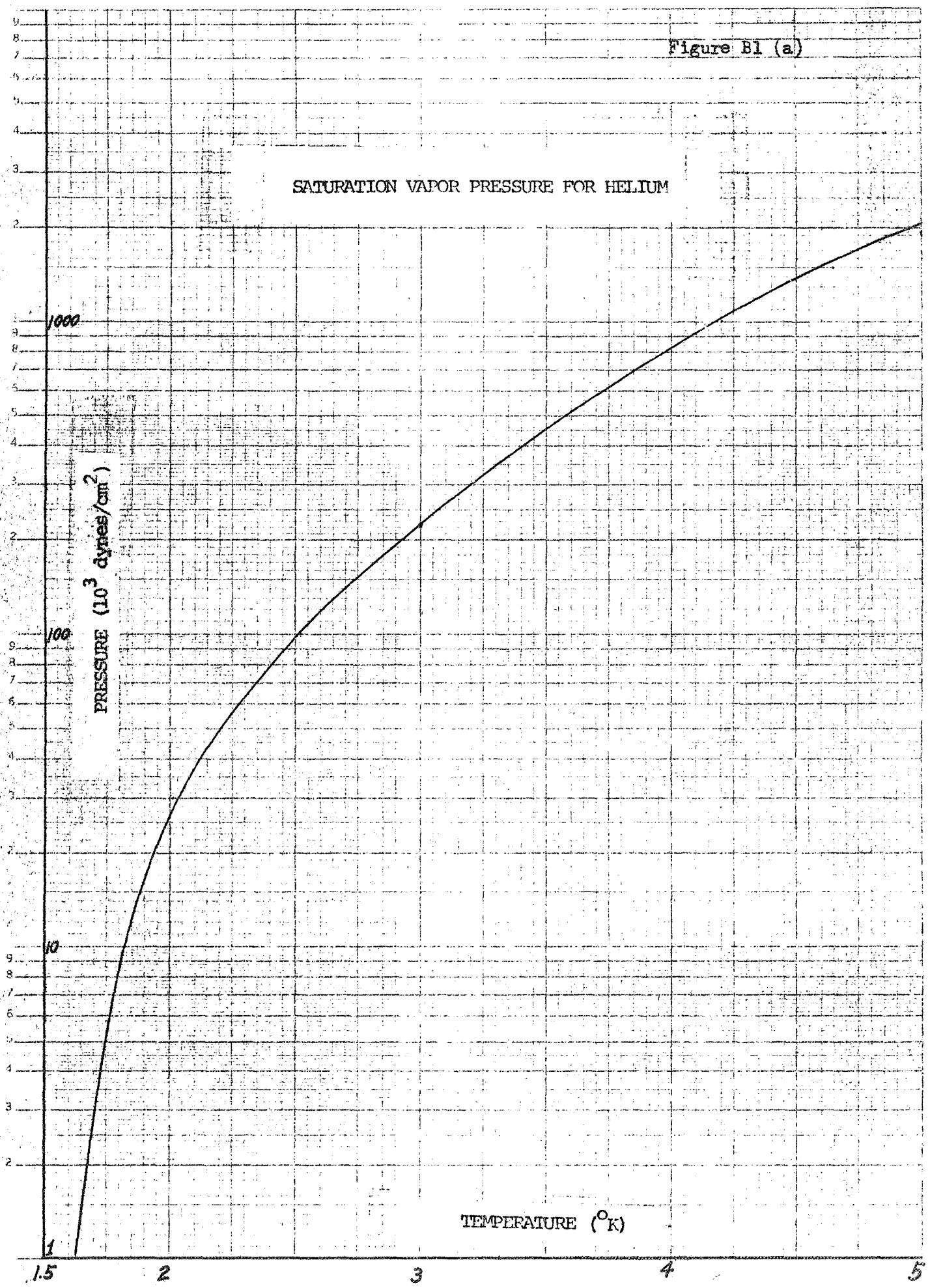
SATURATION VAPOR PRESSURE FOR HELIUM
PRESSURE (10^3 dynes/cm^2)
1000
100
10
1
TEMPERATURE (^{o}K)
1.5
2
3
4
5

Figure B1 (a)

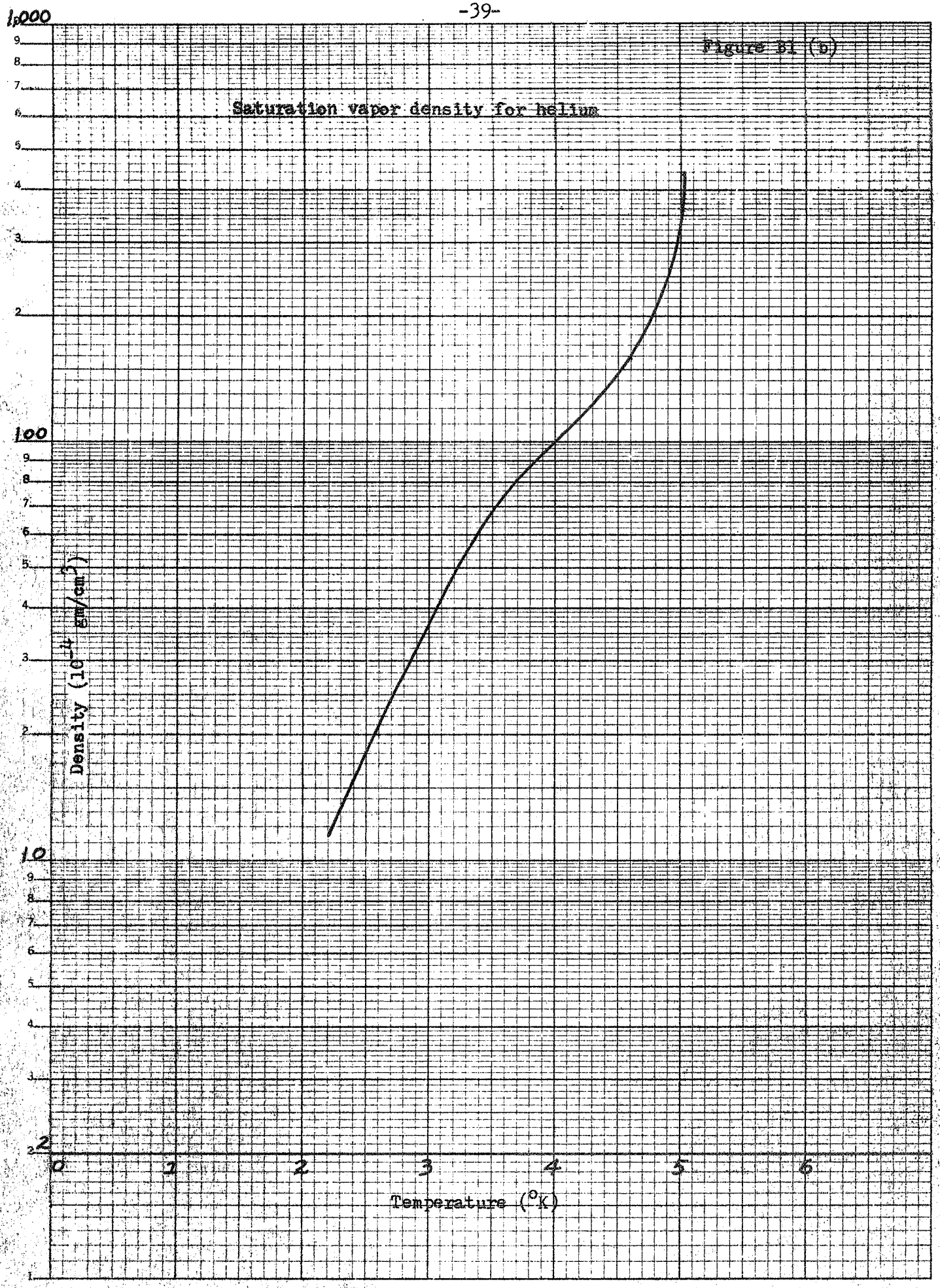
Figure 31 (b)
Saturation vapor density for helium
Density (10^{-4} gm/cm^3)
Temperature (^{o}K)
1,000
100
10
2
0
1
2
3
4
5
6

Figure B1 (c)

SATURATION VAPOR VISCOSITY FOR HELIUM

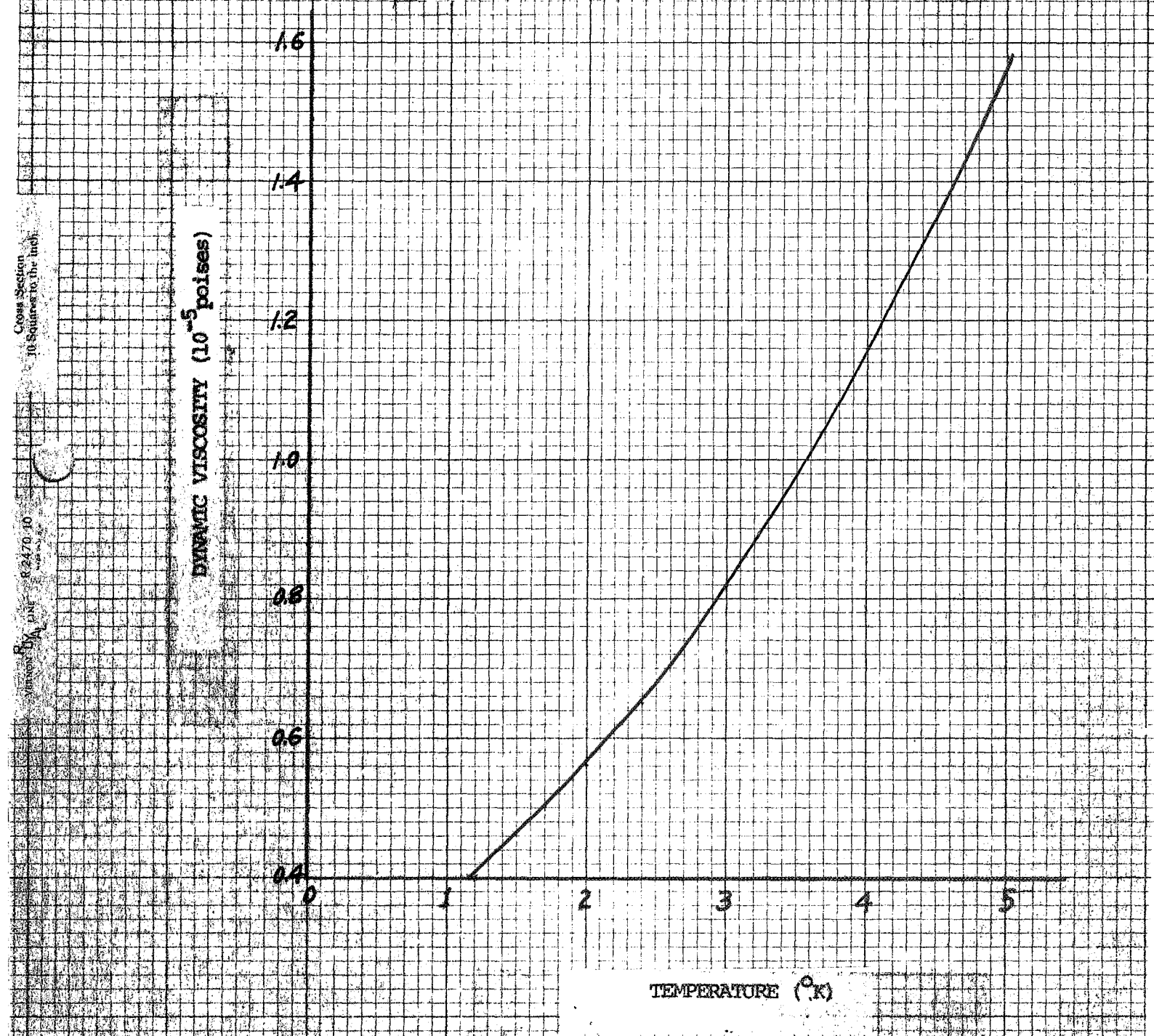

Figure B1 (d)

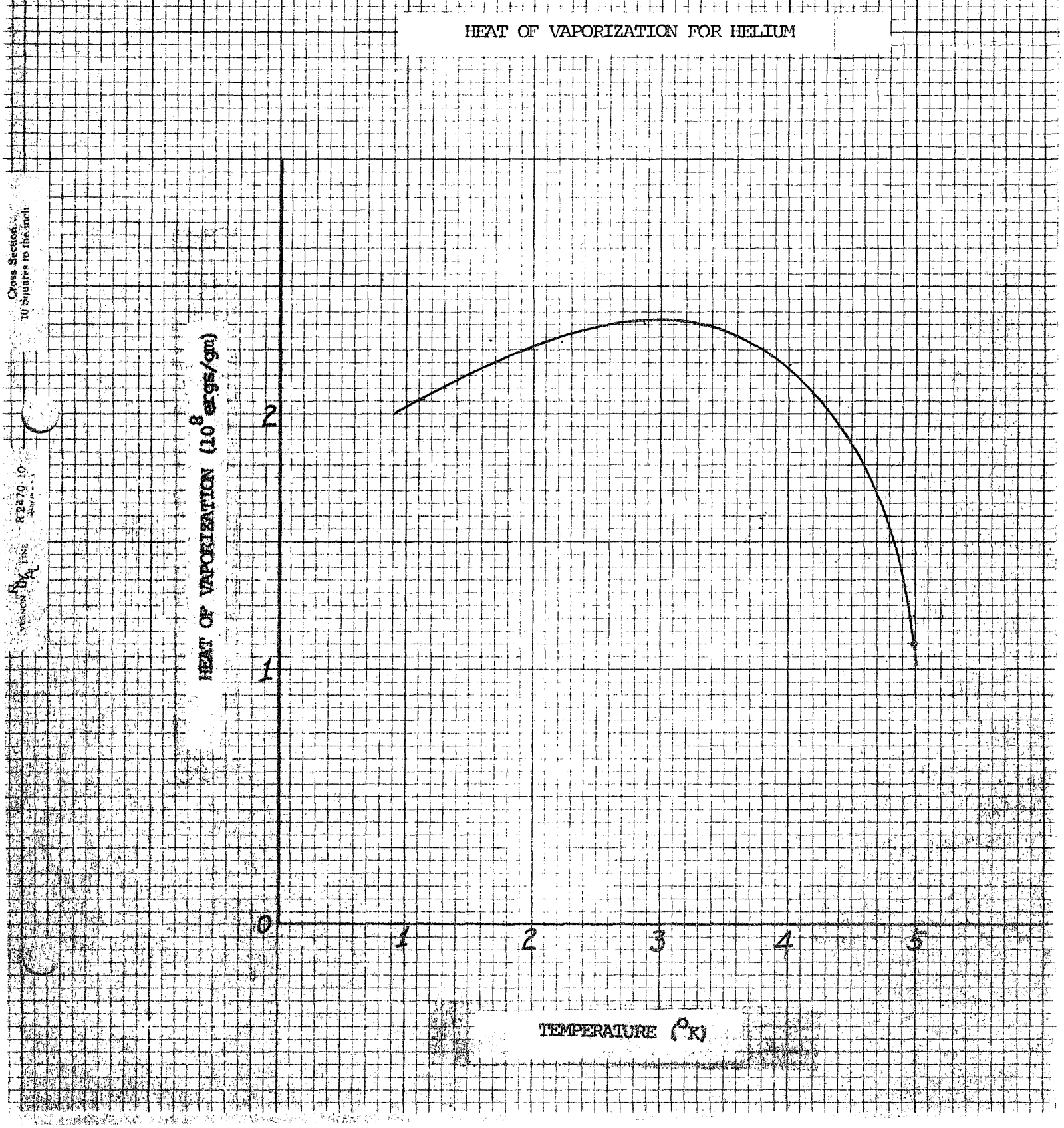
HEAT OF VAPORIZATION FOR HELIUM
HEAT OF VAPORIZATION (10^8 ergs/gm)
2
1
0
1
2
3
4
5
TEMPERATURE (°K)

Figure E1 (e)

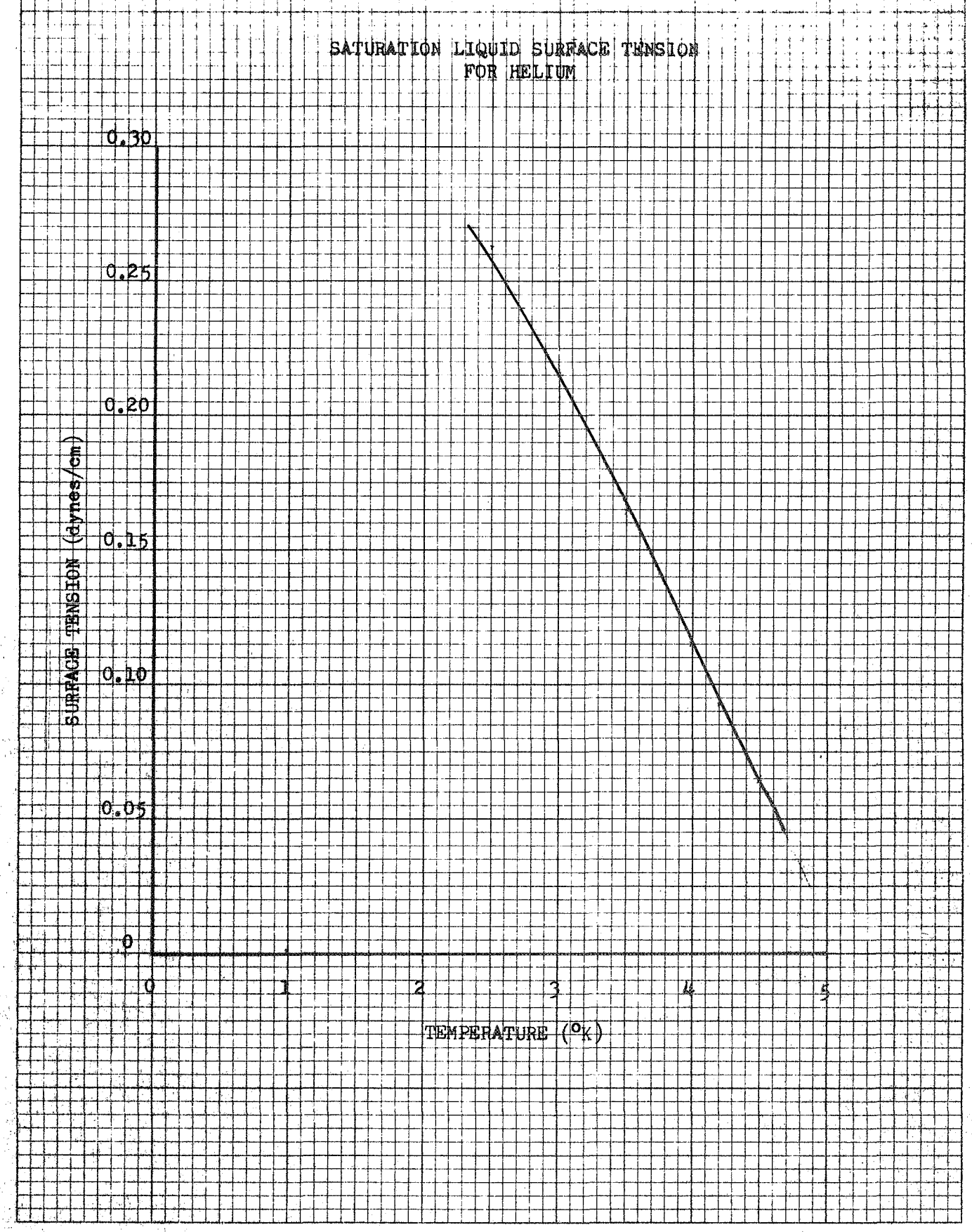

EUGENE DIETZGEN CO.
MADE IN U. S. A.
NO. 340-10 DIETZGEN GRAPH PAPER
10 X 10 PER INCH

Figure B1 (f)

SATURATION LIQUID DENSITY FOR HELIUM

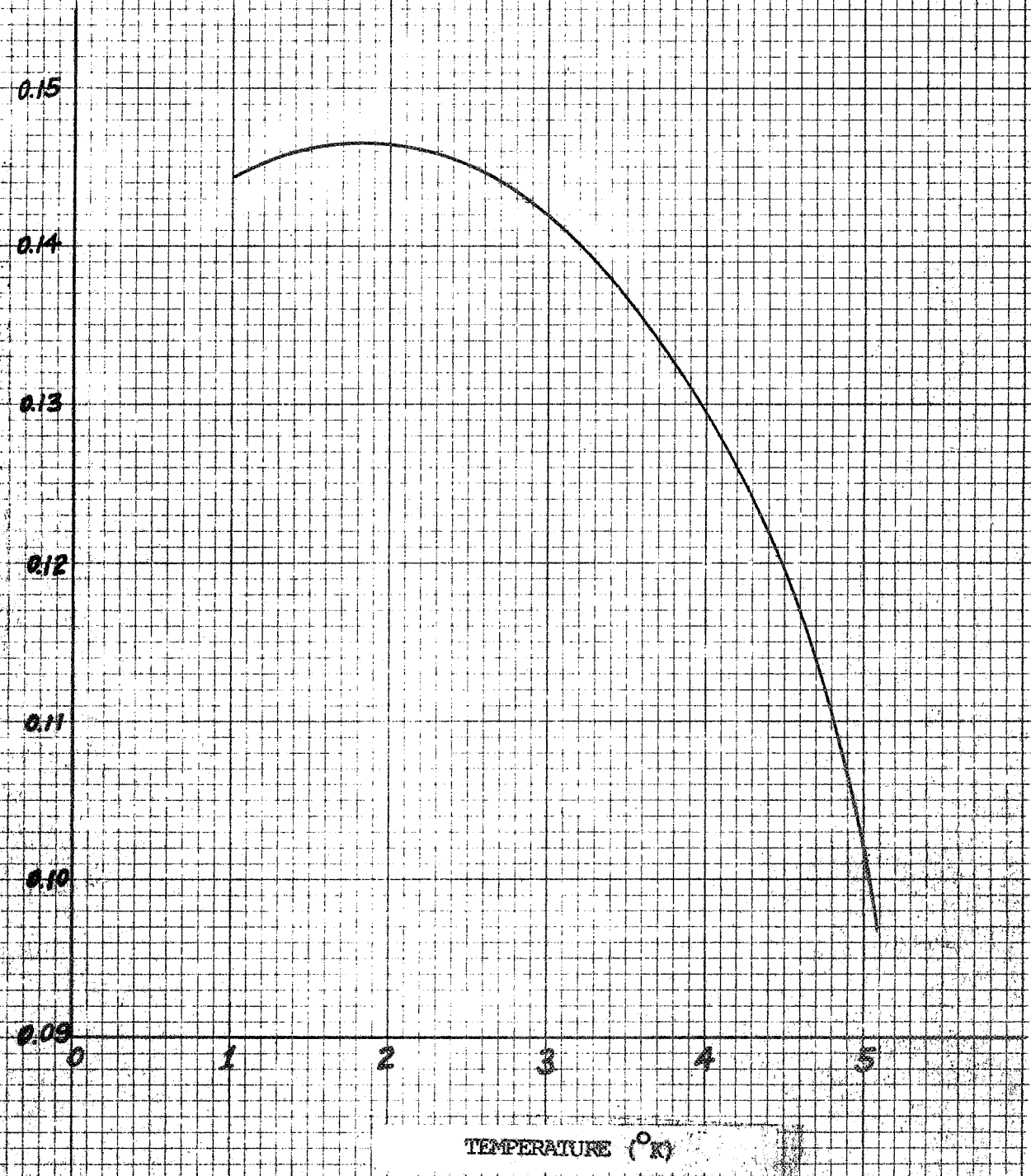

Cross Section
10 Squares to the inch
R 2470 10
VERNON LINE

Figure B1 (g)

SATURATION LIQUID VISCOSITY FOR HELIUM

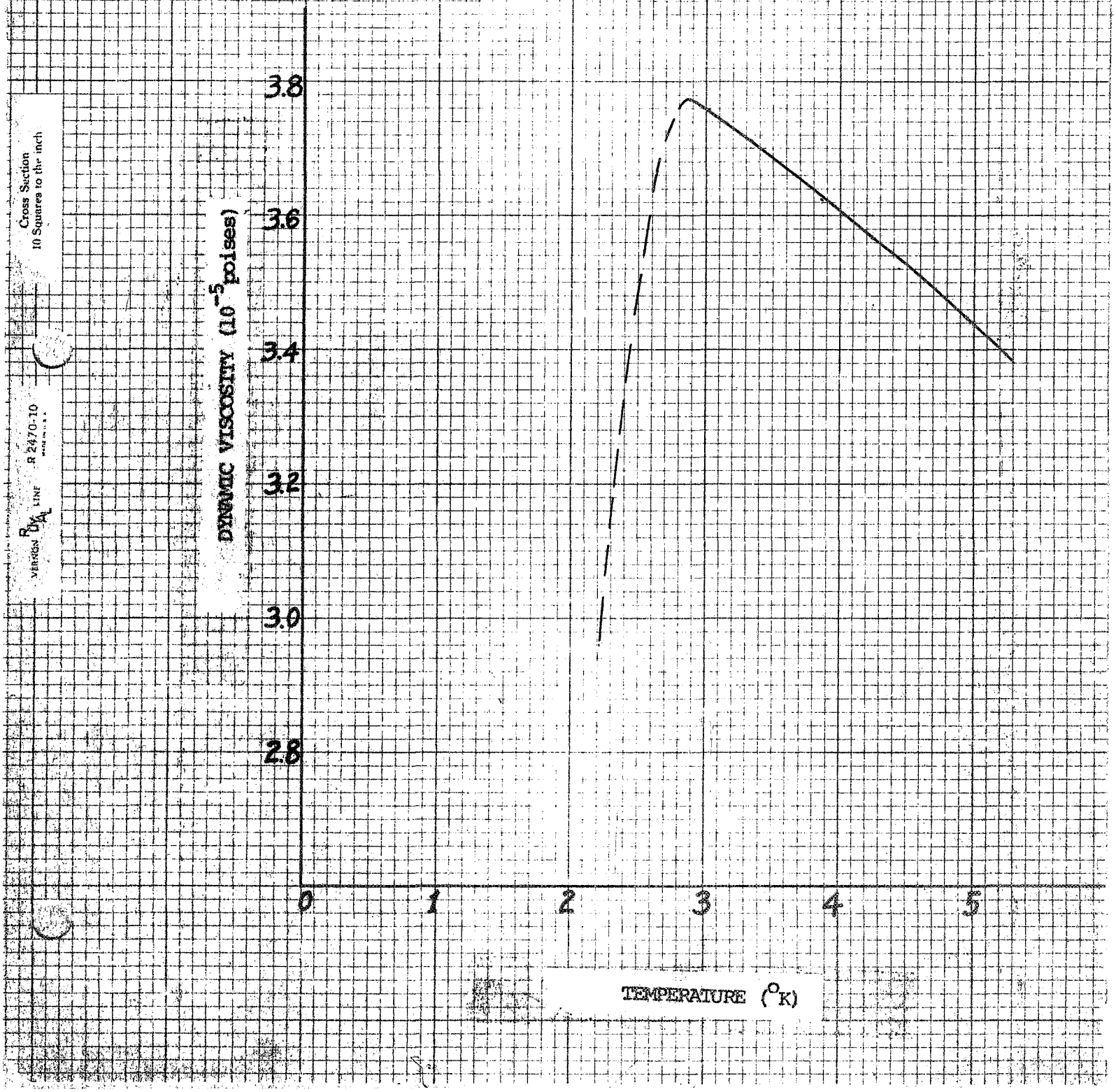

Cross Section
10 Squares to the inch
VERGEN DUAL LINE R 2470-10

Figure B1 (h)

SATURATION LIQUID SPECIFIC HEAT
FOR HELIUM

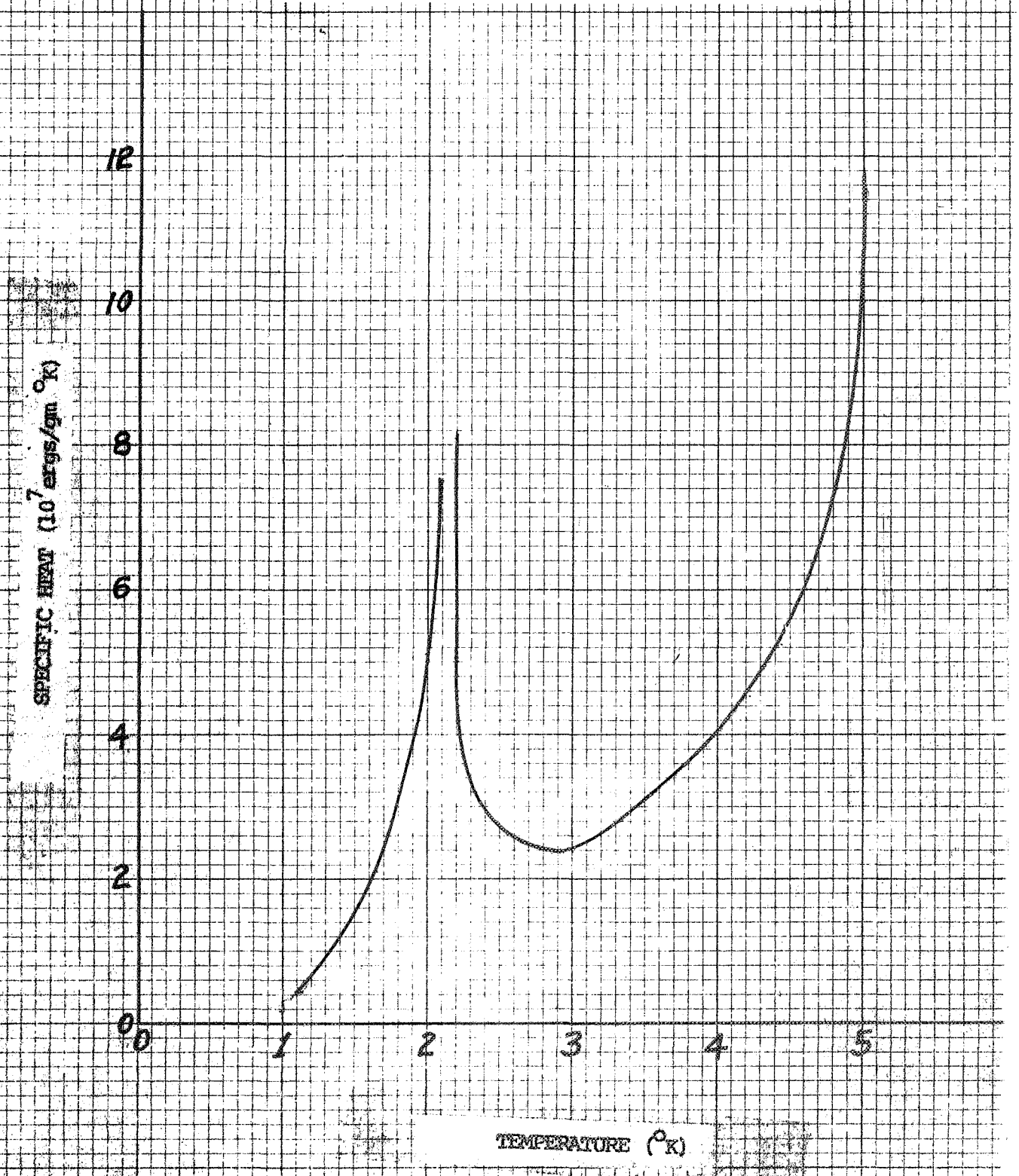

Cross Section
10 Squares to the inch
VERNON R 2470-10

Figure B1 (i)

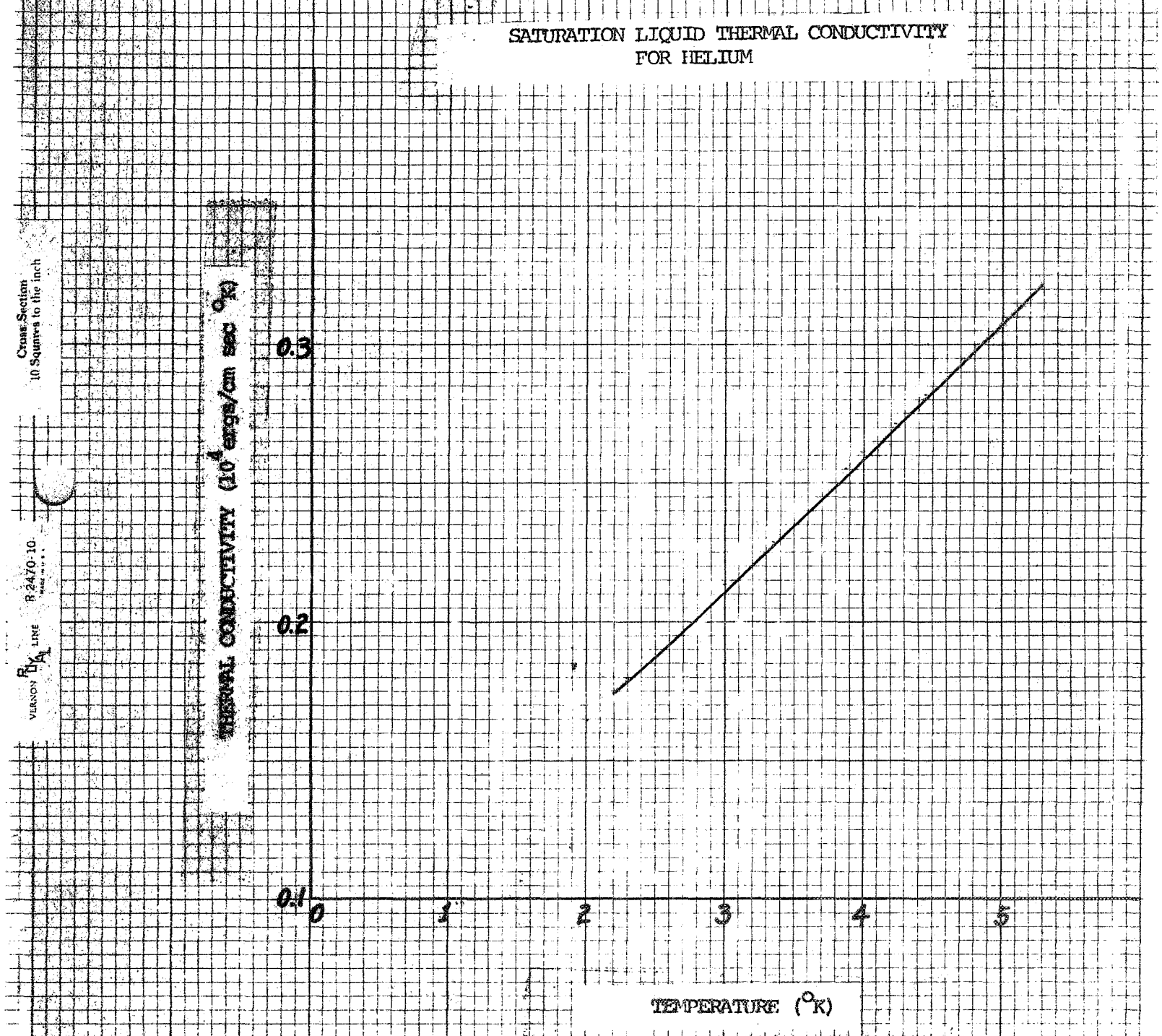
SATURATION LIQUID THERMAL CONDUCTIVITY
FOR HELIUM
THERMAL CONDUCTIVITY (10^4 ergs/cm sec °K)
0.3
0.2
0.1
0
1
2
3
4
5
TEMPERATURE (°K)

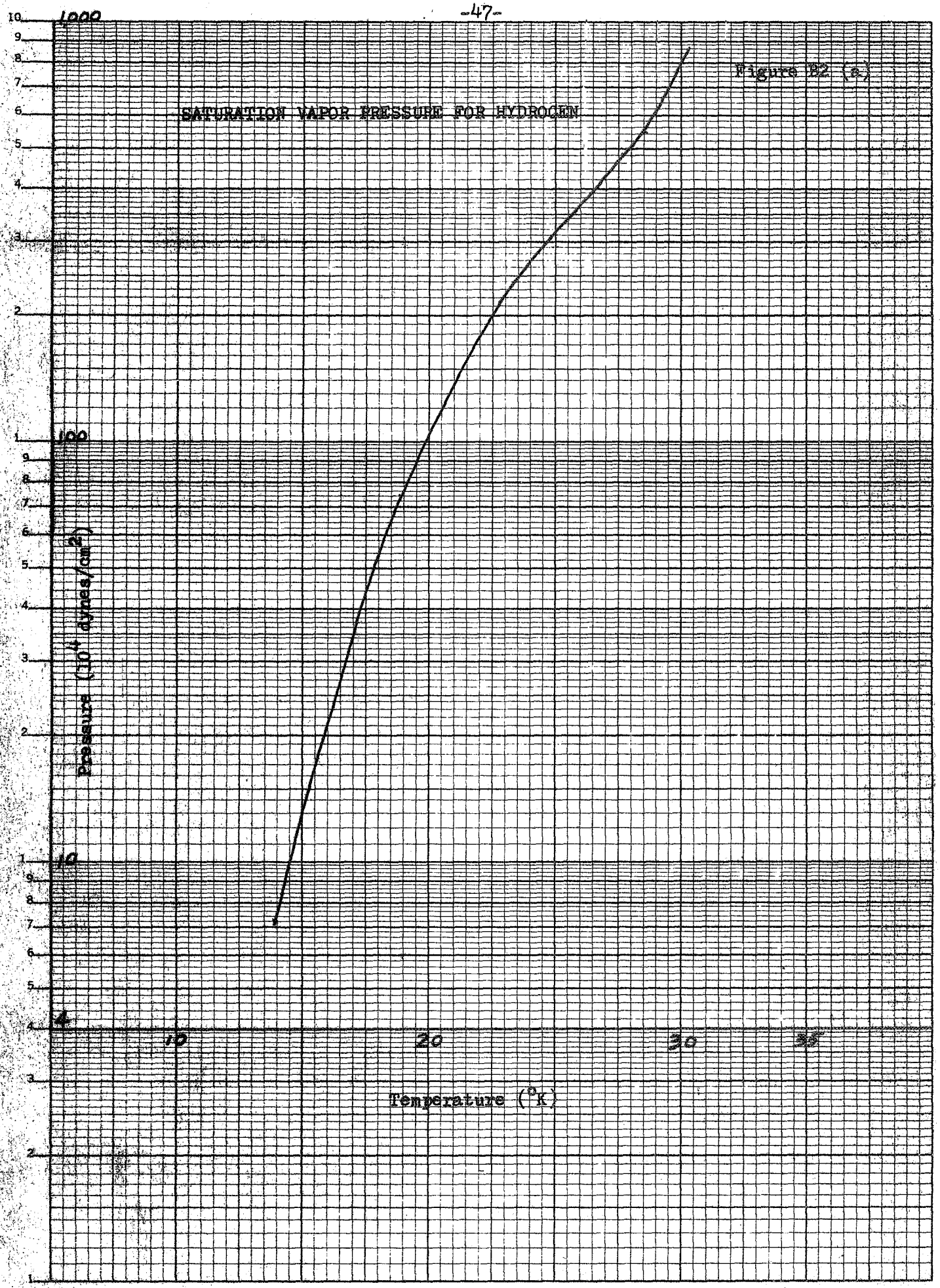
SATURATION VAPOR PRESSURE FOR HYDROGEN
Pressure (10^4 dynes/cm^2)
1000
100
10
4
10
20
30
35
Temperature (°K)

Figure B2 (a)

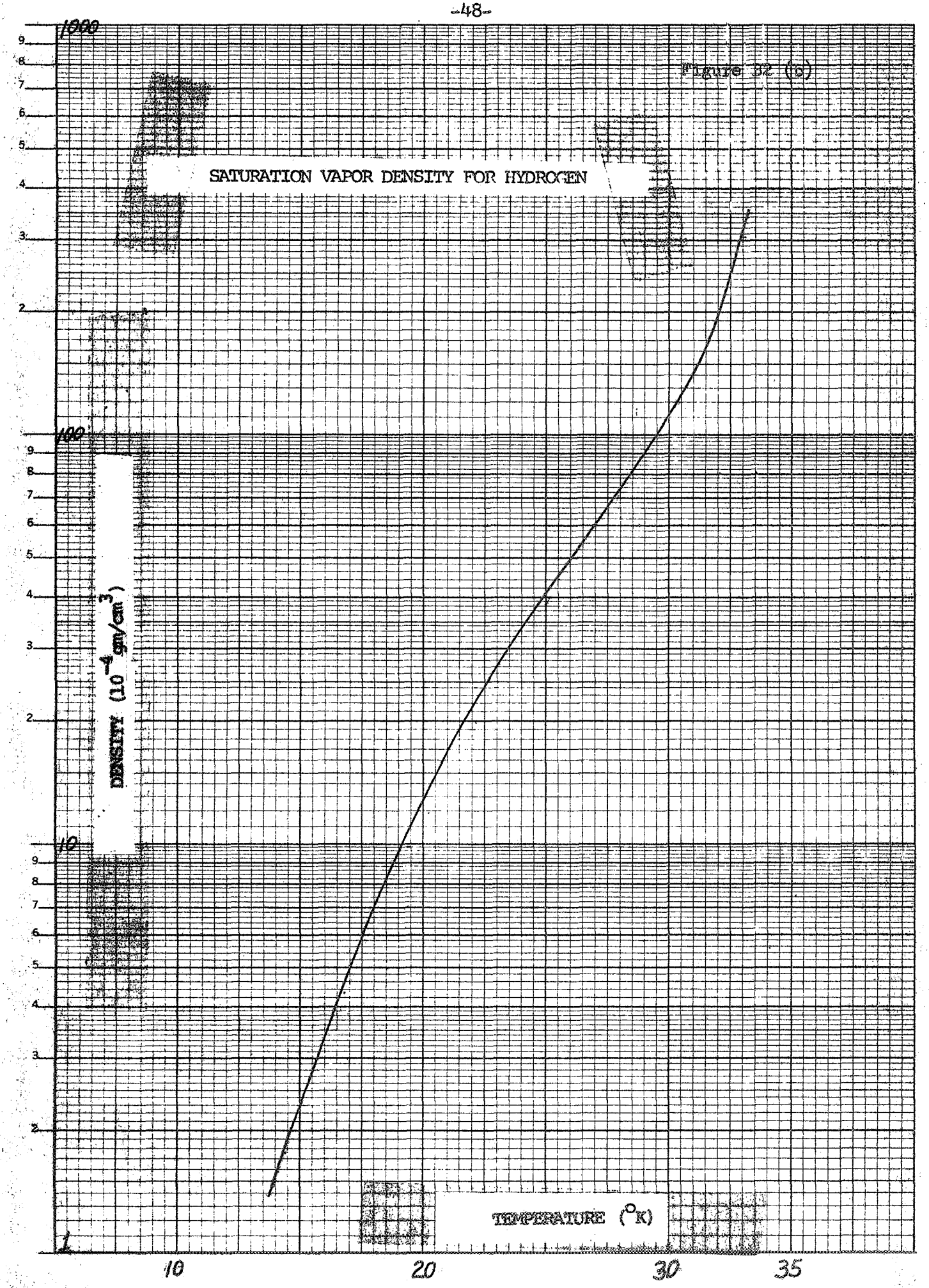

Semi-Logarithmic
3 Cycles x 10 to the inch
VERNON R 2470 SL 3

Figure B2 (c)

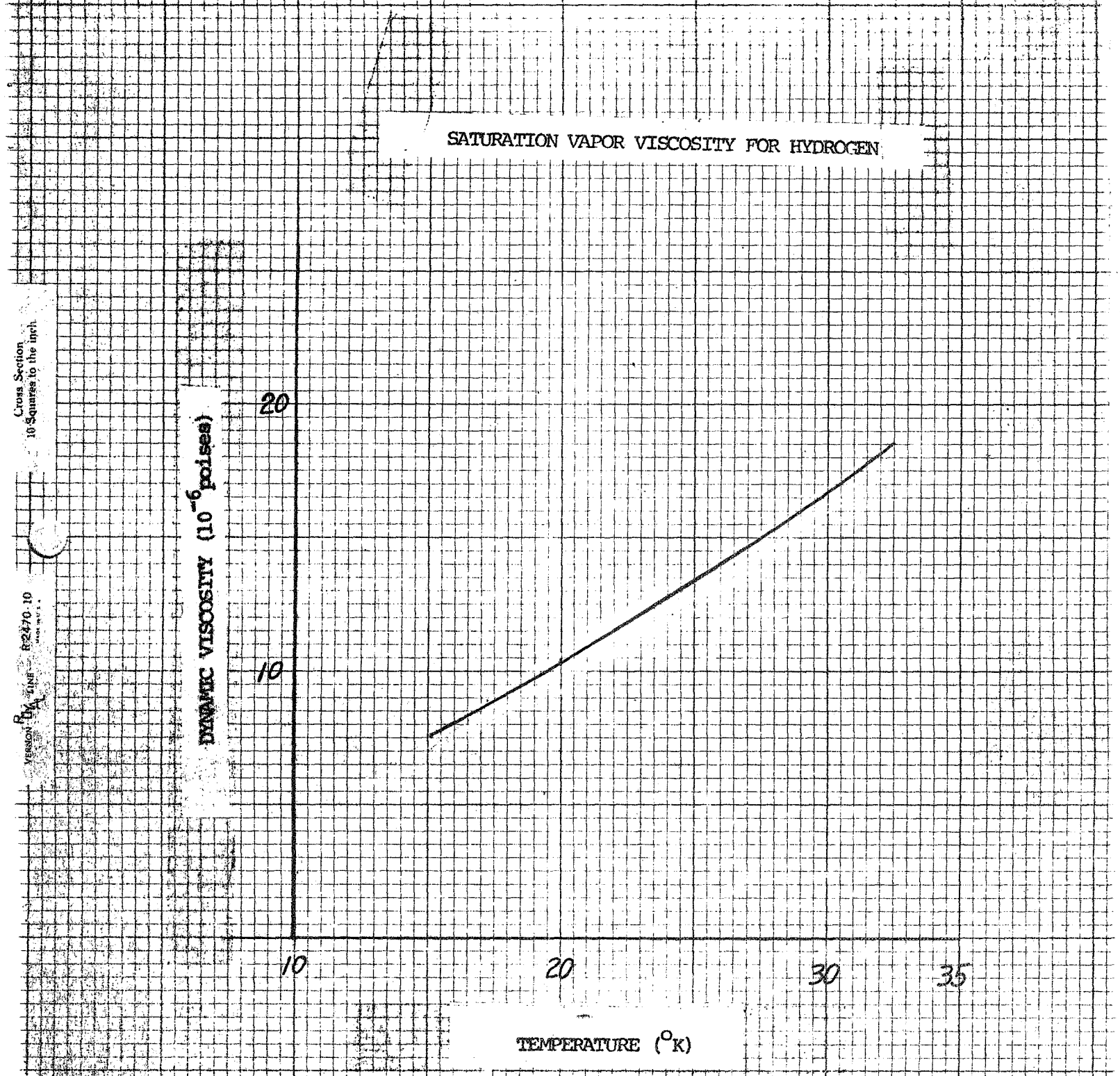
SATURATION VAPOR VISCOSITY FOR HYDROGEN
DYNAMIC VISCOSITY (10^{-6} poises)
20
10
10
20
30
35
TEMPERATURE (^{o}K)

Figure B2 (d)

HEAT OF VAPORISATION FOR HYDROGEN

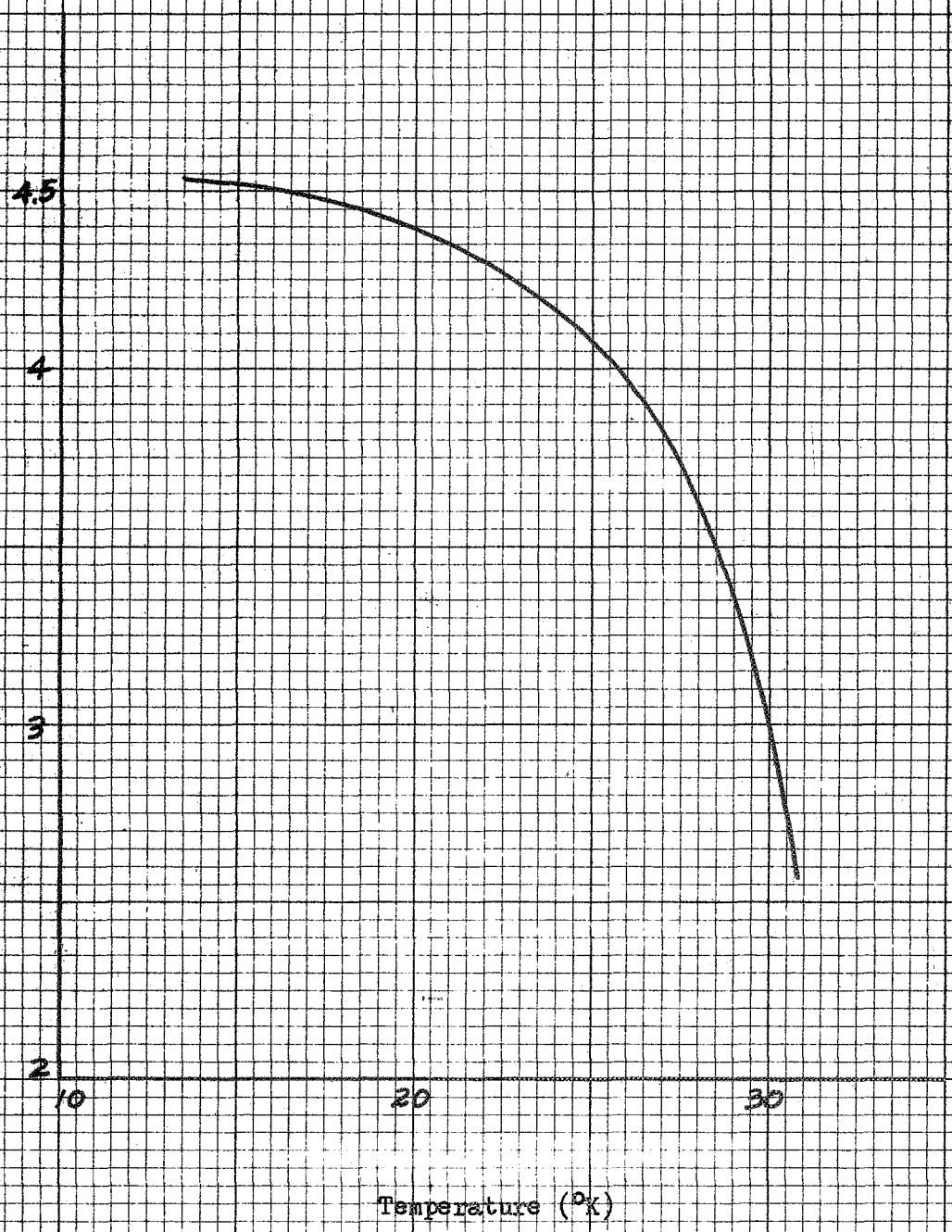

Figure 32 (a)

SATURATION LIQUID SURFACE TENSION
FOR HYDROGEN

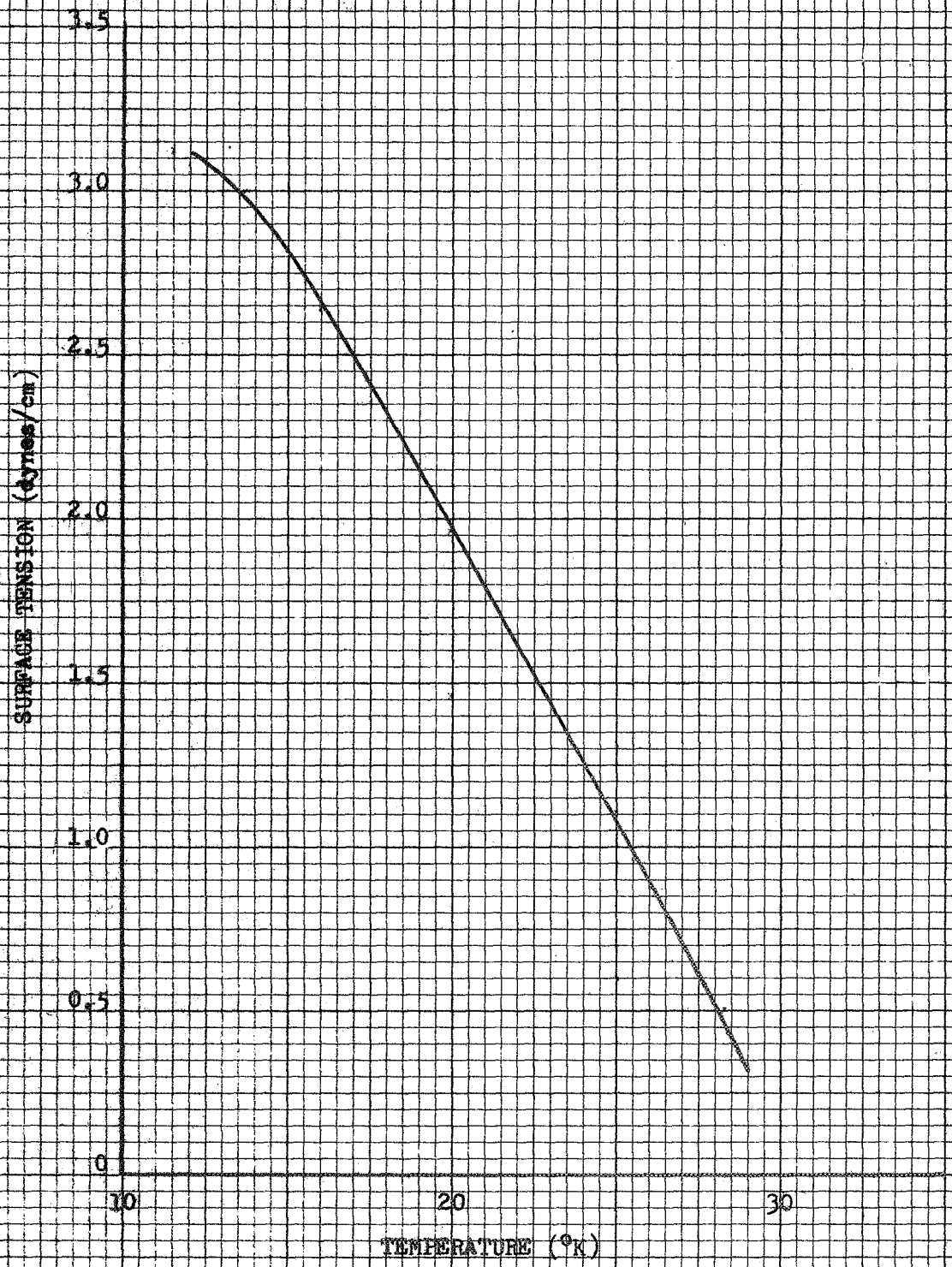

EUGENE DIETZGEN CO.
MADE IN U. S. A.
NO. 340-10 DIETZGEN GRAPH PAPER
10 X 10 PER INCH

Figure 32 (b)

Figure B2 (f)

SATURATION LIQUID DENSITY FOR HYDROGEN

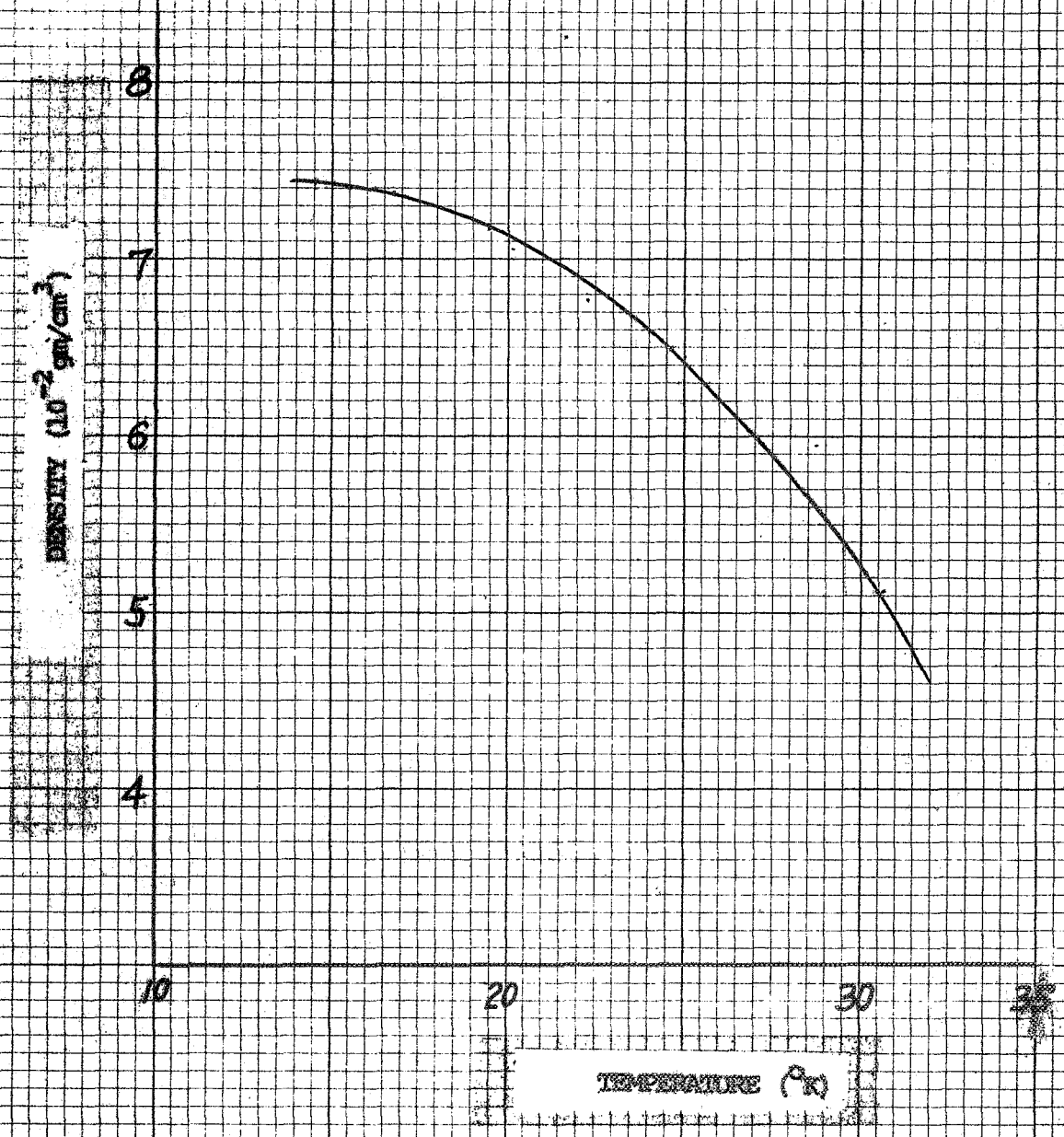

Cross Section
10 Squares to the inch
R 2470-10
VERNON

Figure B2 (g)

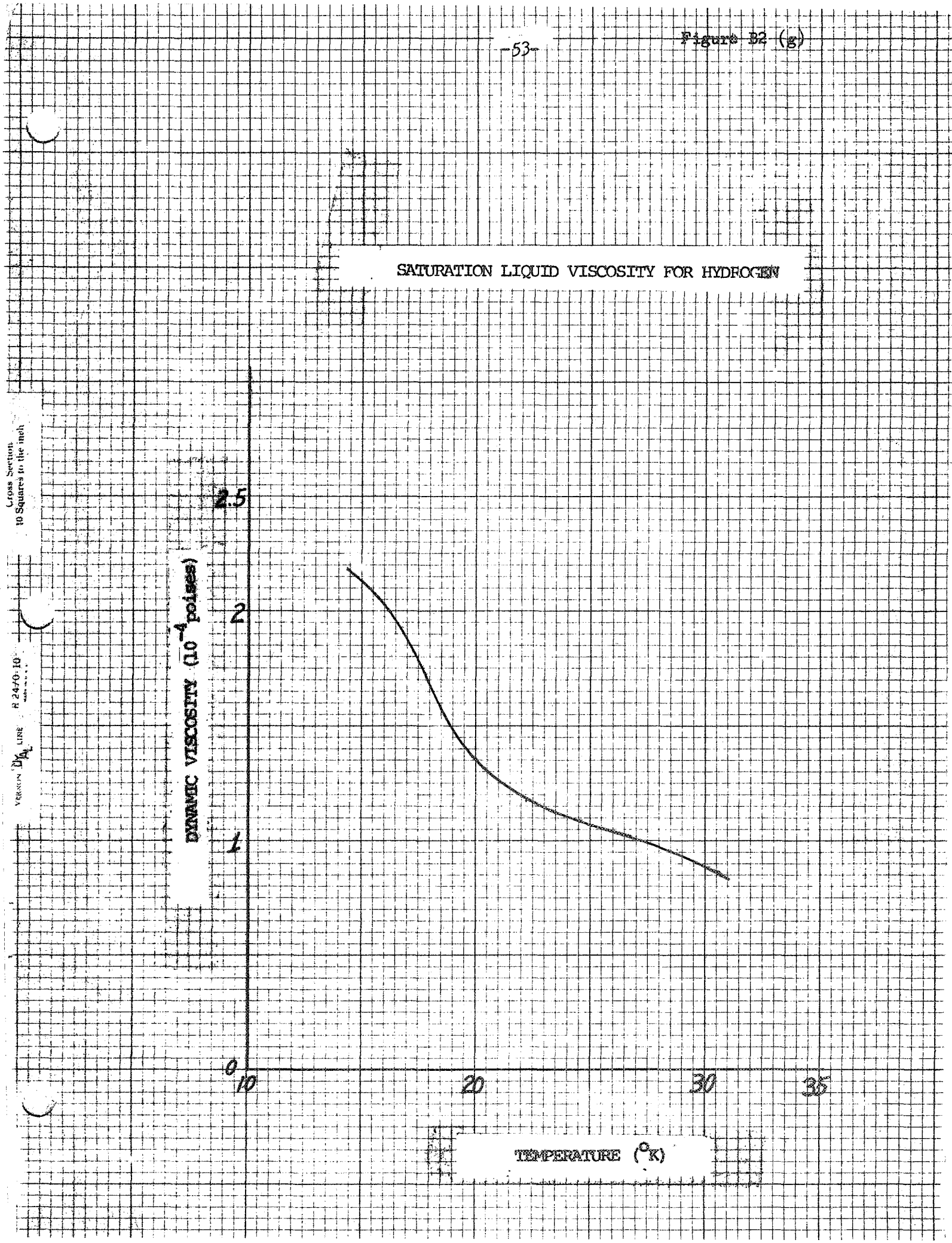
SATURATION LIQUID VISCOSITY FOR HYDROGEN
DYNAMIC VISCOSITY (10^{-4} poises)
2.5
2
1
0
10
20
30
35
TEMPERATURE (°K)

Figure B2 (h)

SATURATION LIQUID SPECIFIC HEAT
FOR HYDROGEN

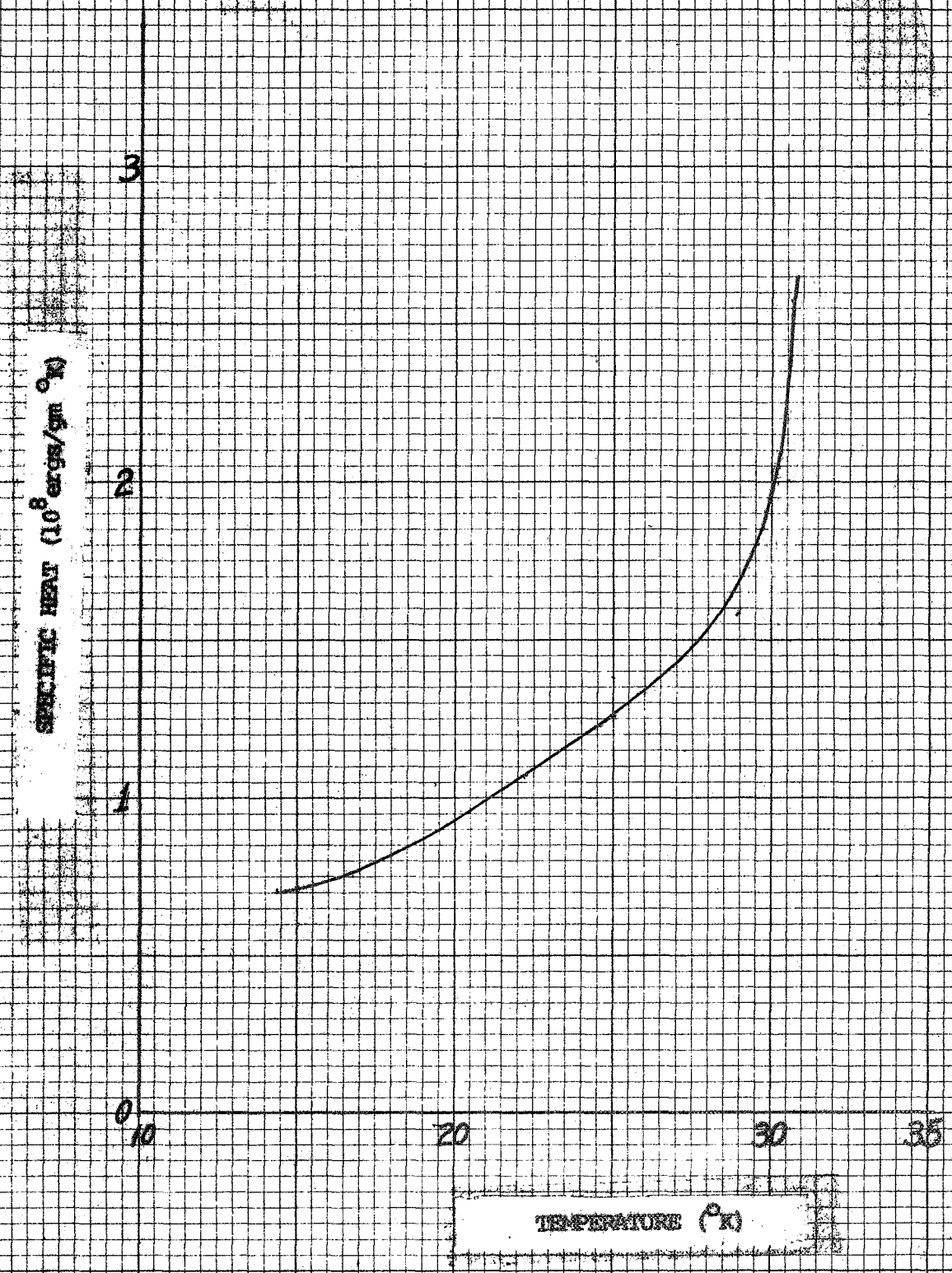

Cross Section
10 Squares to the inch
VERNON LINE R 2470-10

Figure B2 (i)

SATURATION LIQUID THERMAL CONDUCTIVITY
FOR HYDROGEN

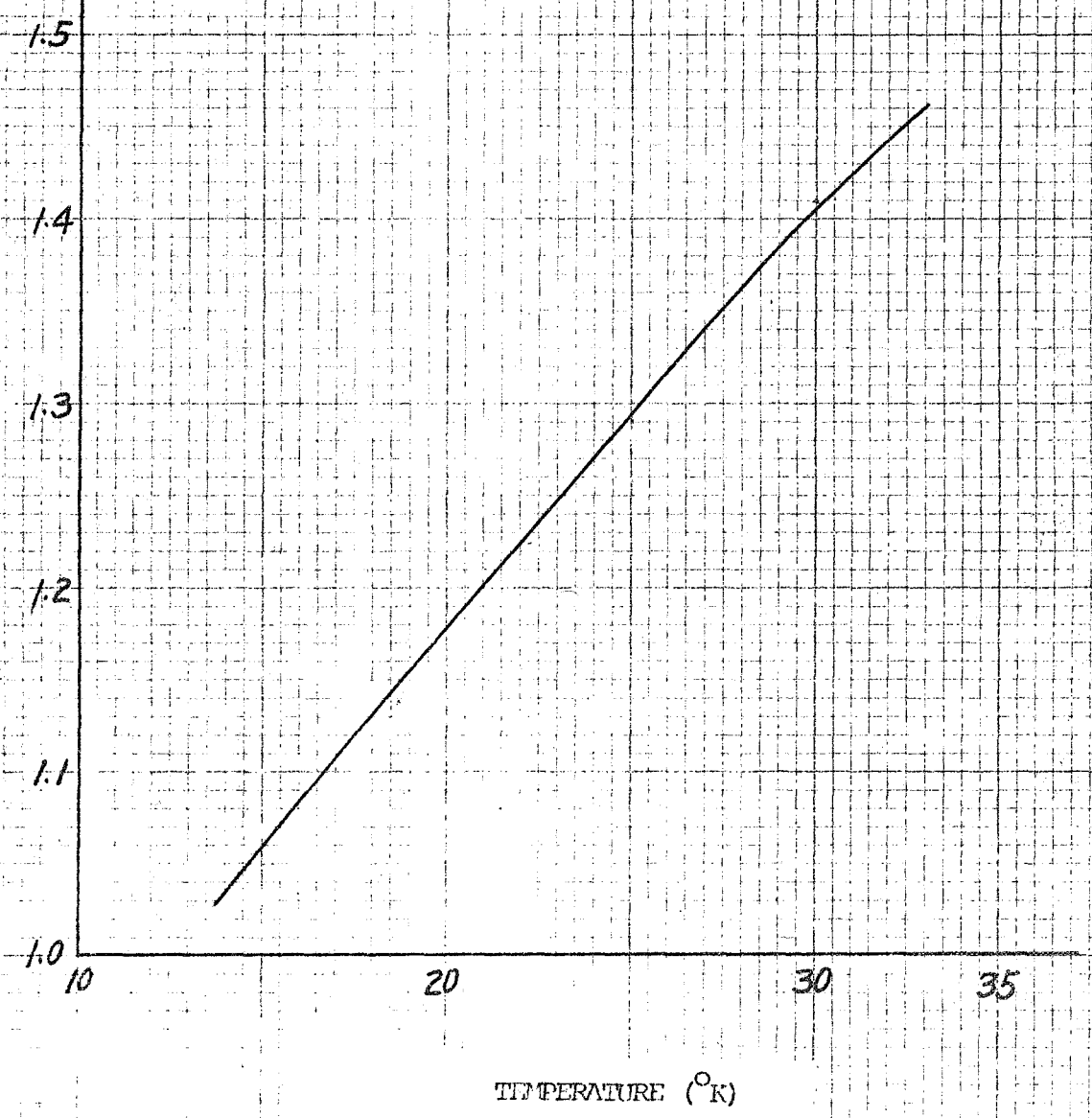

Figure B3 (a)

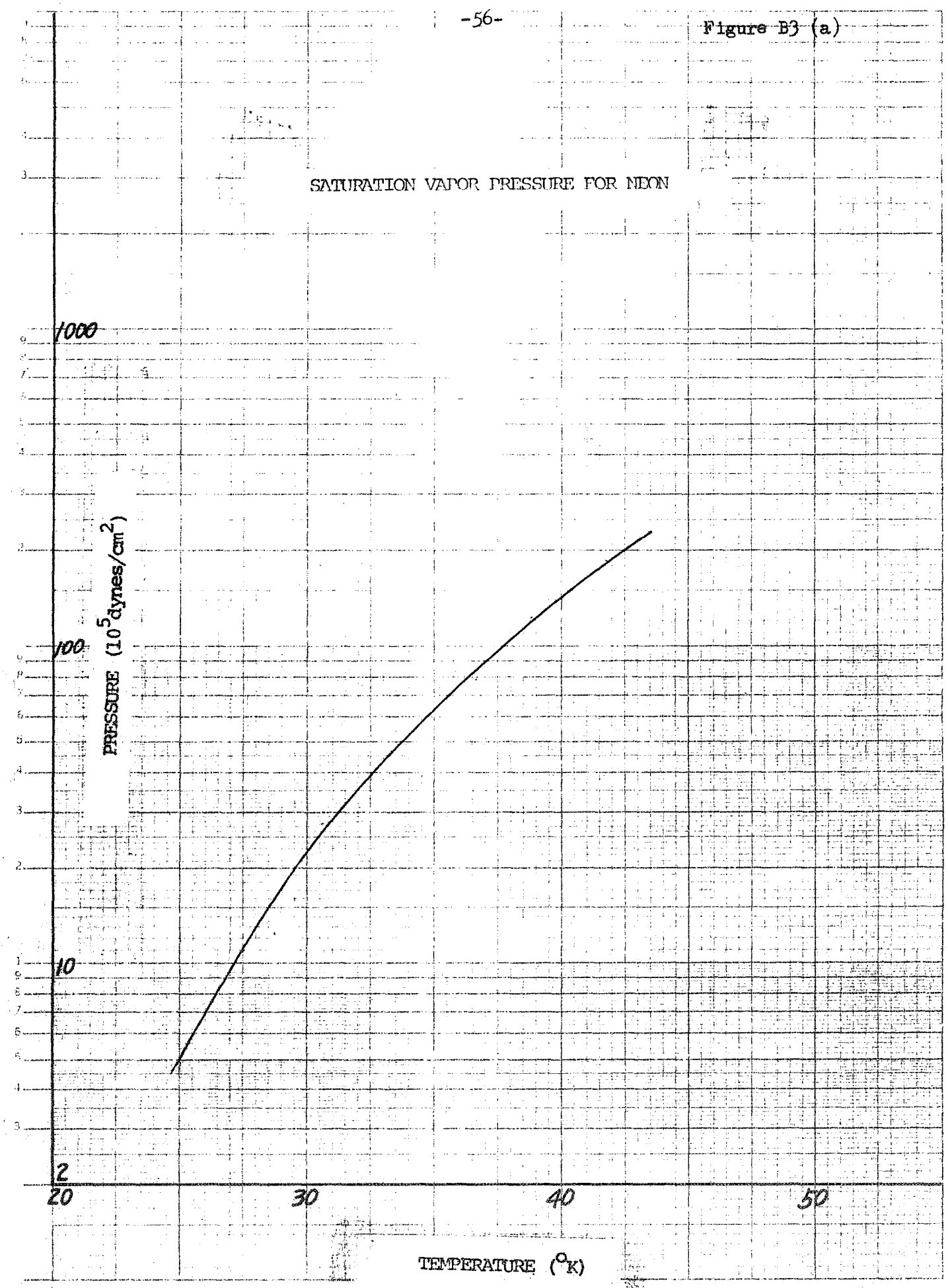
SATURATION VAPOR PRESSURE FOR NEON
1000
100
10
2
PRESSURE (10^5 dynes/cm^2)
20
30
40
50
TEMPERATURE (^oK)

Figure B3 (b)

Saturation vapor density for neon

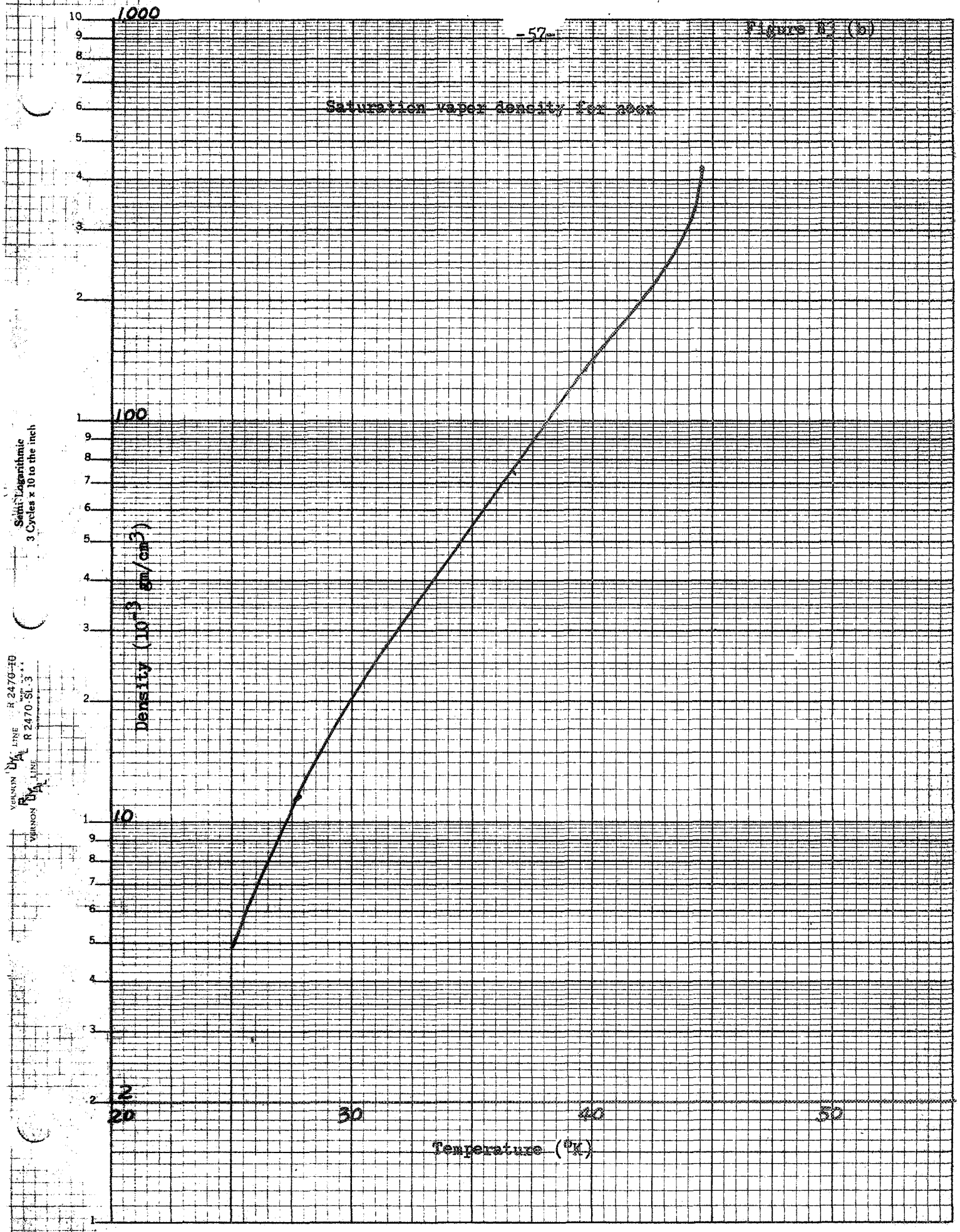

Figure B3(a)

SATURATION VAPOR VISCOSITY FOR NEON

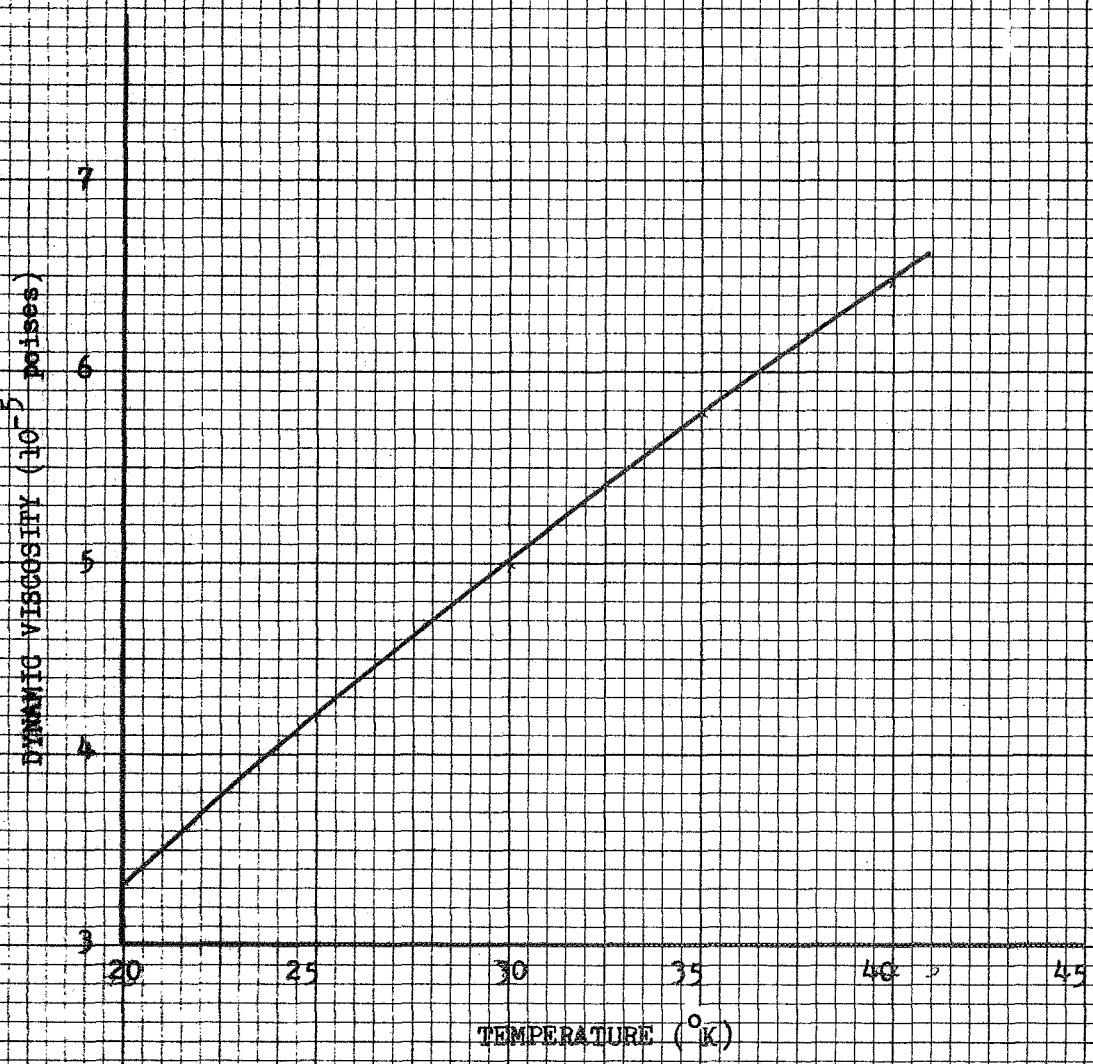

EUGENE DIETZGEN CO.
MADE IN U. S. A.
NO. 340-10 DIETZGEN GRAPH PAPER
10 X 10 PER INCH

Figure B3 (d)

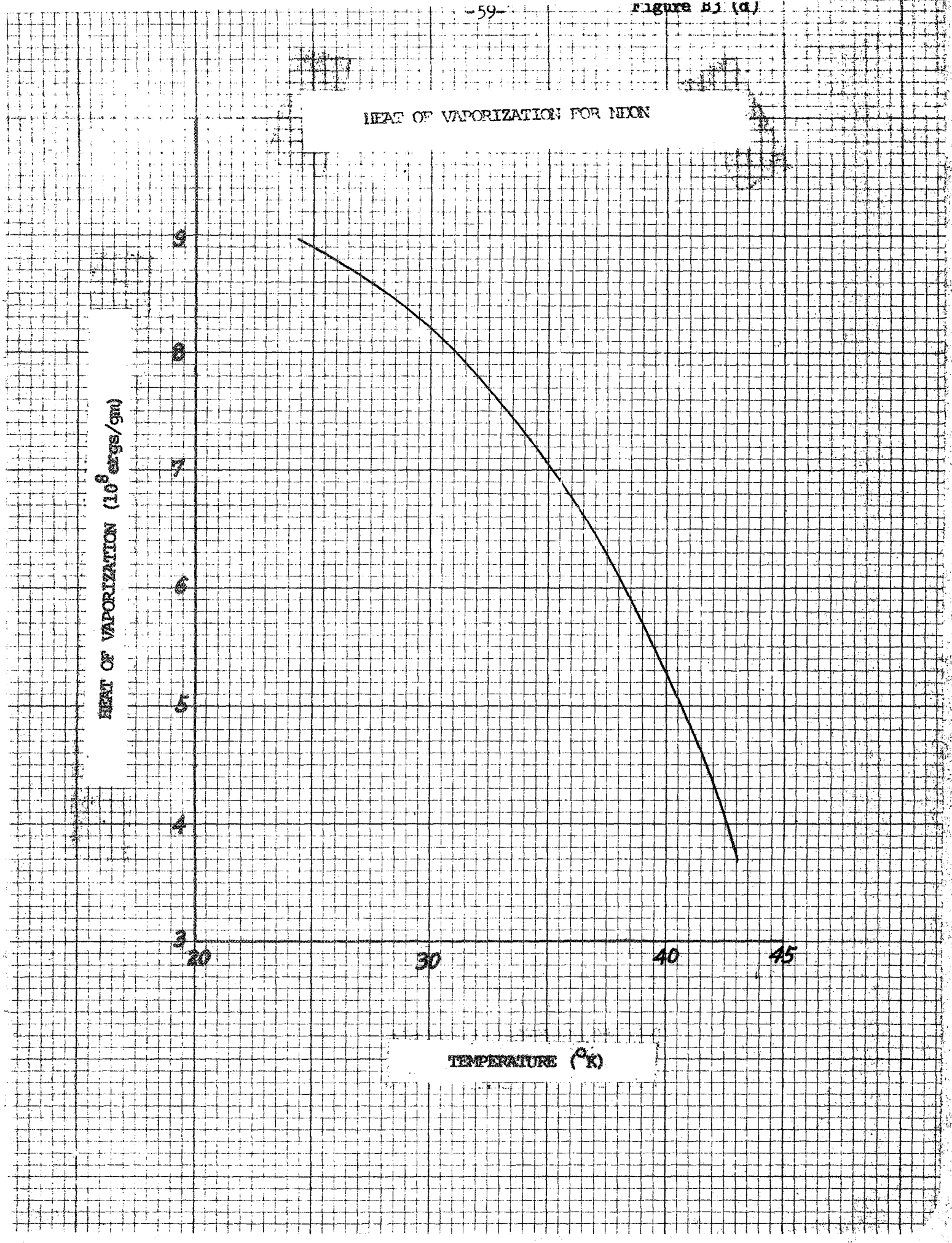
HEAT OF VAPORIZATION FOR NEON
HEAT OF VAPORIZATION (10^8 ergs/gm)
9
8
7
6
5
4
3
20
30
40
45
TEMPERATURE (^oK)

Figure B3 (e)

SATURATION LIQUID SURFACE TENSION
FOR NEON

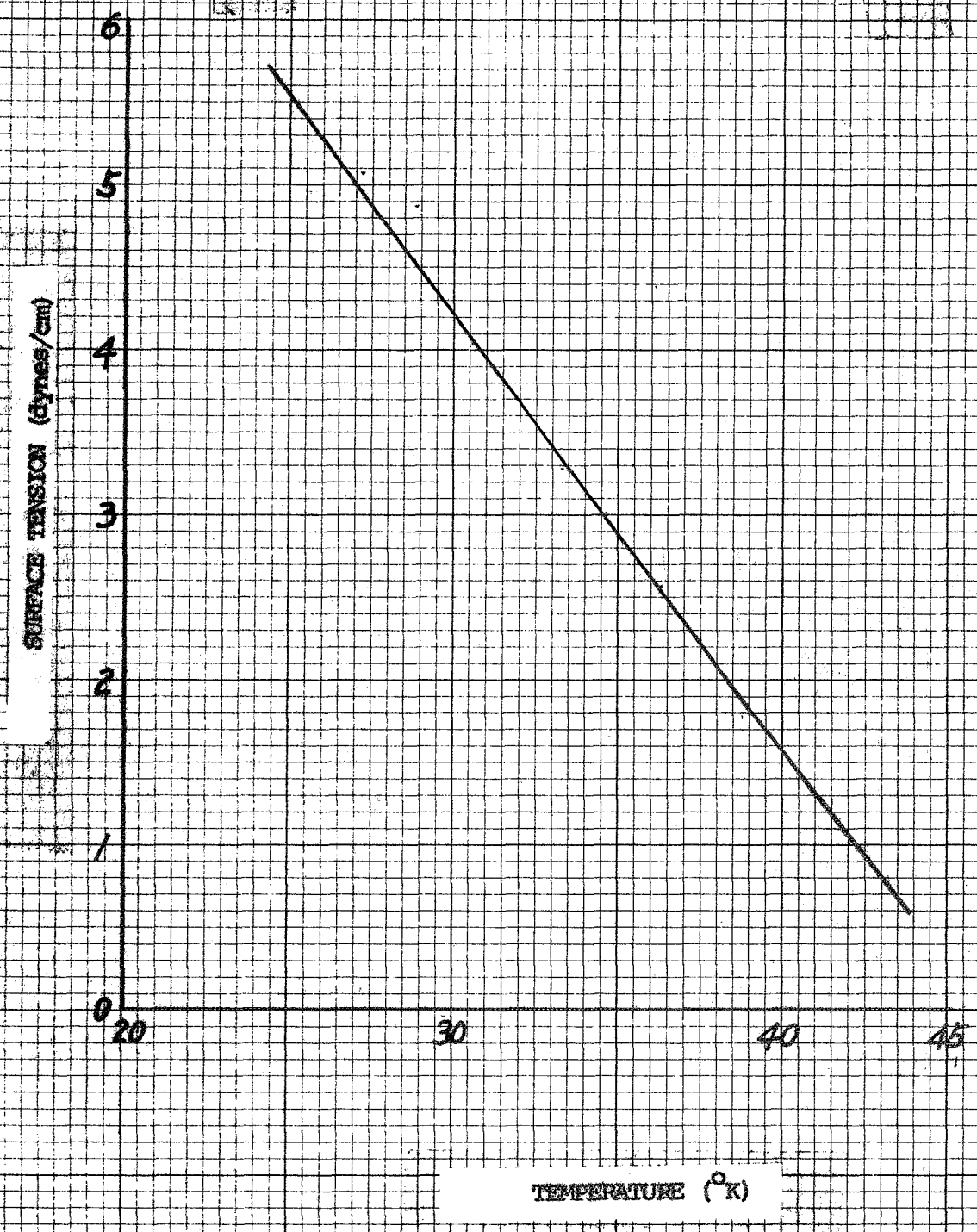

Cross Section
10 Squares to the inch
VERNON LINE

Figure B3 (f)

SATURATION LIQUID DENSITY FOR NEON

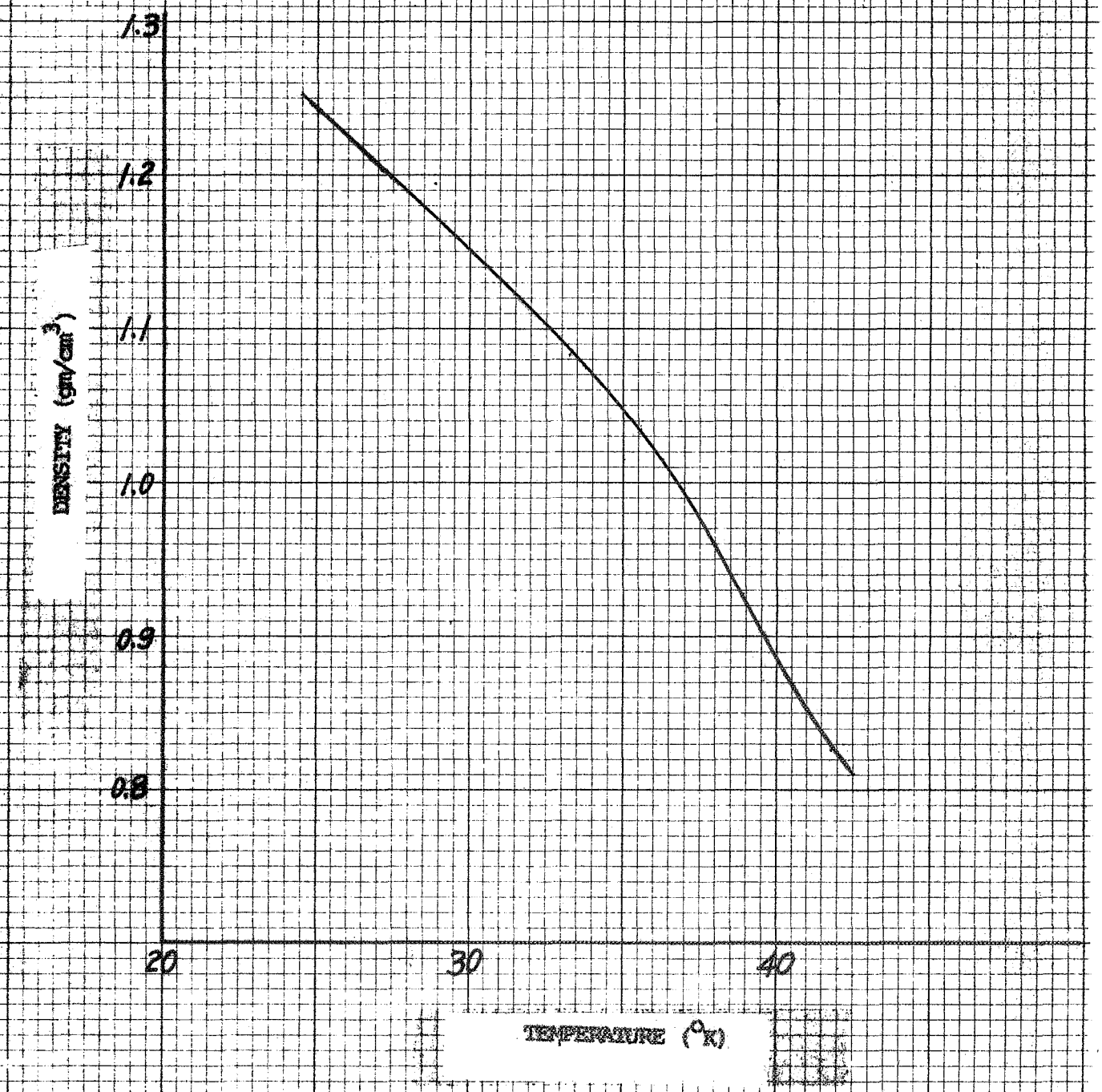

Cross Section
10 Squares to the inch
VERNON R 2470-10

Figure B3 (g)

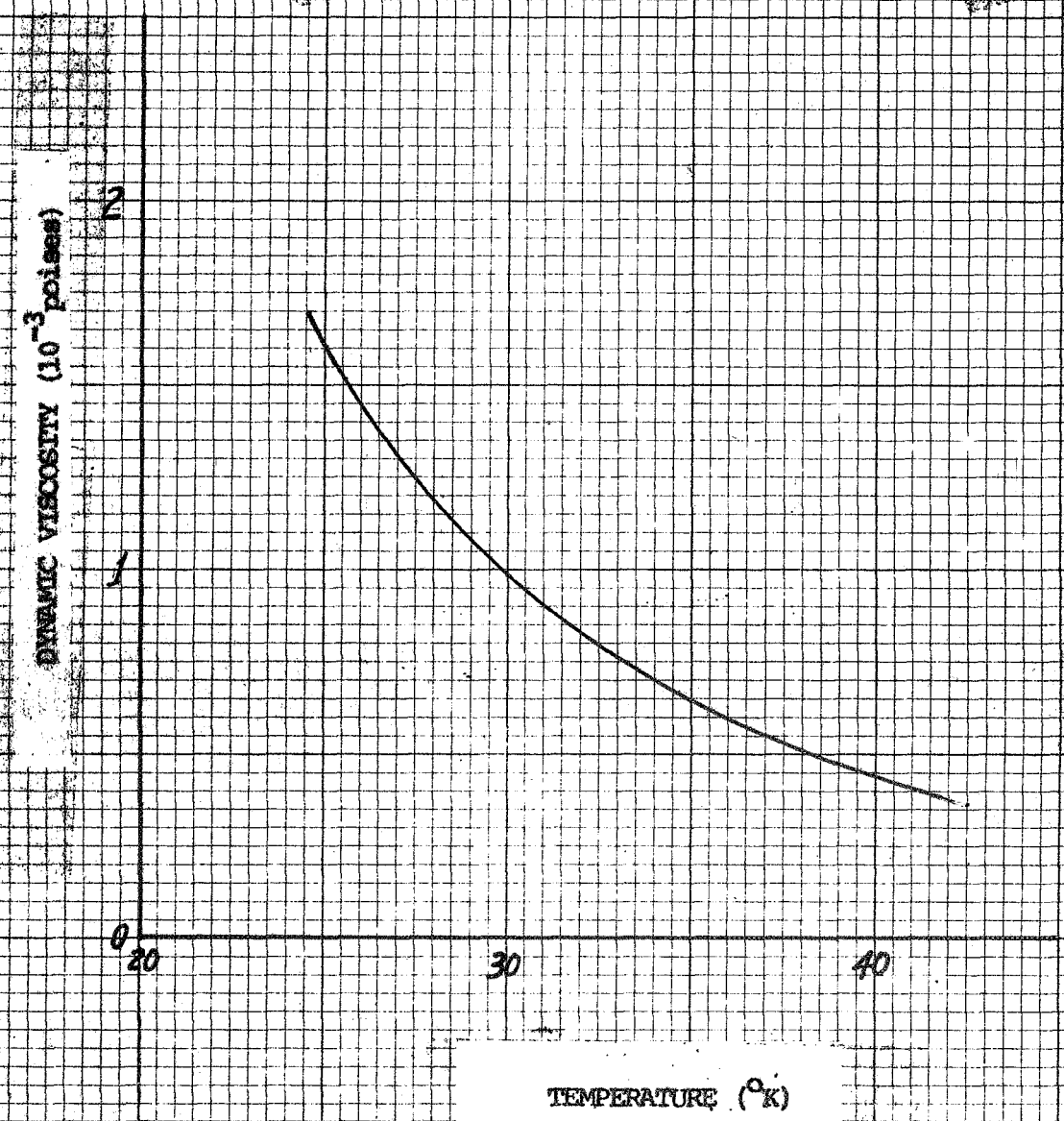

Cross Section
10 Squares to the inch
R 2470-10

Figure B3 (h)

SATURATION LIEQUID SPECIFIC HEAT
FOR NEON

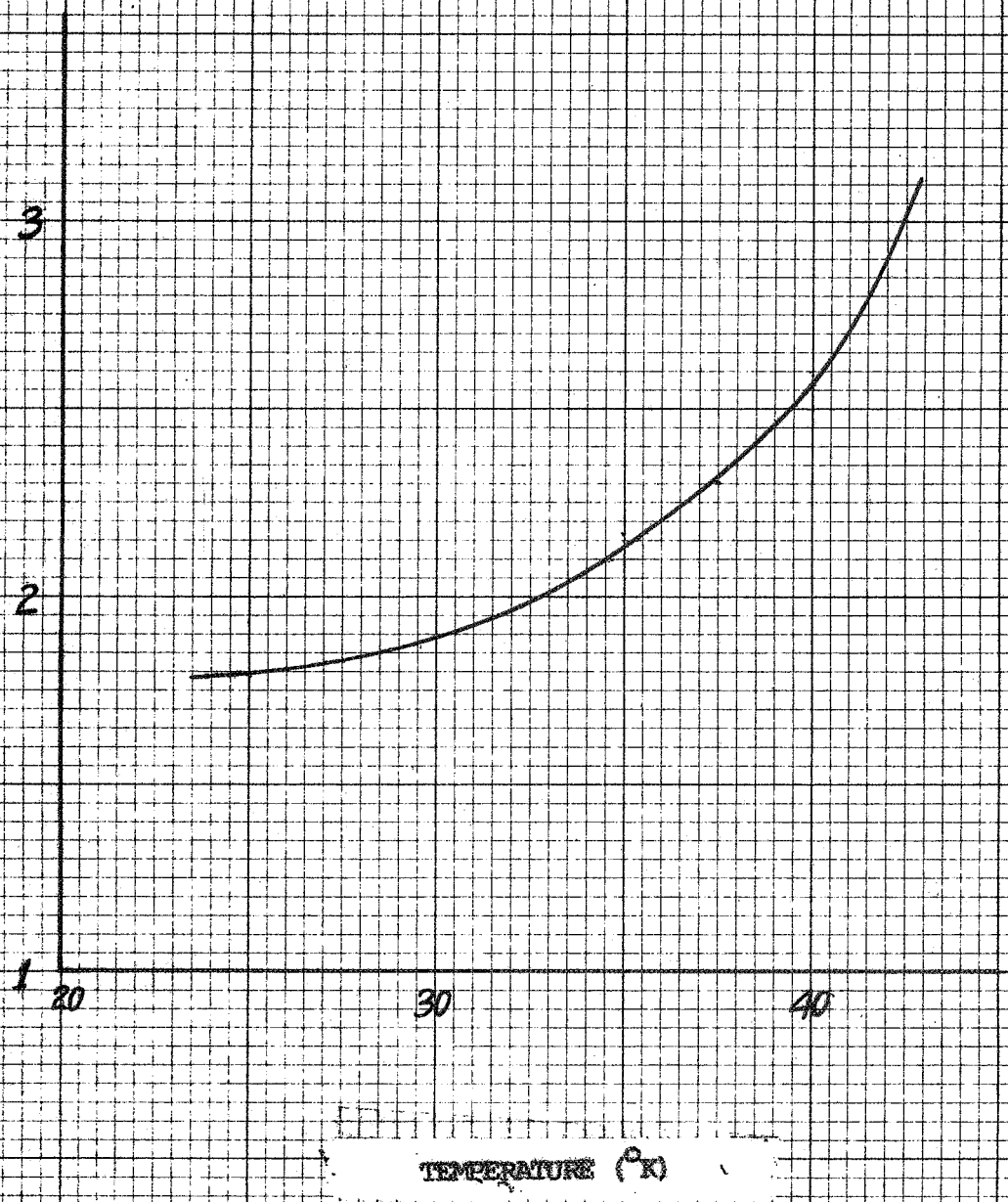

Cross Section
10 Squares to the inch
R 2470-10
VERNON ROYAL LINE

Figure B3 (1)

SATURATION LIQUID THERMAL CONDUCTIVITY
FOR NEON

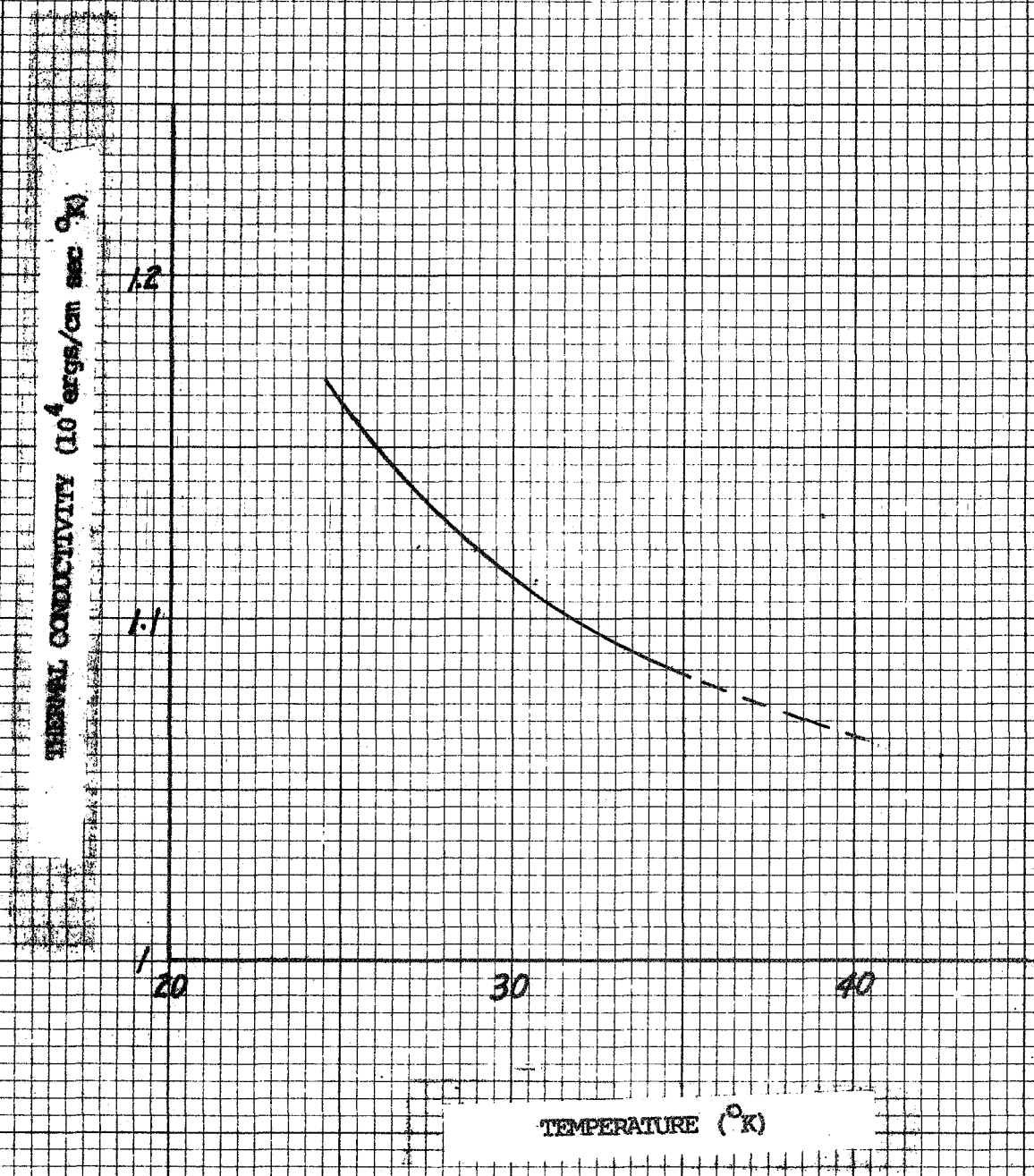

Figure B4 (a)

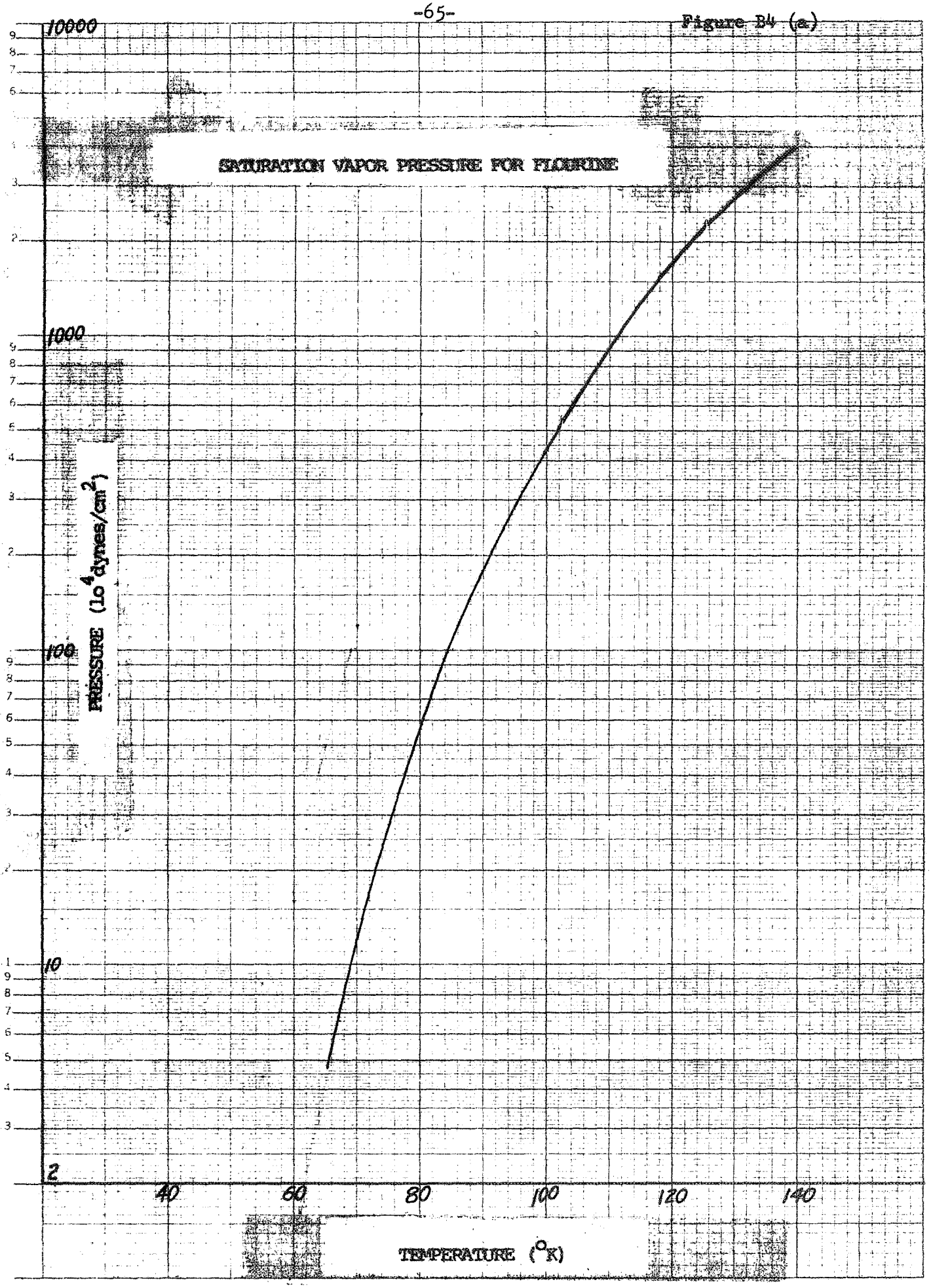
SATURATION VAPOR PRESSURE FOR FLUORINE
PRESSURE (10^4 dynes/cm^2)
10000
1000
100
10
2
40
60
80
100
120
140
TEMPERATURE ($^{\circ}$K)

Figure B4 (b)

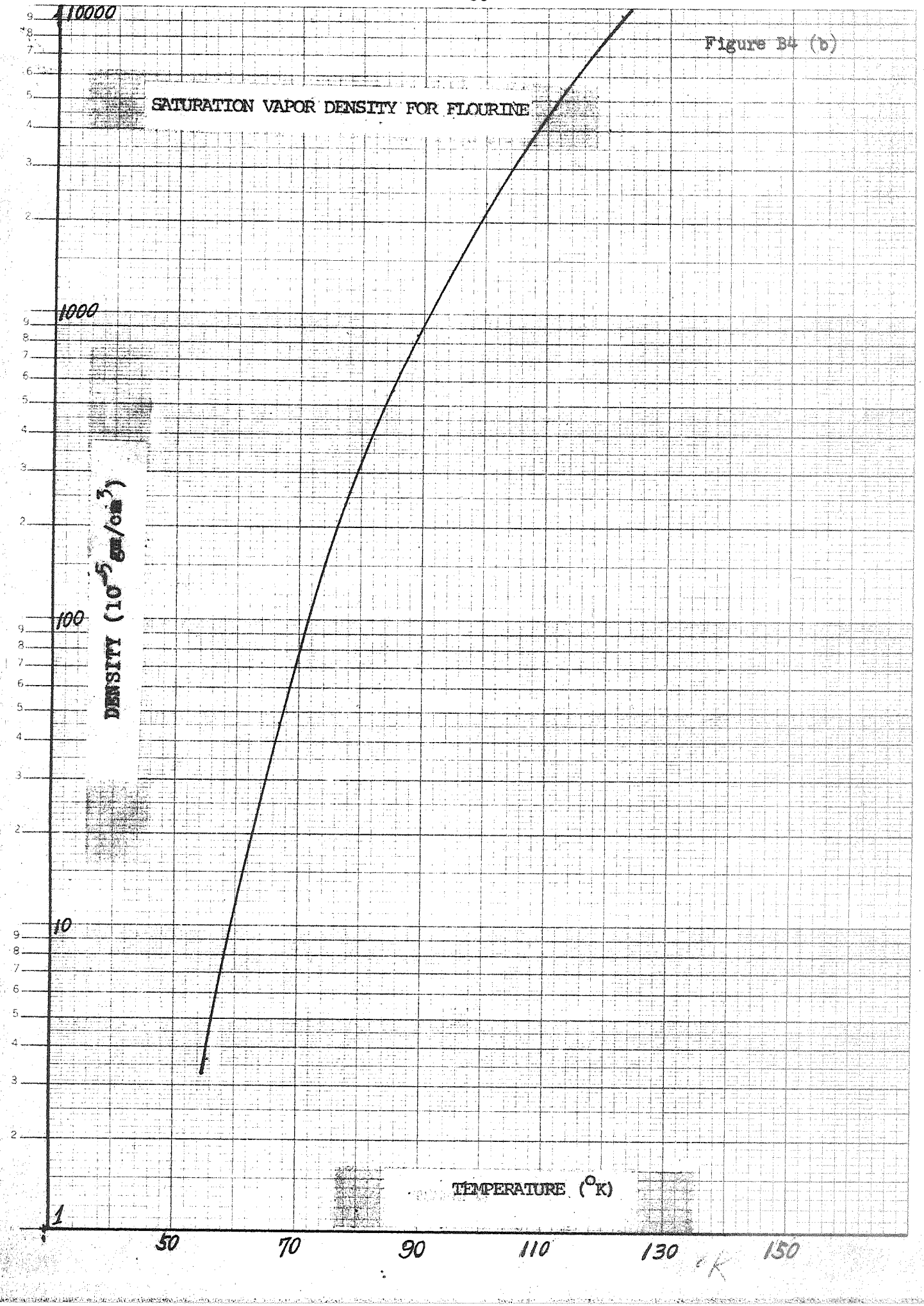
SATURATION VAPOR DENSITY FOR FLOURINE
DENSITY (10^{-5} gm/cm^3)
10000
1000
100
10
1
TEMPERATURE (^{o}K)
50
70
90
110
130
150
°K

Figure E4 (c)

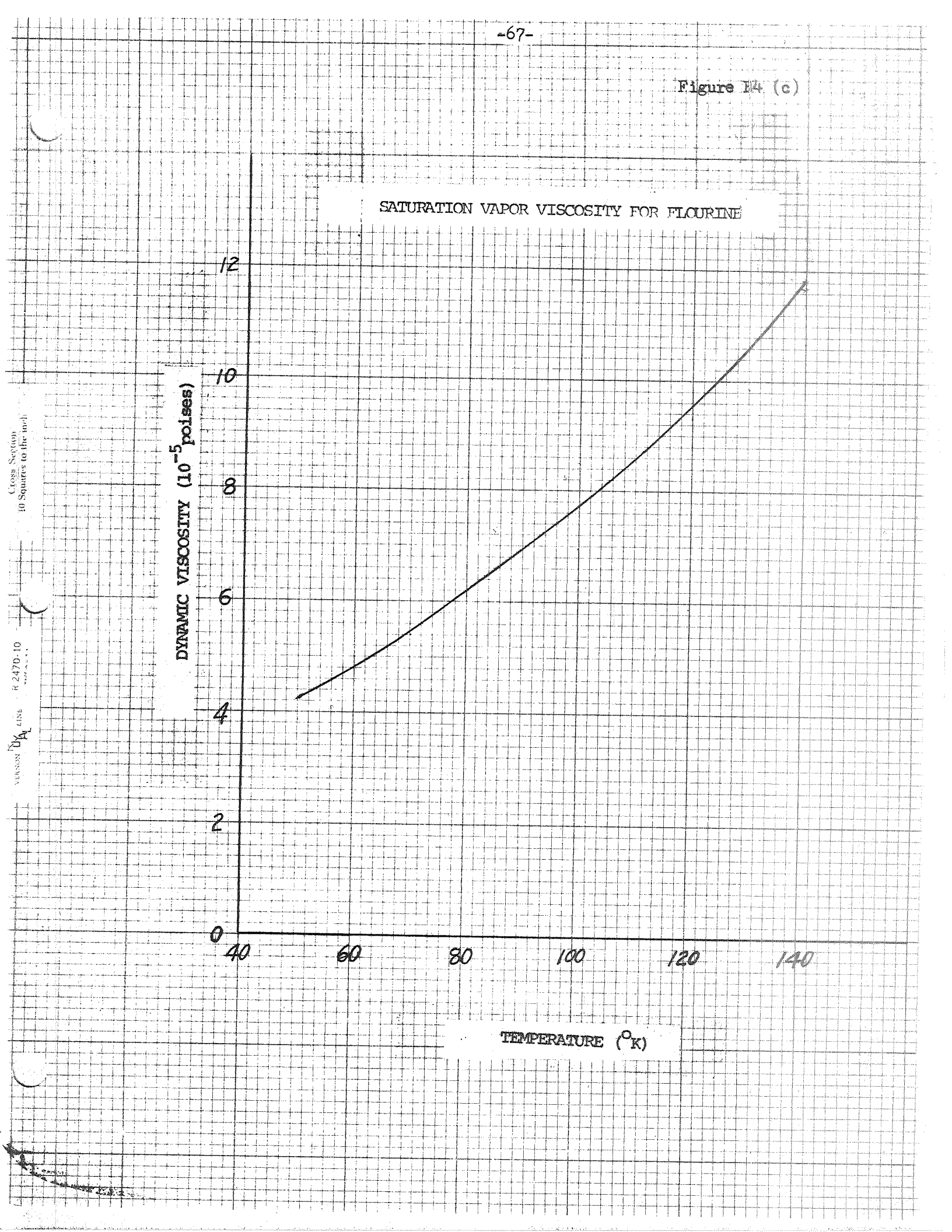
SATURATION VAPOR VISCOSITY FOR FLOURINE
DYNAMIC VISCOSITY (10^{-5} poises)
0
2
4
6
8
10
12
40
60
80
100
120
140
TEMPERATURE (^{o}K)

Figure B4 (d)

HEAT OF VAPORIZATION FOR FLOURINE

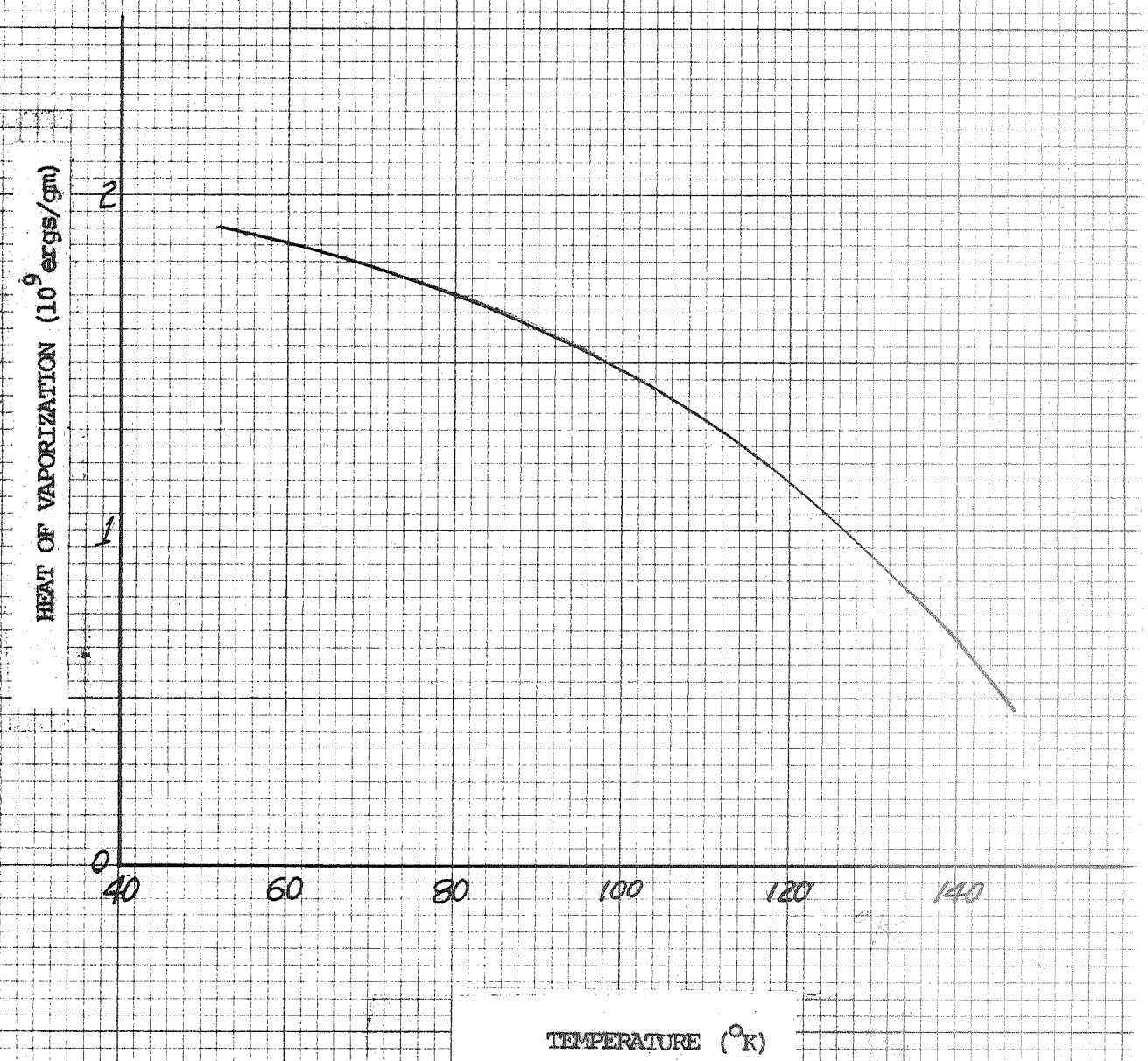

Figure B4(e)

SATURATION LIQUID SURFACE TENSION
FOR FLOURINE

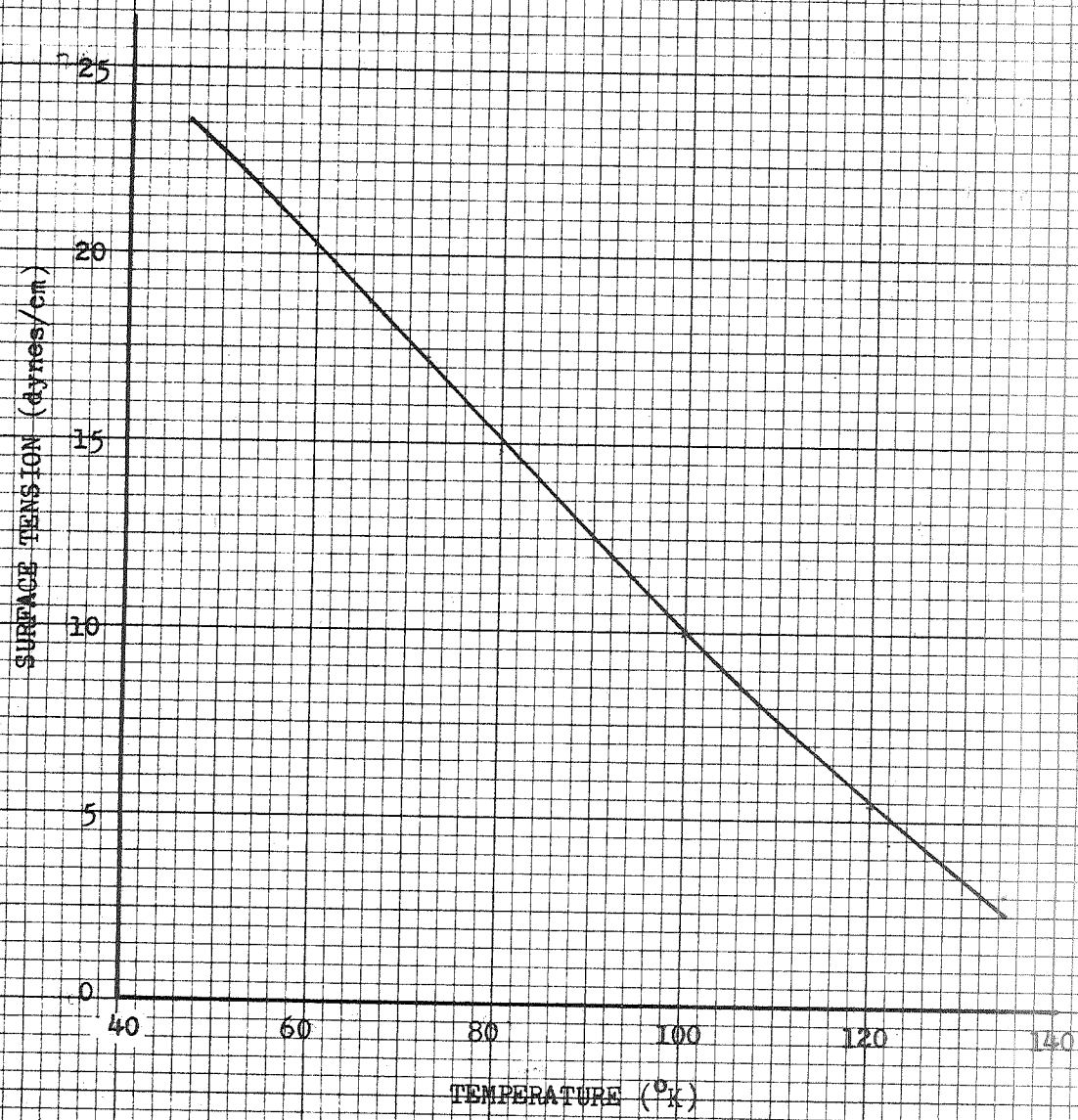

EUGENE DIETZGEN CO.
MADE IN U. S. A.
NO. 340-10 DIETZGEN GRAPH PAPER
10 X 10 PER INCH

Figure B4 (f)

SATURATION LIQUID DENSITY FOR FLOURINE

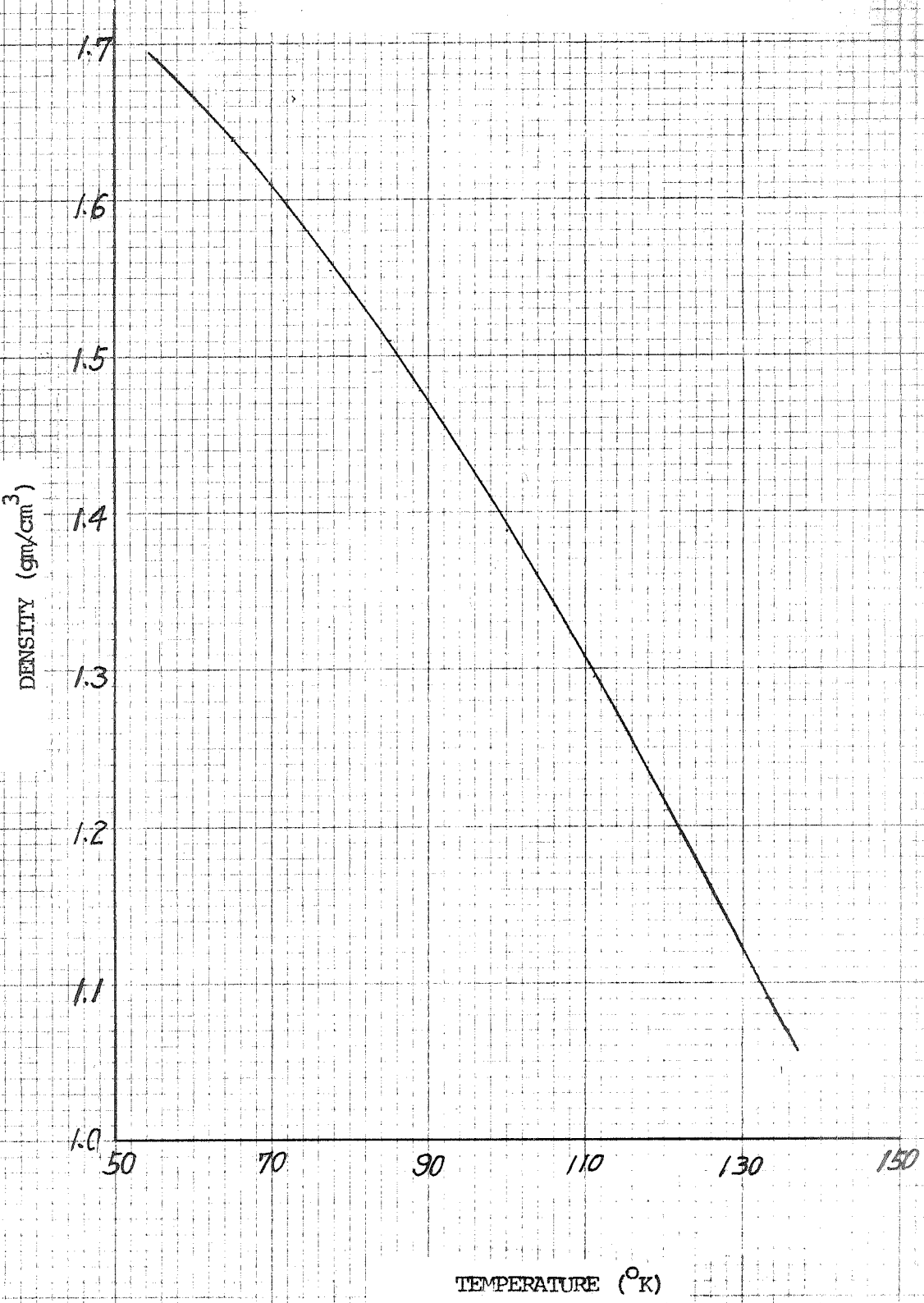

Figure B4 (g)

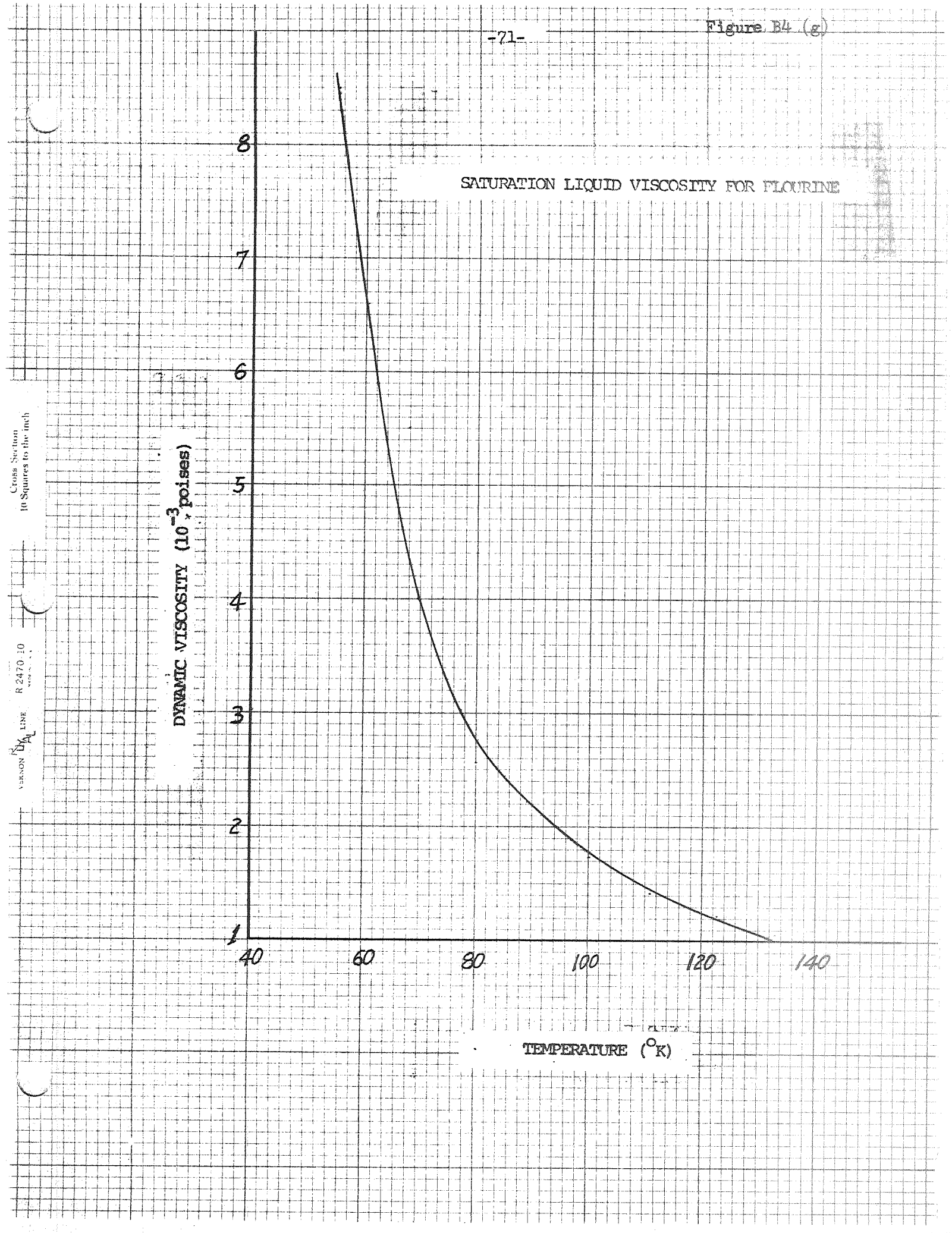
SATURATION LIQUID VISCOSITY FOR FLOURINE
DYNAMIC VISCOSITY (10^{-3} poises)
8
7
6
5
4
3
2
1
40
60
80
100
120
140
TEMPERATURE (^{o}K)

Figure B4 (h)

SATURATION LIQUID SPECIFIC HEAT
FOR FLOURINE

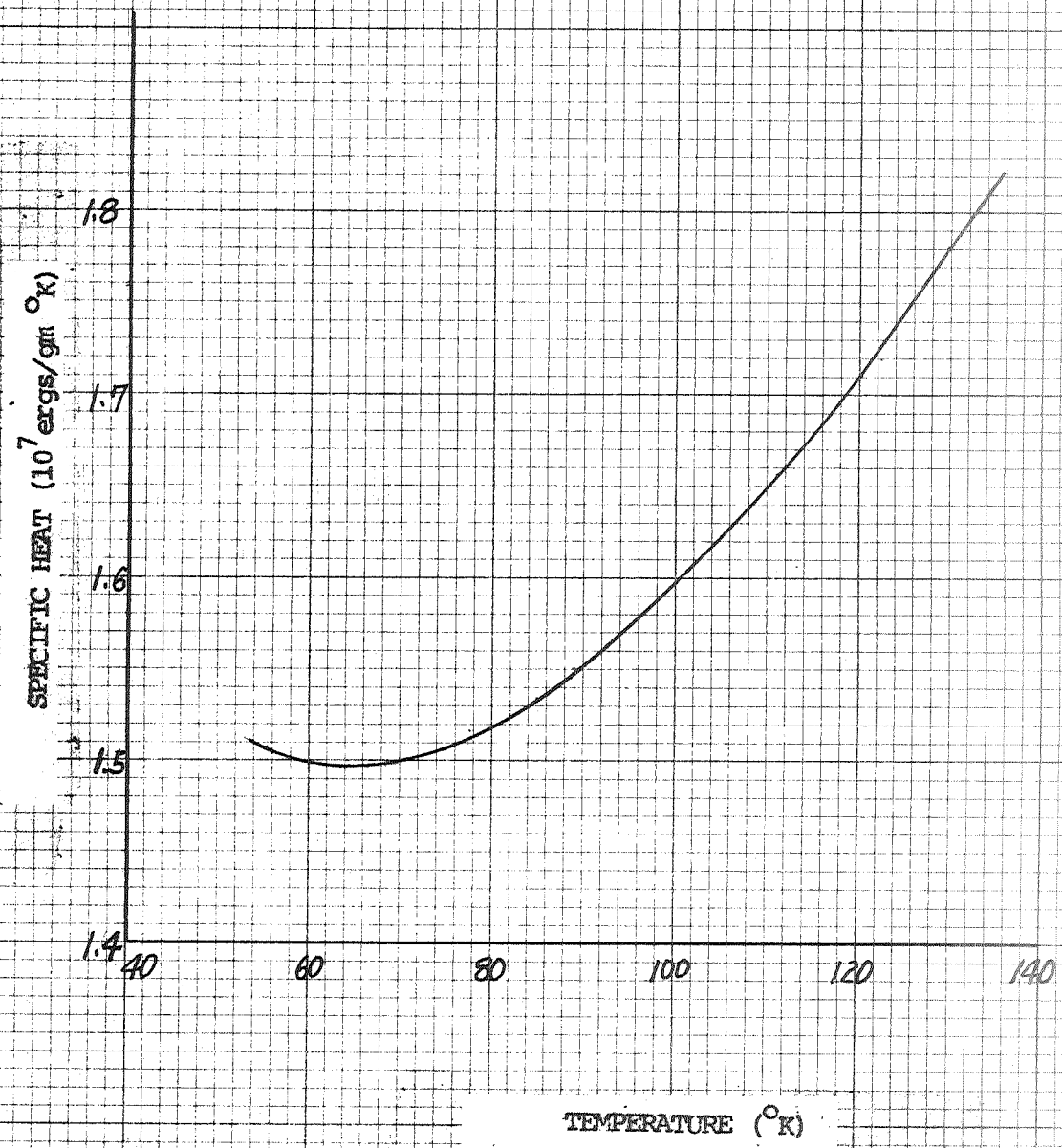

Cross Section
10 Squares to the inch
VERNON R 2470-10

Figure B4 (i)

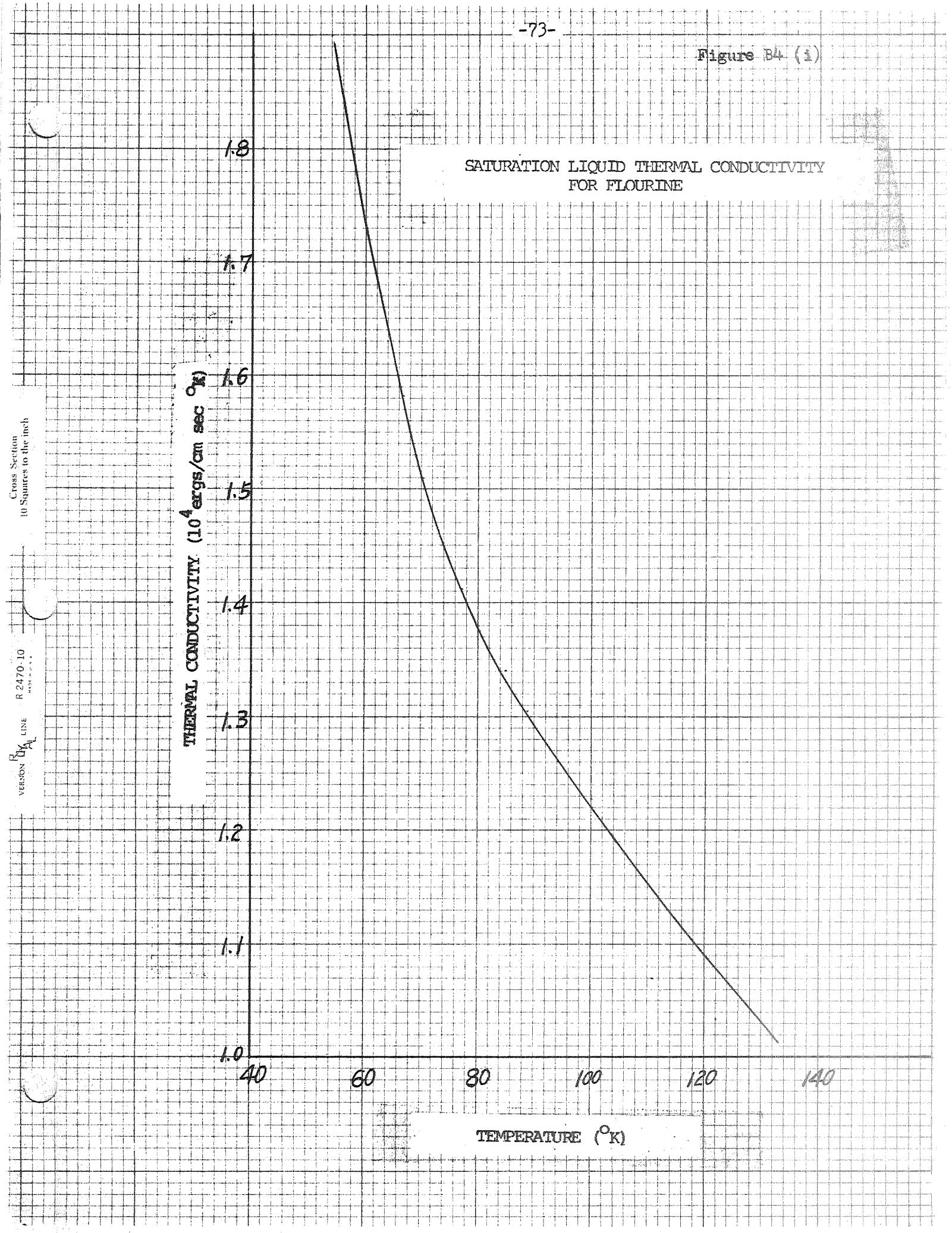
SATURATION LIQUID THERMAL CONDUCTIVITY
FOR FLOURINE
THERMAL CONDUCTIVITY (10^4 ergs/cm sec °K)
1.8
1.7
1.6
1.5
1.4
1.3
1.2
1.1
1.0
40
60
80
100
120
140
TEMPERATURE (°K)
Cross Section
10 Squares to the inch
R 2470-10

Figure D5 (a)

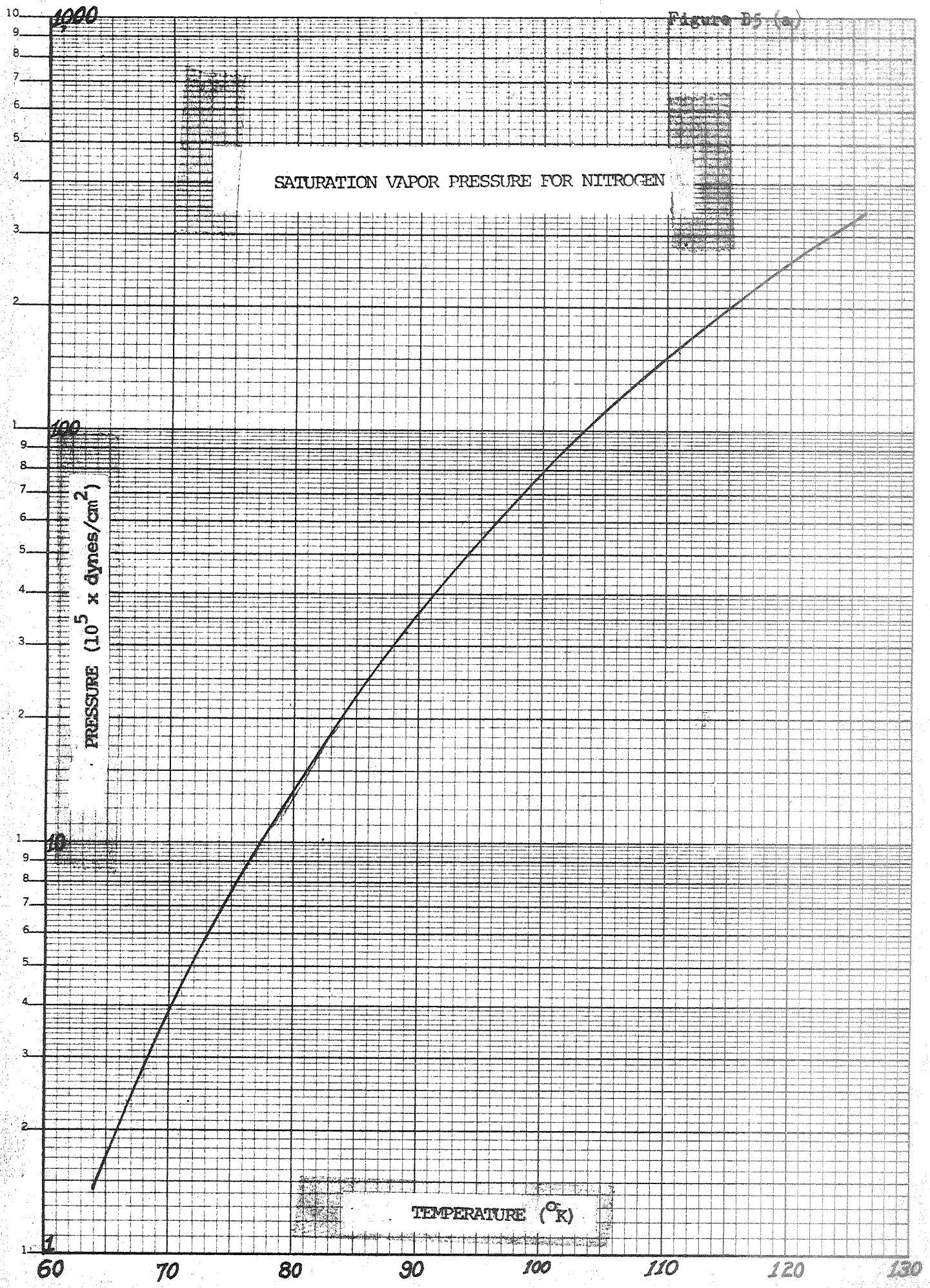

Semi-Logarithmic
3 Cycles x 10 to the inch
VERNON RULING LINE R 2470 SL 3

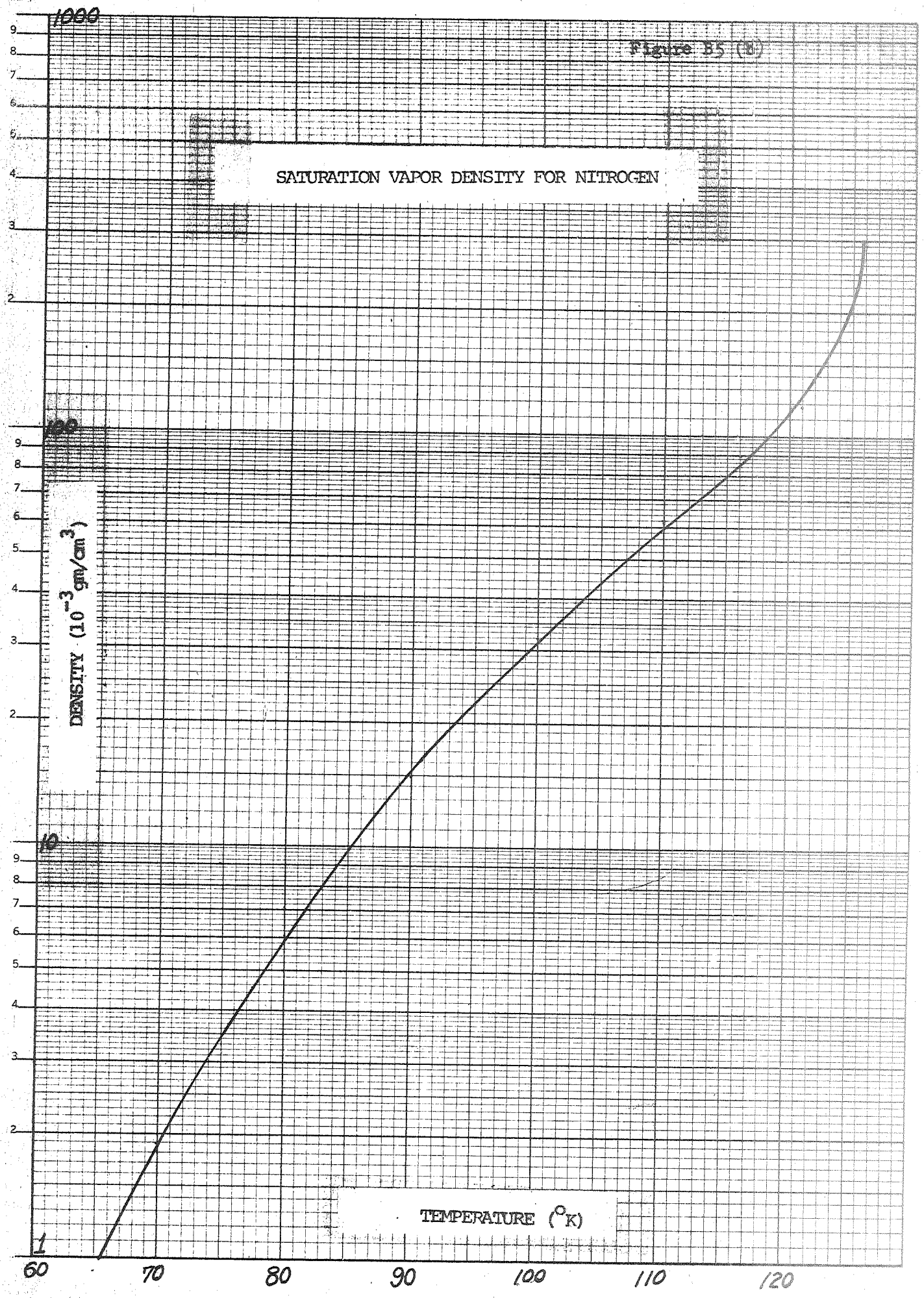

Semi-Logarithmic
3 Cycles x 10 to the inch
R 2470 SL 3
VERNON DIAZO LINE

Figure B5 (c)

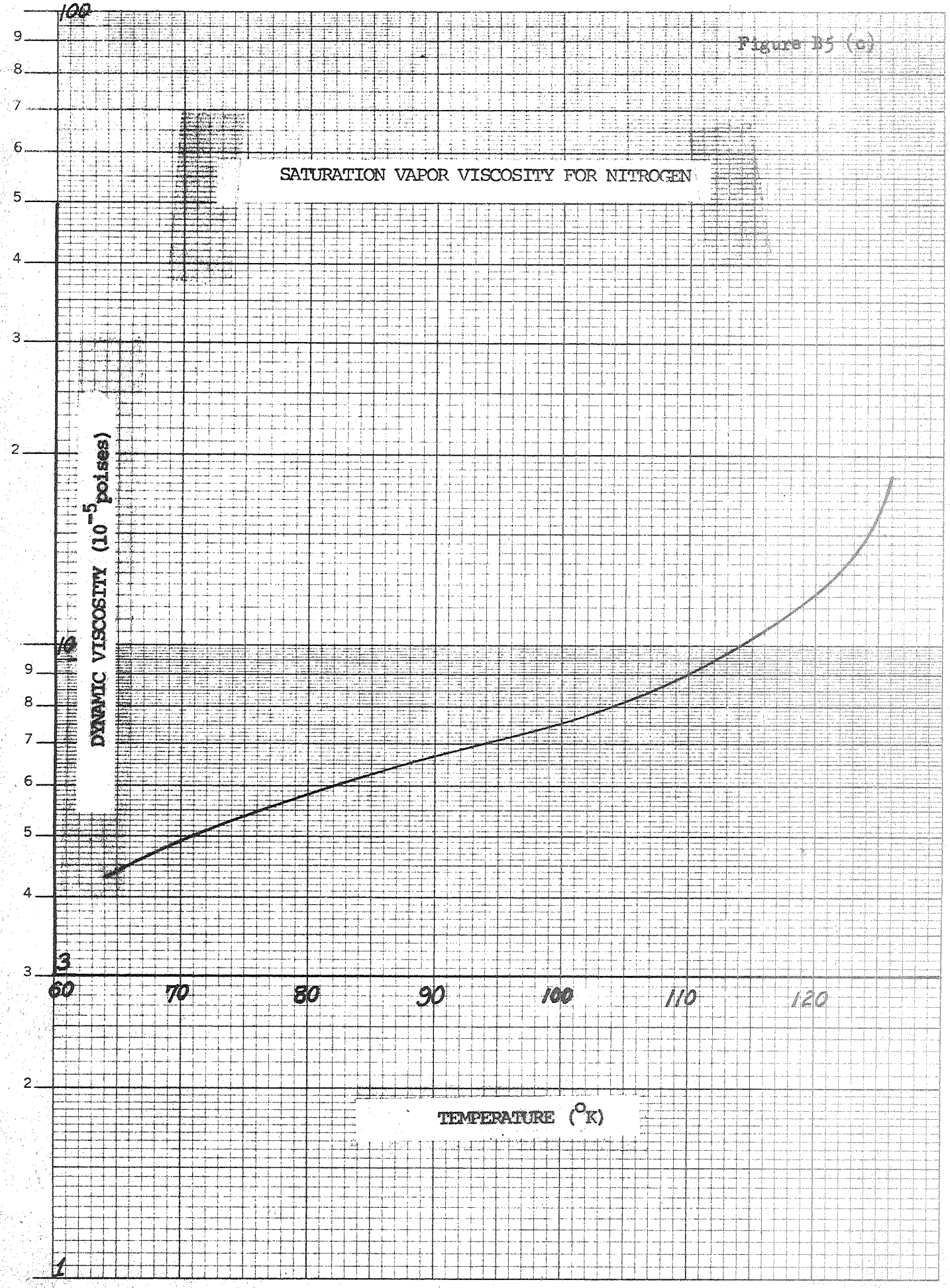

Semi-Logarithmic
2 Cycles x 10 to the inch
VERNON DIAL LINE R 2470 SL 2

Figure B5 (d)

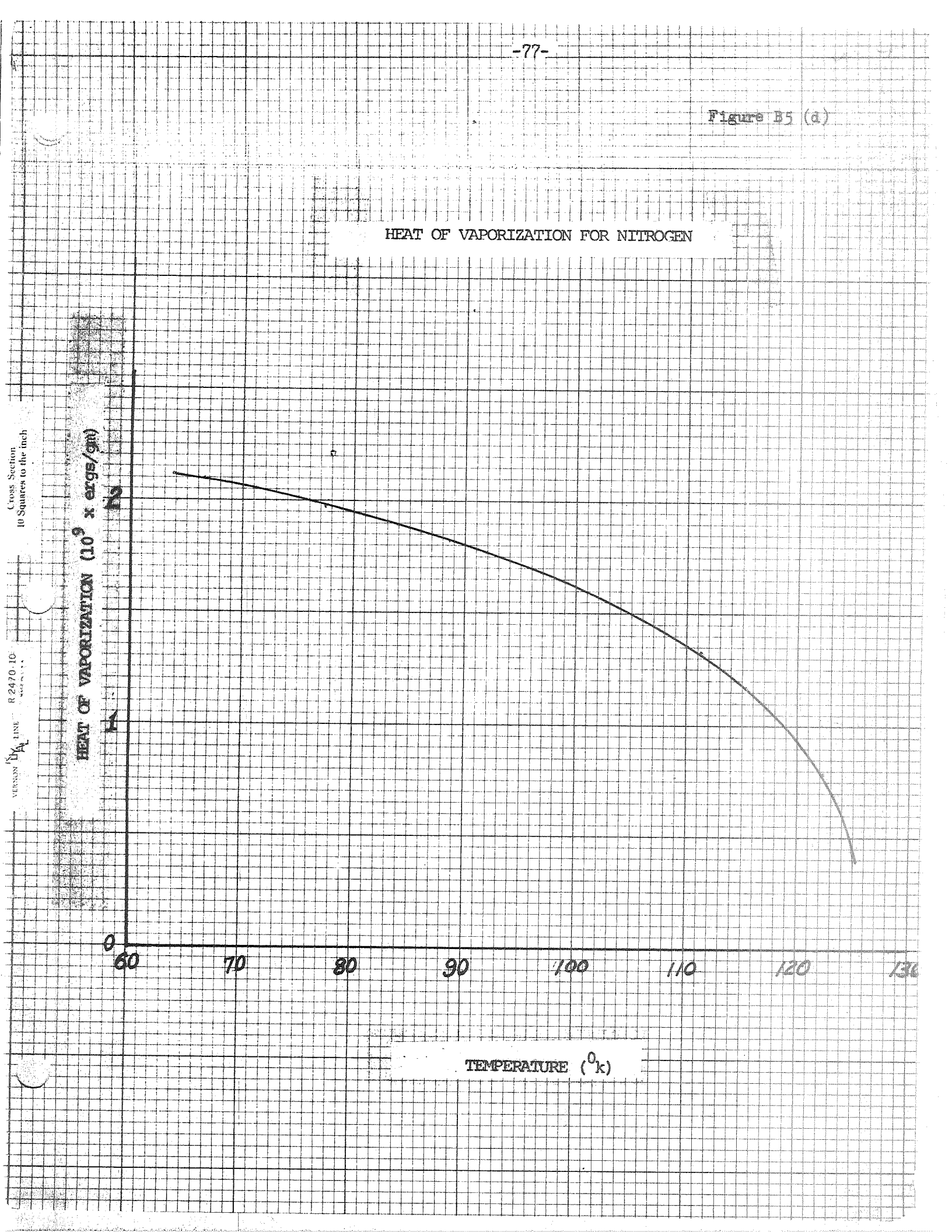
HEAT OF VAPORIZATION FOR NITROGEN
HEAT OF VAPORIZATION (10^9 x ergs/gm)
2
1
0
60
70
80
90
100
110
120
130
TEMPERATURE (^{0}k)

Figure B5 (e)

SATURATION LIQUID SURFACE TENSION
FOR NITROGEN

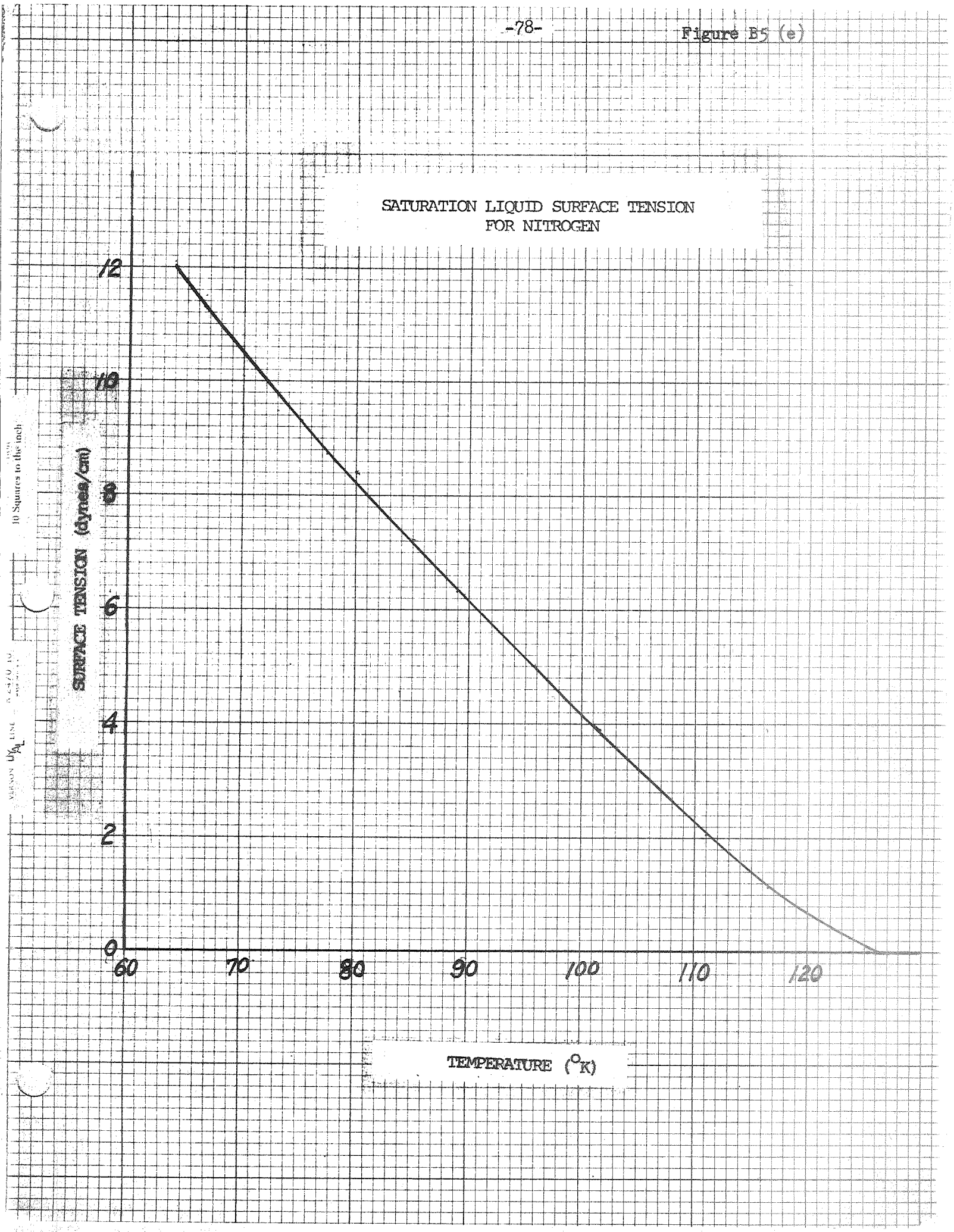

Figure B5 (f)

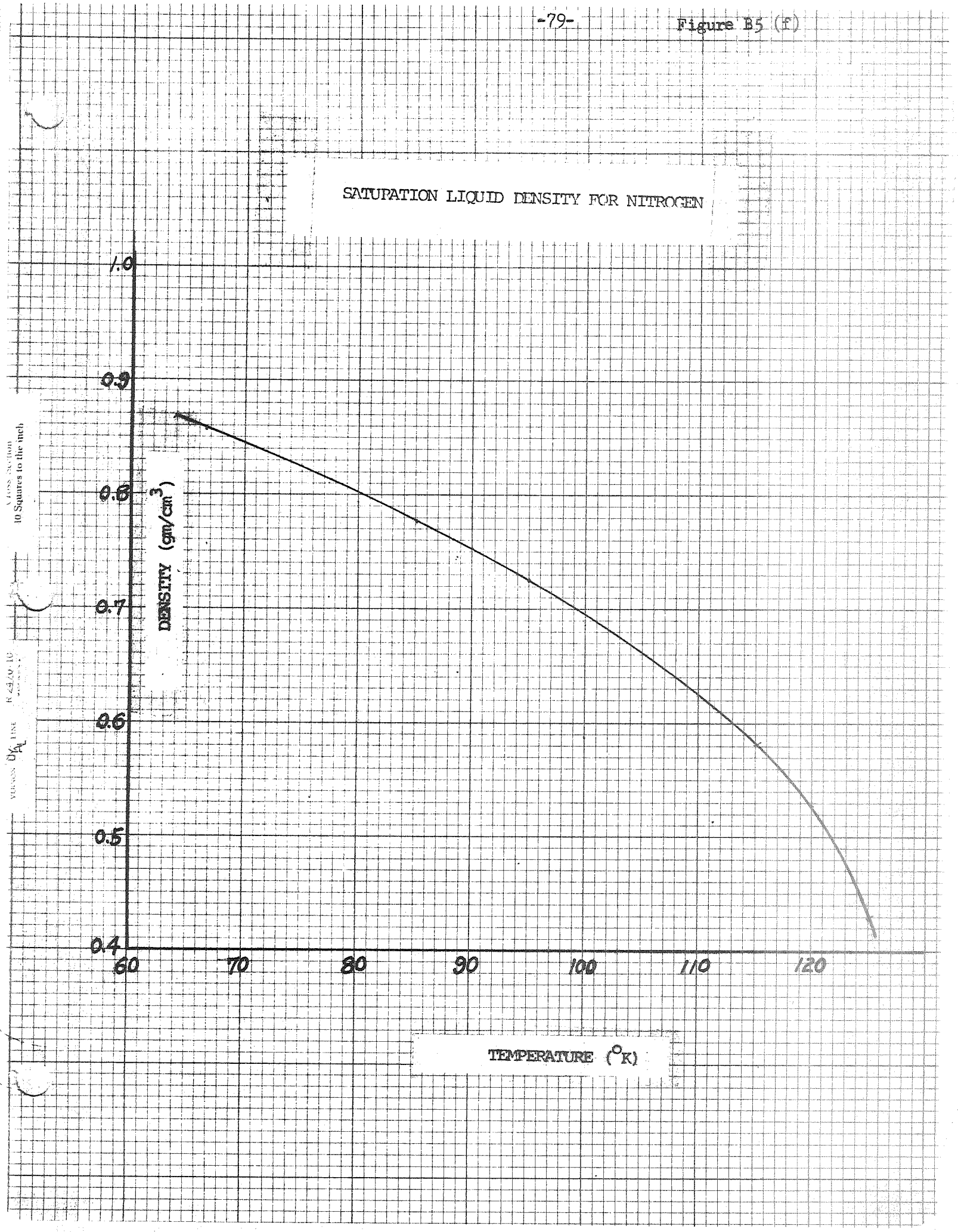
SATURATION LIQUID DENSITY FOR NITROGEN
1.0
0.9
0.8
0.7
0.6
0.5
0.4
DENSITY (gm/cm^3)
60
70
80
90
100
110
120
TEMPERATURE (^{o}K)

Figure B5 (g)

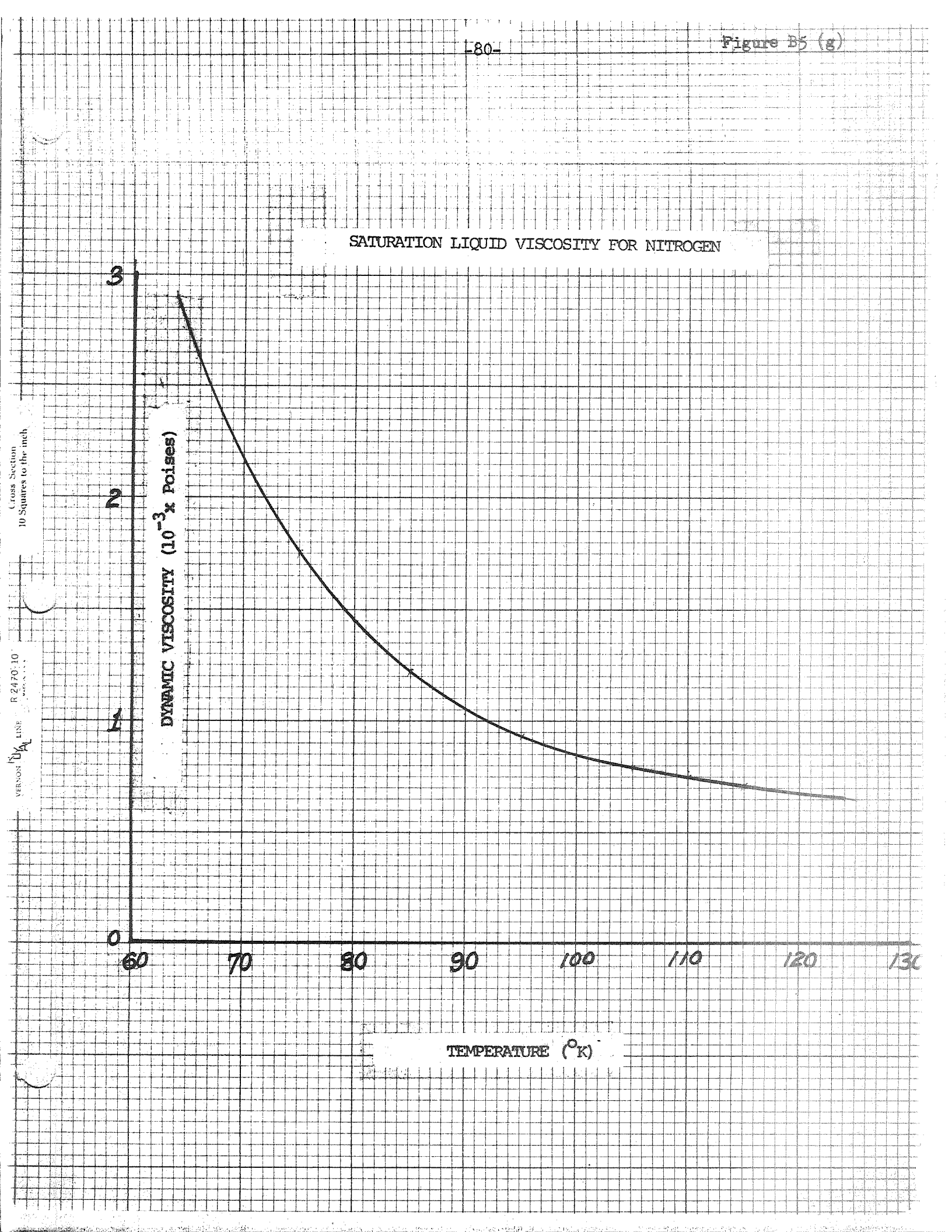
SATURATION LIQUID VISCOSITY FOR NITROGEN
DYNAMIC VISCOSITY (10^{-3} x Poises)
3
2
1
0
60
70
80
90
100
110
120
130
TEMPERATURE (°K)

Figure B5 (h)

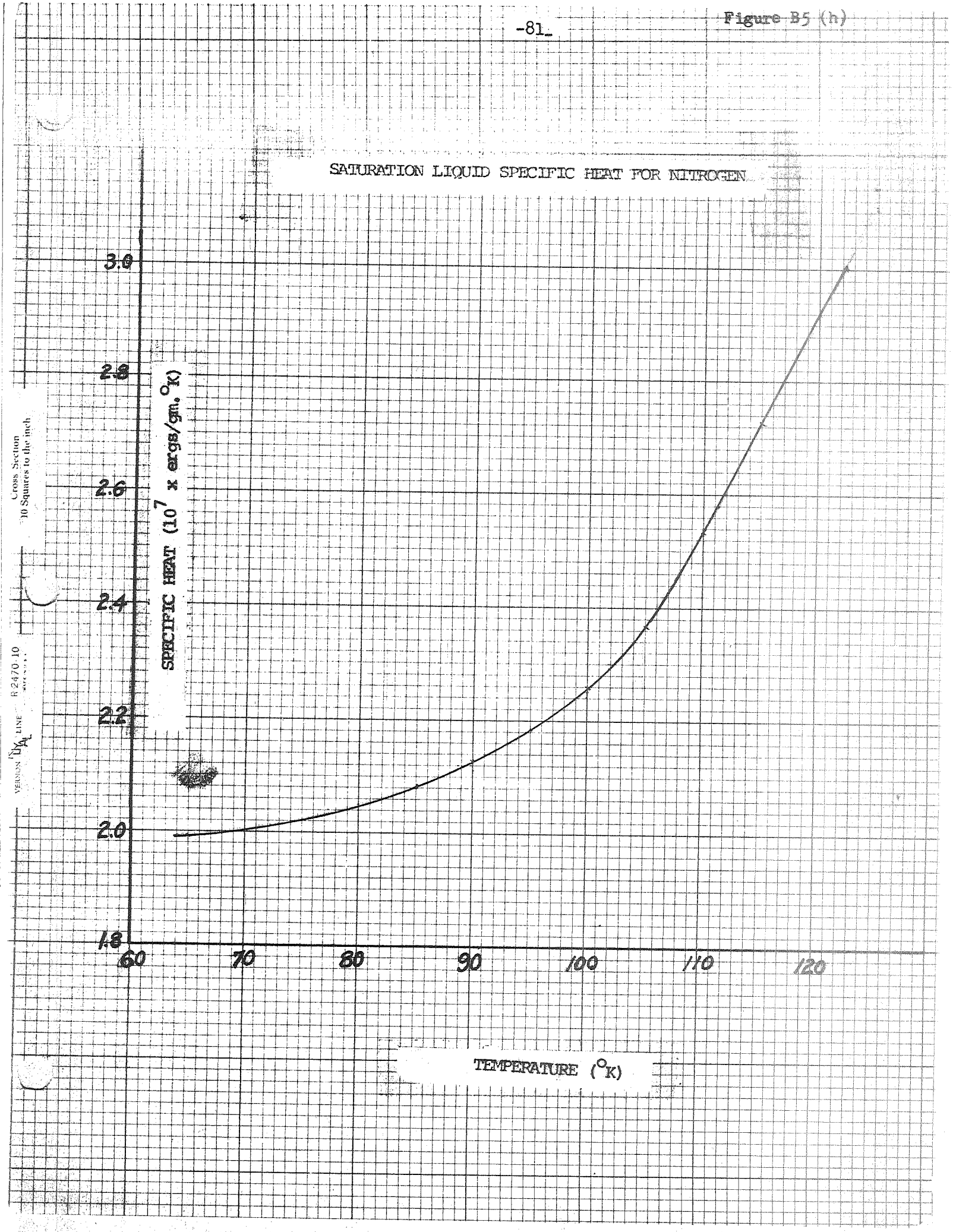
SATURATION LIQUID SPECIFIC HEAT FOR NITROGEN
SPECIFIC HEAT (10^7 x ergs/gm. ^oK)
3.0
2.8
2.6
2.4
2.2
2.0
1.8
60
70
80
90
100
110
120
TEMPERATURE (^oK)

SATURATION LIQUID THERMAL CONDUCTIVITY
FOR NITROGEN

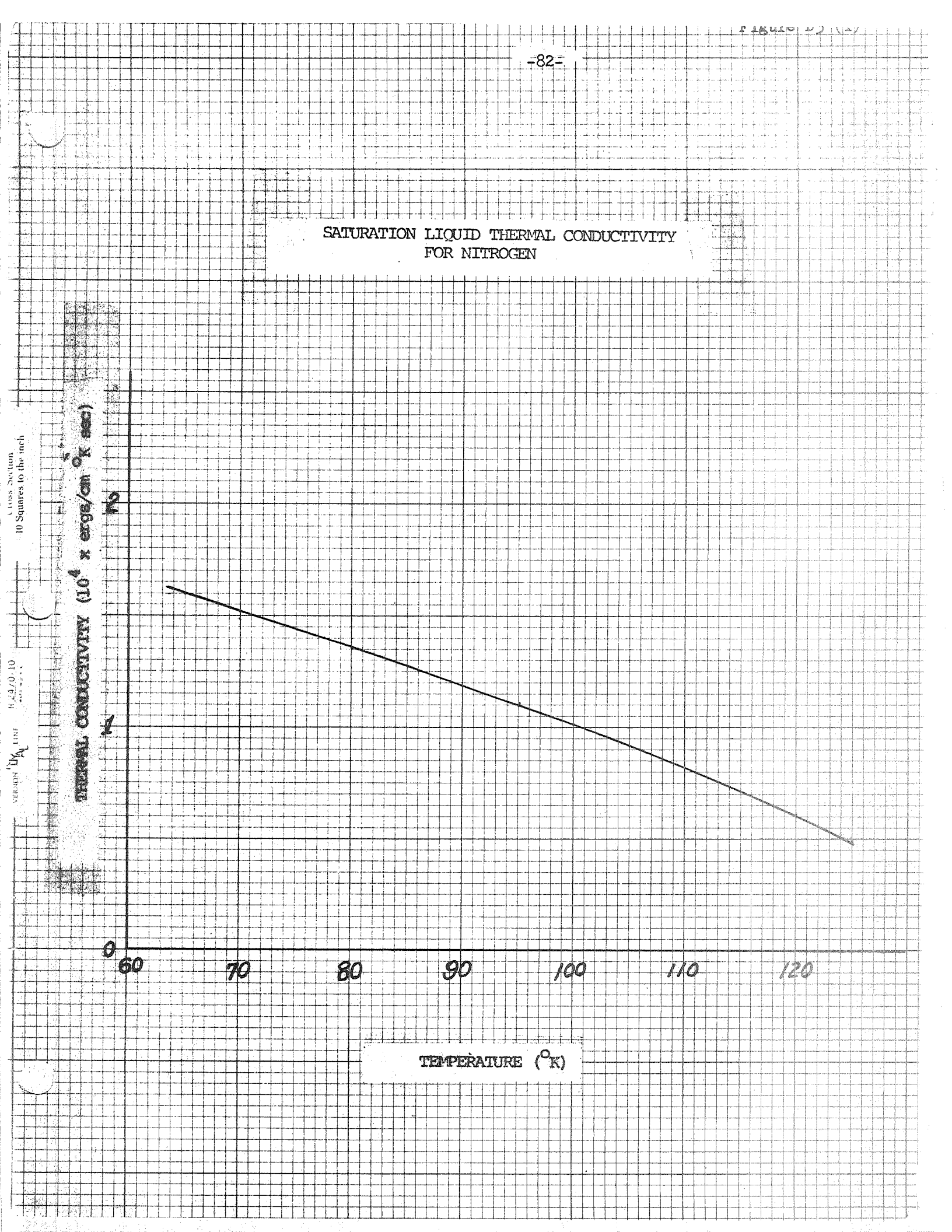

Figure B6 (a)

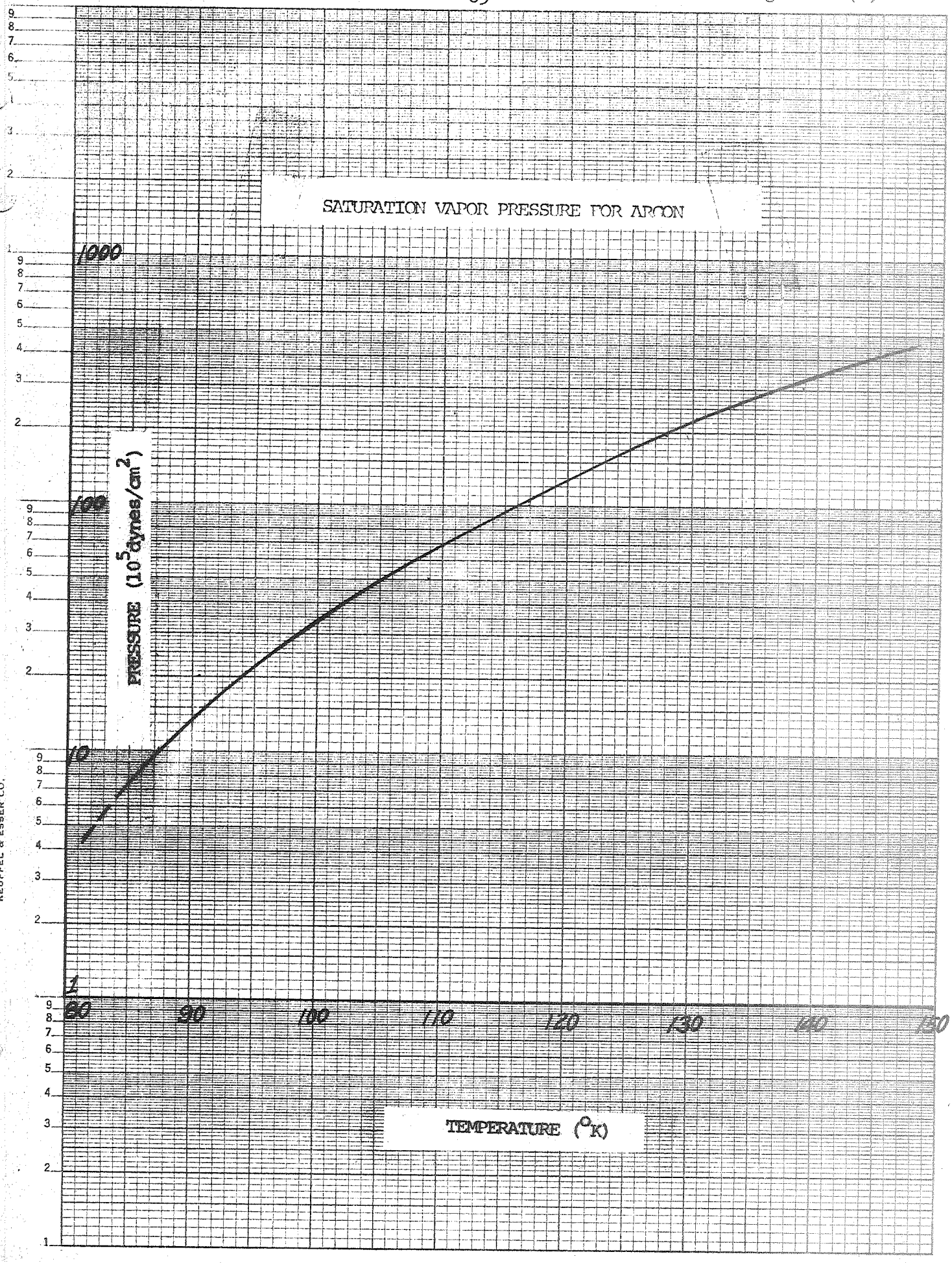
SATURATION VAPOR PRESSURE FOR ARGON
PRESSURE (10^5 dynes/cm^2)
1000
100
10
1
80
90
100
110
120
130
140
150
TEMPERATURE (°K)
K&E SEMI-LOGARITHMIC 46 6210
5 CYCLES X 70 DIVISIONS MADE IN U.S.A.
KEUFFEL & ESSER CO.

Figure B6 (a)

SATURATION VAPOR DENSITY FOR ARGON

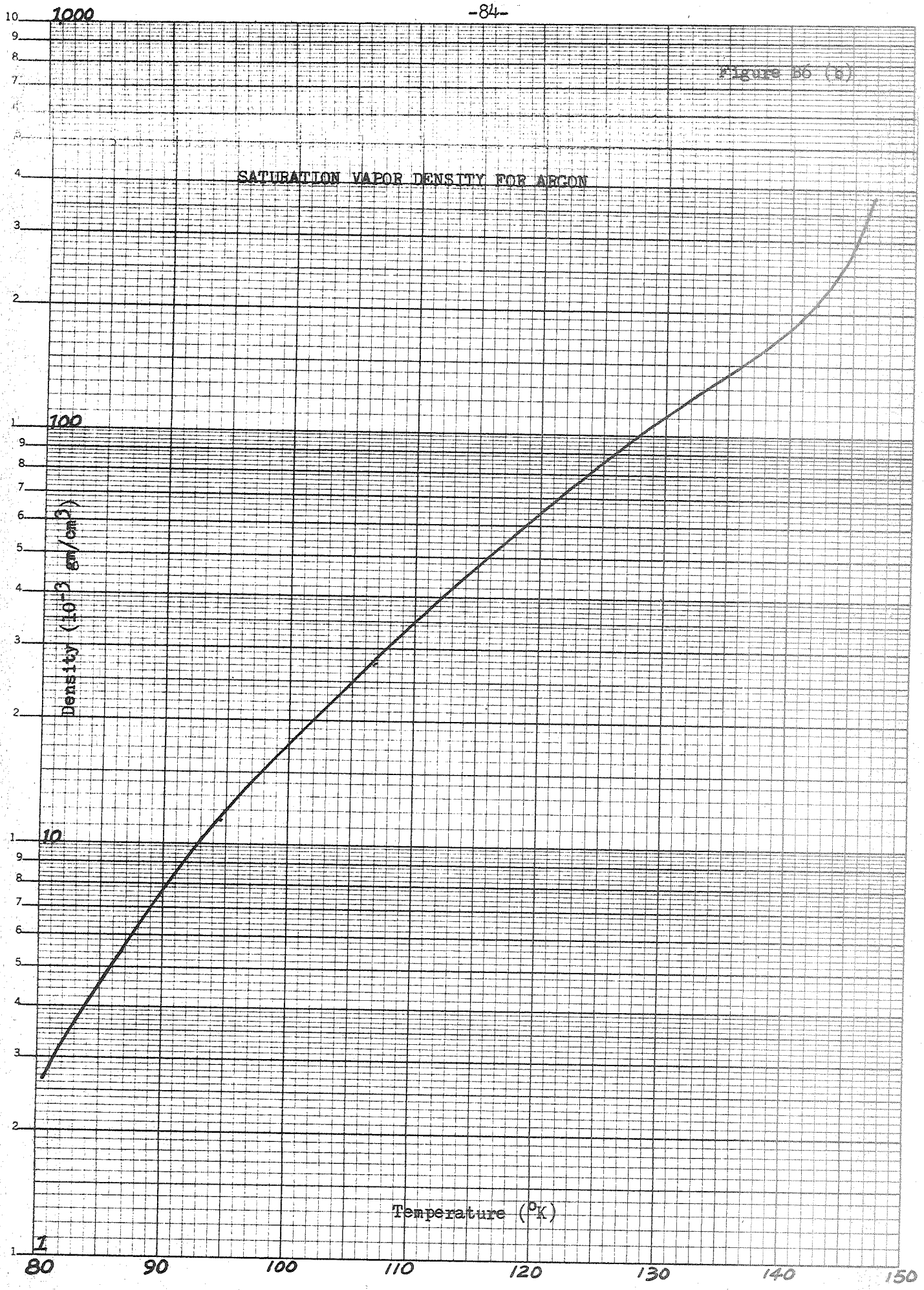

Semi-Logarithmic-
3 Cycles x 10 to the inch
R 2470 SL-3
VERNON RUX LINE

Figure B6 (c)

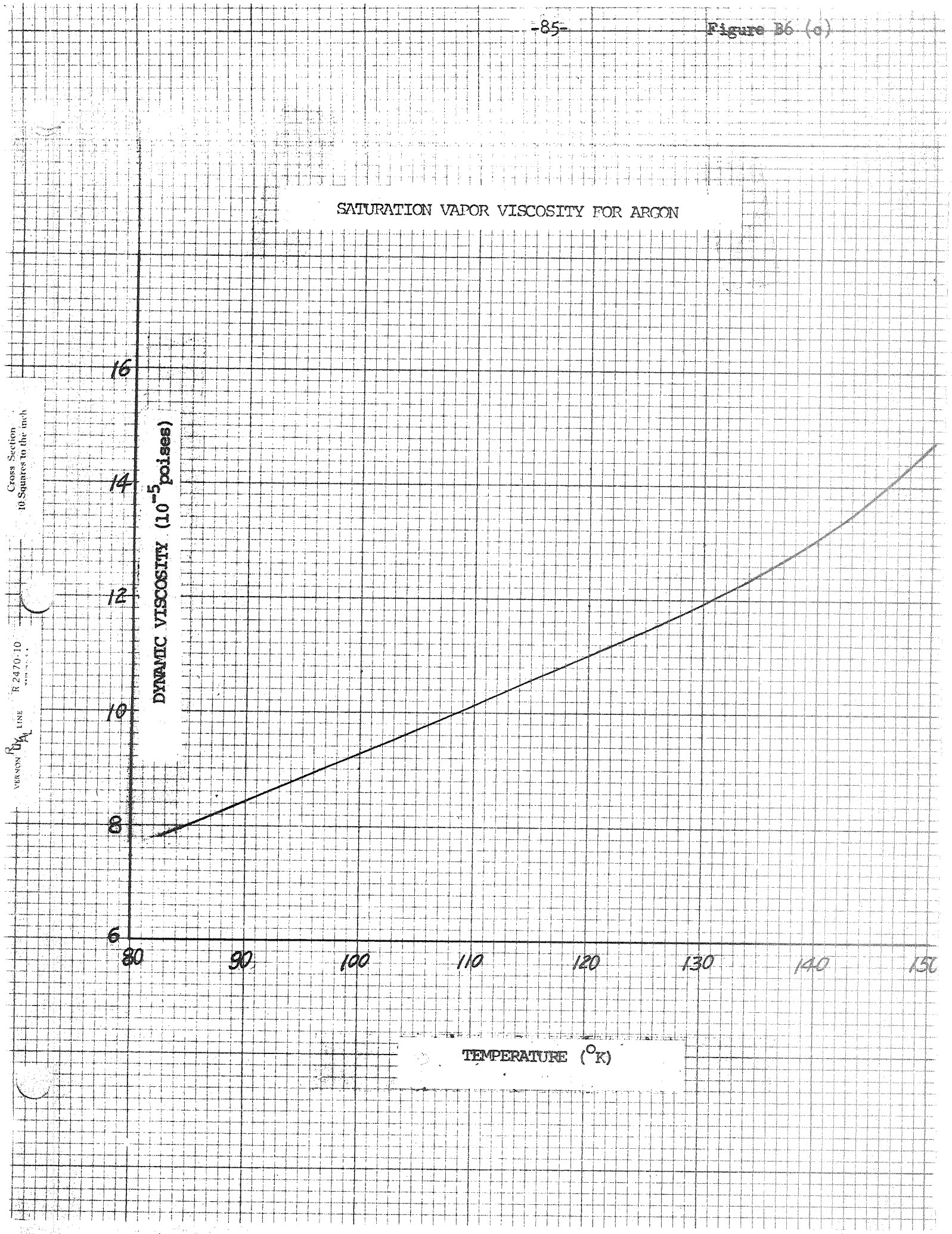
SATURATION VAPOR VISCOSITY FOR ARGON
DYNAMIC VISCOSITY (10^{-5} poises)
16
14
12
10
8
6
80
90
100
110
120
130
140
150
TEMPERATURE (^{o}K)

Figure B6 (d)

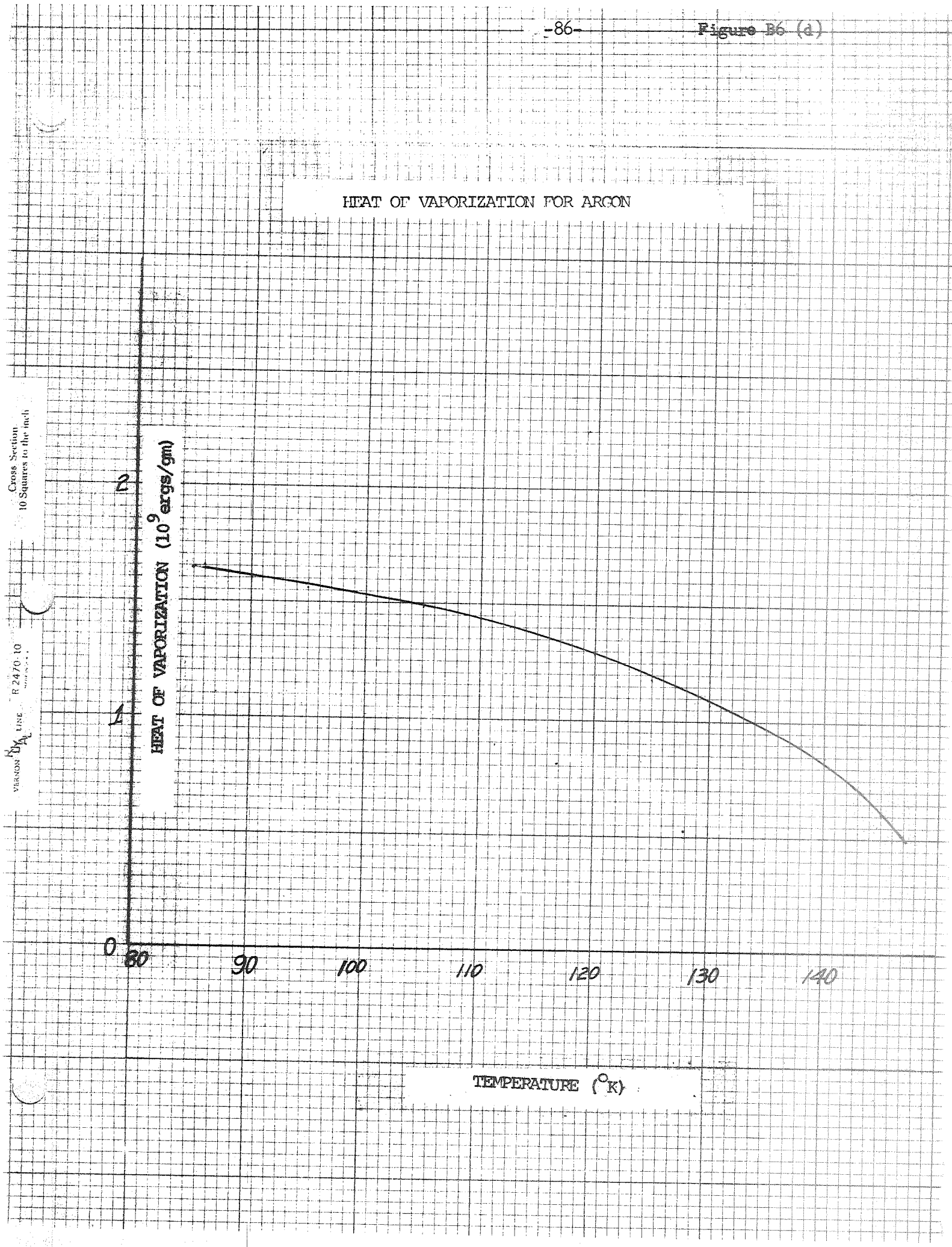
HEAT OF VAPORIZATION FOR ARGON
HEAT OF VAPORIZATION (10^9 ergs/gm)
2
1
0
80
90
100
110
120
130
140
TEMPERATURE (^oK)

Figure B6 (e)

Saturation Liquid Surface Tension for Argon

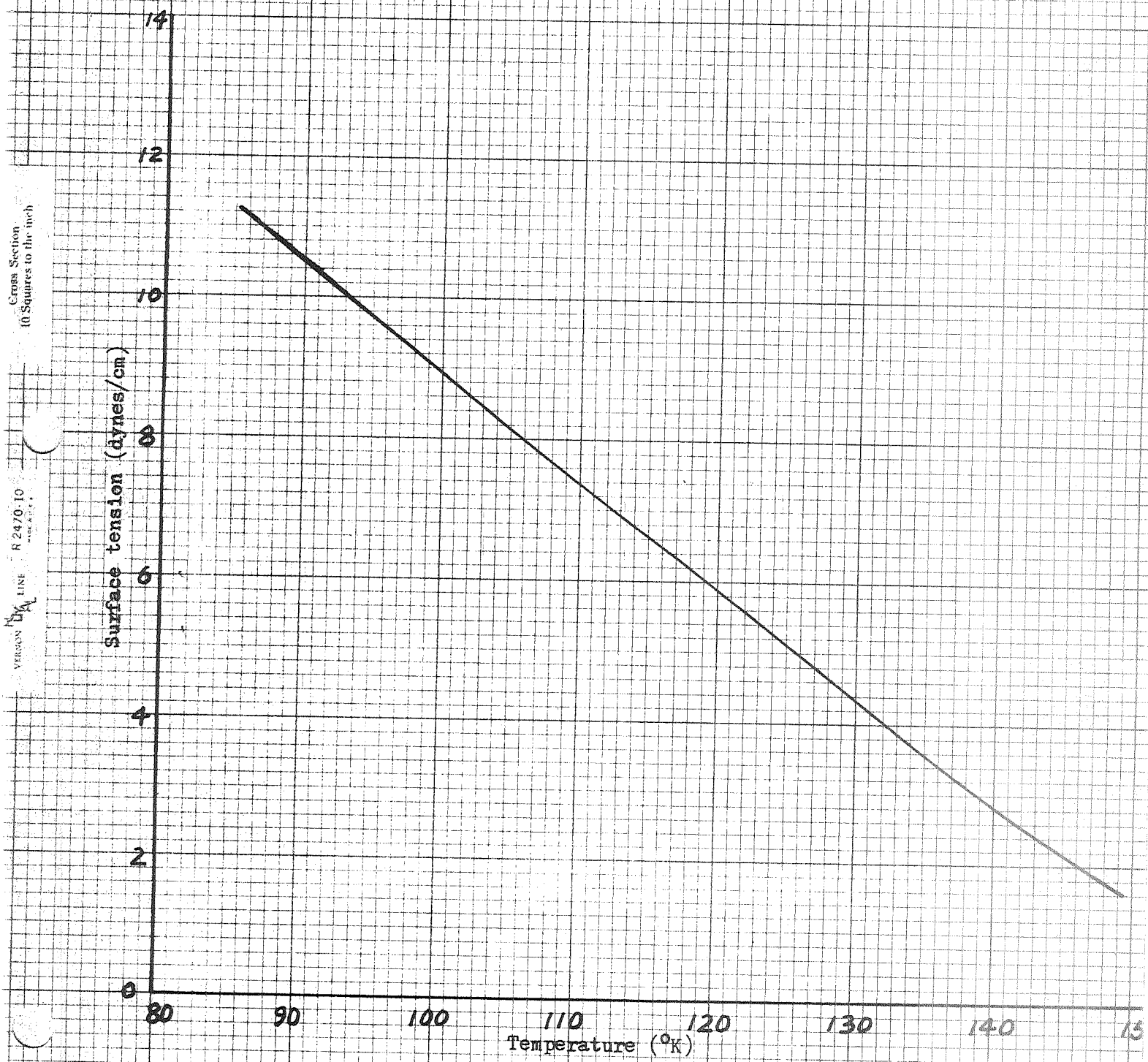

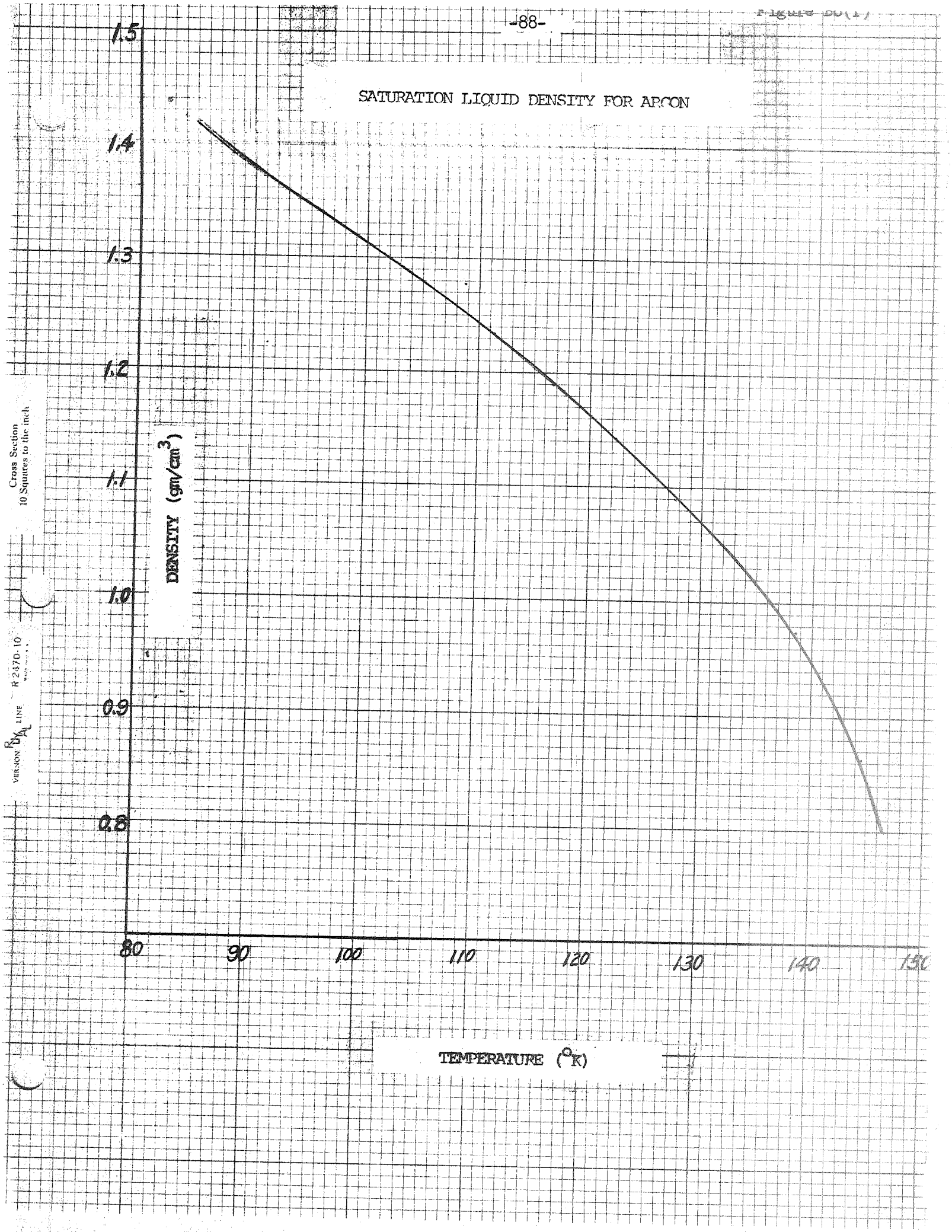

Cross Section
10 Squares to the inch
VERSION DUAL LINE R 2470-10

Figure B6 (g)

SATURATION LIQUID VISCOSITY FOR ARGON

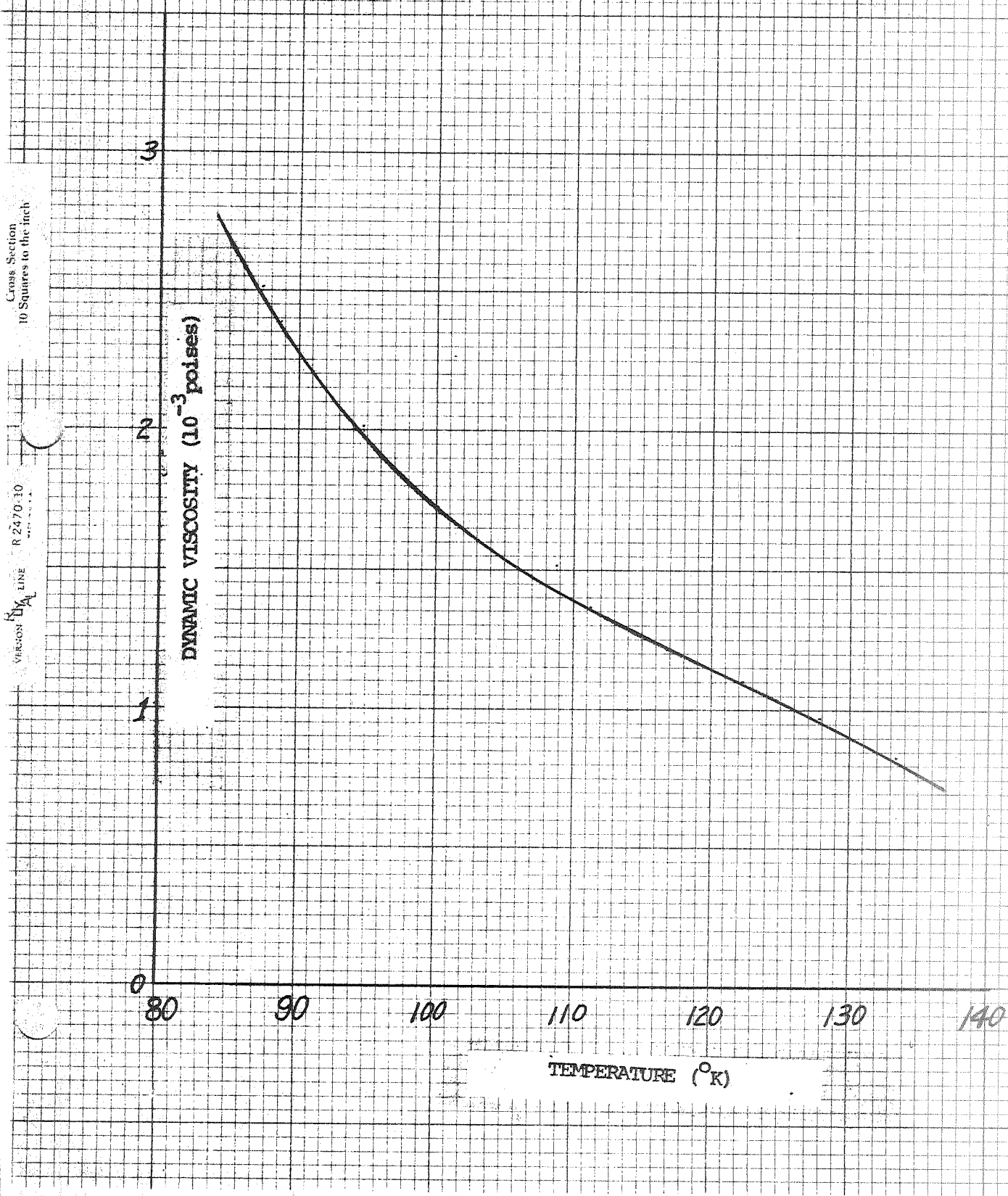

Cross Section
10 Squares to the inch
VERGON LINE R 2470-10

Figure B6 (h)

Saturation Liquid Specific Heat for Argon

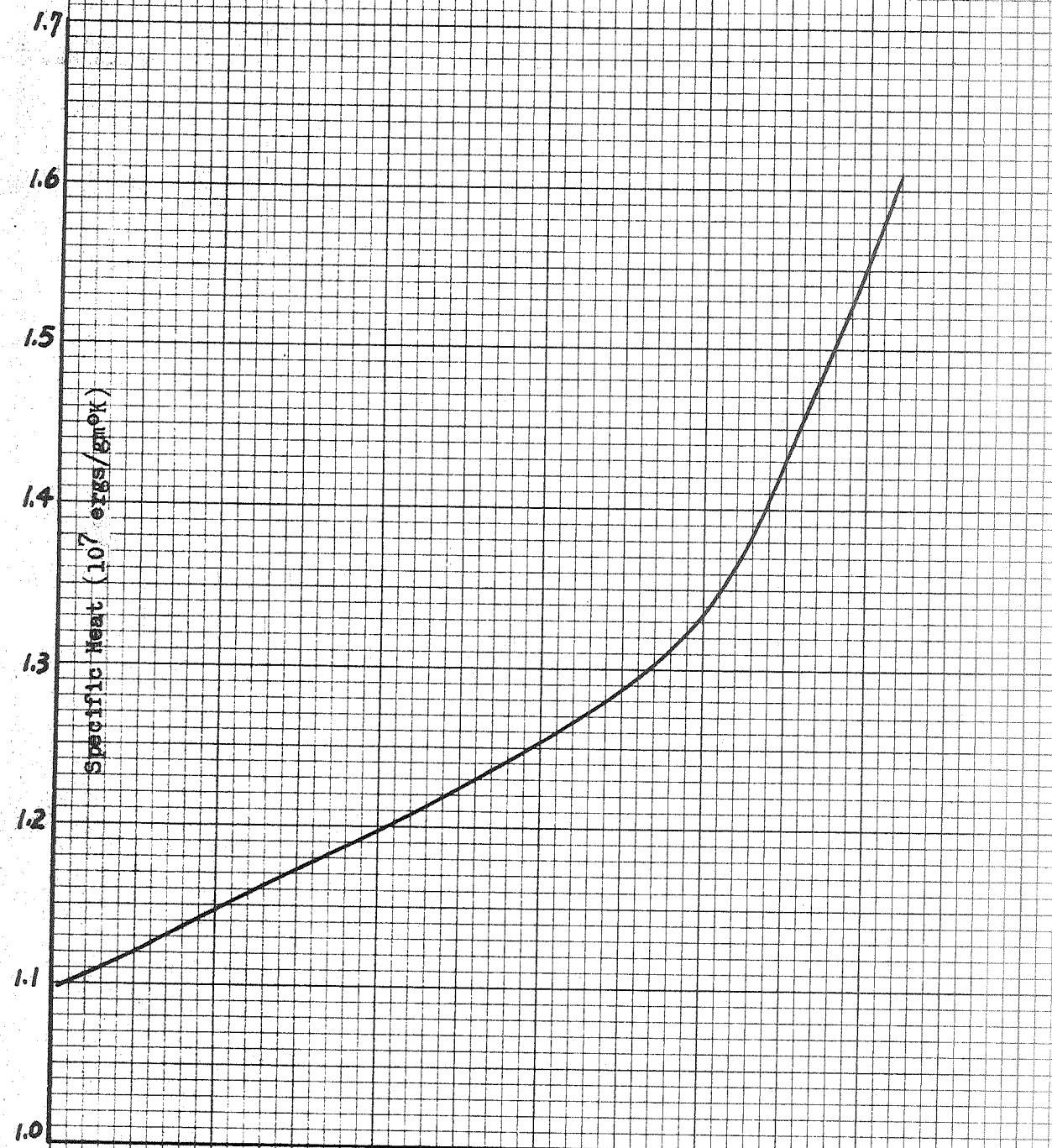

EUGENE DIETZGEN CO.
MADE IN U. S. A.
NO. 340-10 DIETZGEN GRAPH PAPER
10 X 10 PER INCH

Figure B6 (1)

SATURATION LIQUID THERMAL CONDUCTIVITY
FOR ARGON

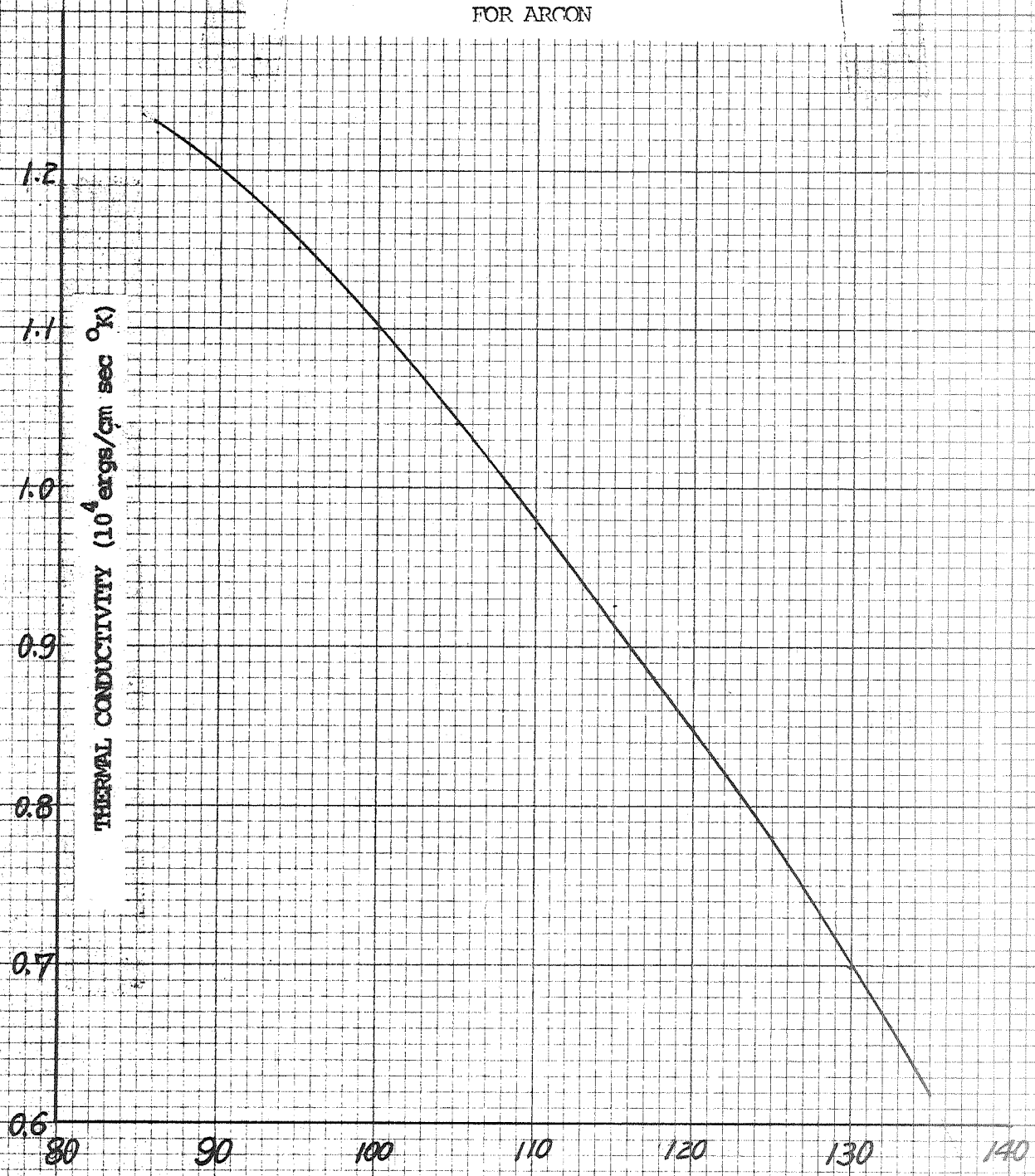

Cross Section
10 Squares to the inch
VERNON BLUE LINE R 2470-10

Figure 87 (a)

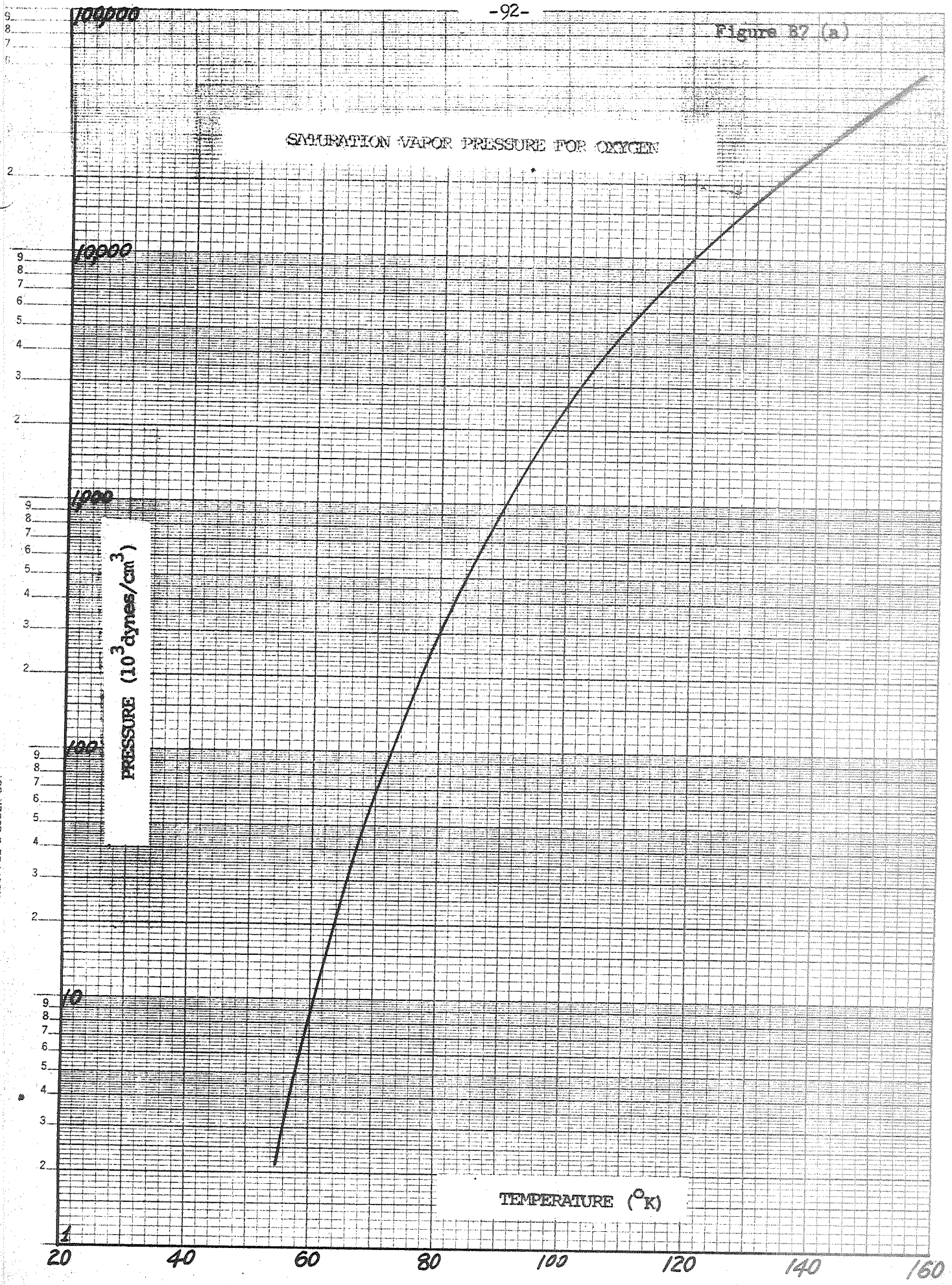
SATURATION VAPOR PRESSURE FOR OXYGEN
PRESSURE (10^3 dynes/cm^3)
TEMPERATURE ($^\circ$K)
100000
10000
1000
100
10
1
20
40
60
80
100
120
140
160
SEMI-LOGARITHMIC 46 6210
5 CYCLES X 70 DIVISIONS MADE IN U.S.A.
KEUFFEL & ESSER CO.

Figure B7 (b)

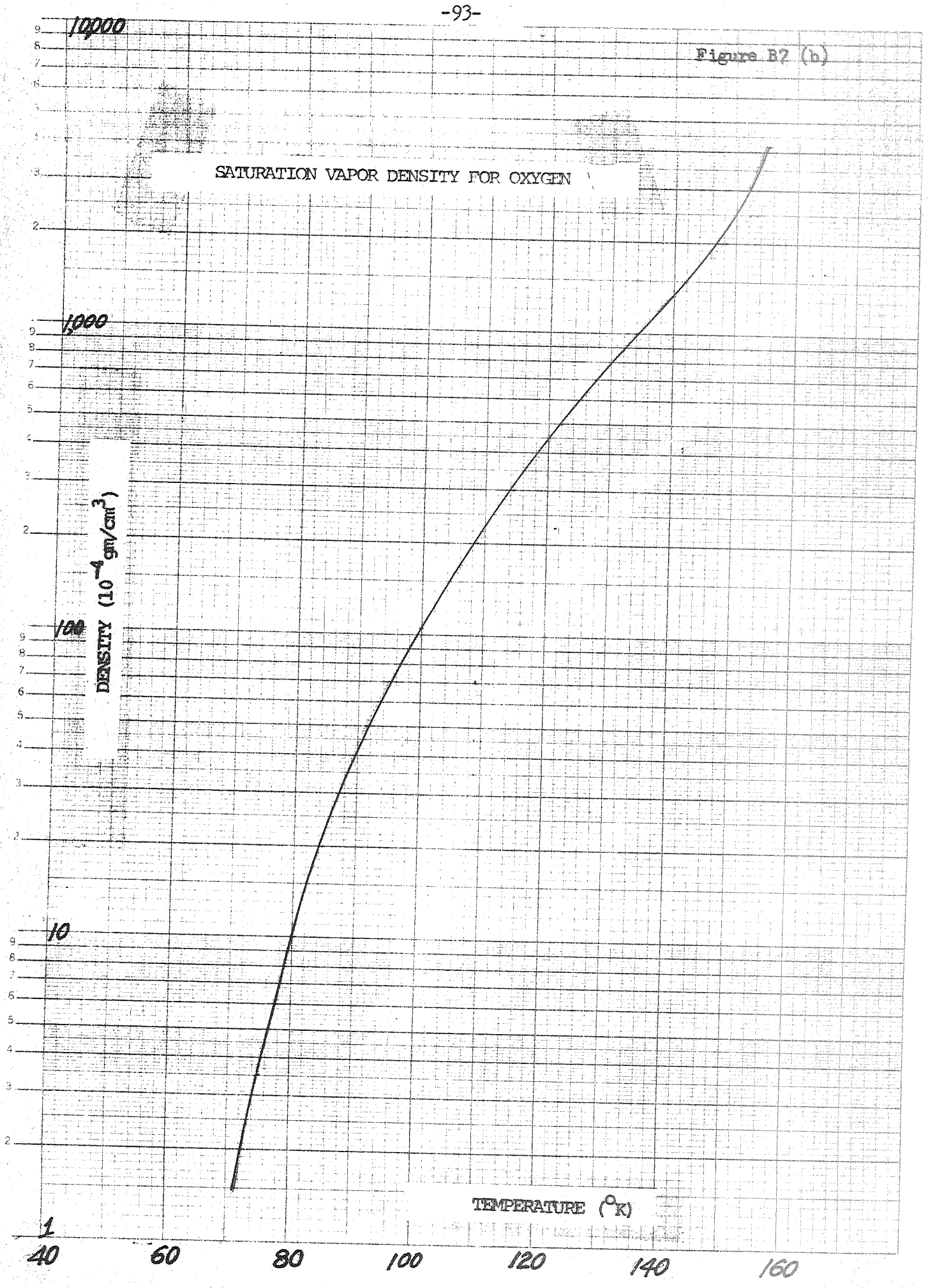
SATURATION VAPOR DENSITY FOR OXYGEN
DENSITY (10^{-4} gm/cm^3)
10,000
1,000
100
10
1
TEMPERATURE (^{o}K)
40
60
80
100
120
140
160

Figure B7 (c)

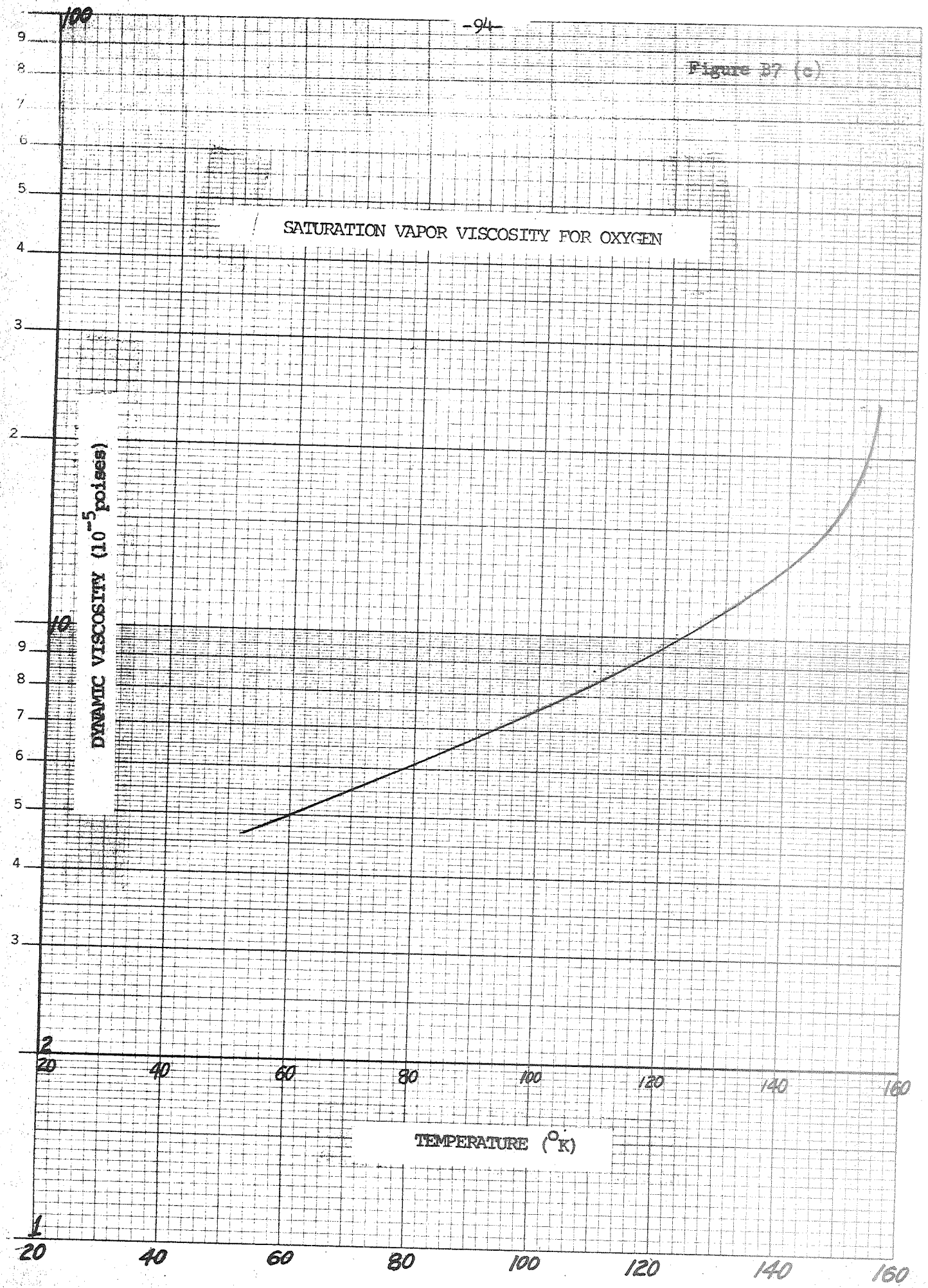

Semi-Logarithmic
2 Cycles x 10 to the inch
R 2470 SL 2
VERNON

Figure B7 (d)

HEAT OF VAPORIZATION FOR OXYGEN

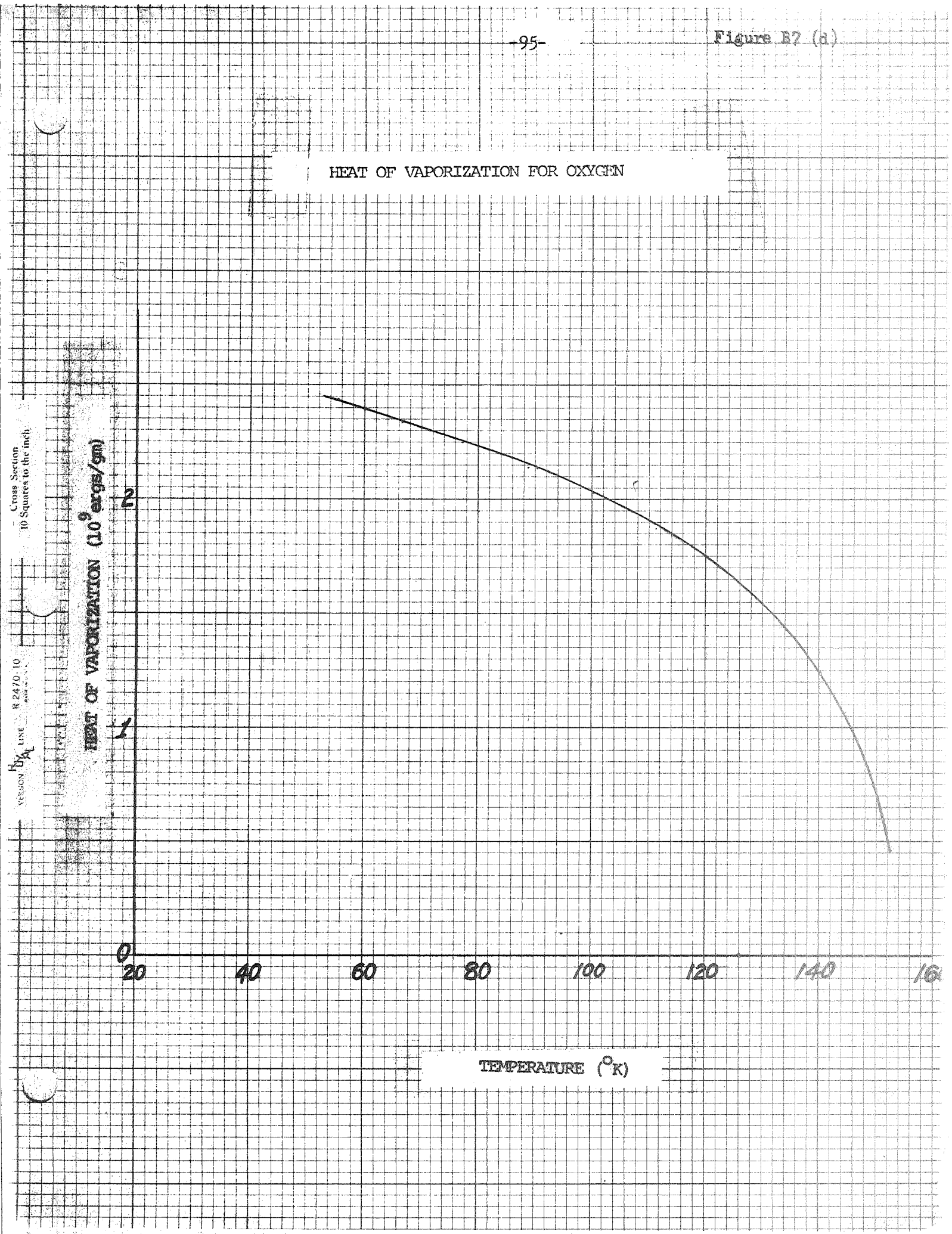

Figure B7 (e)

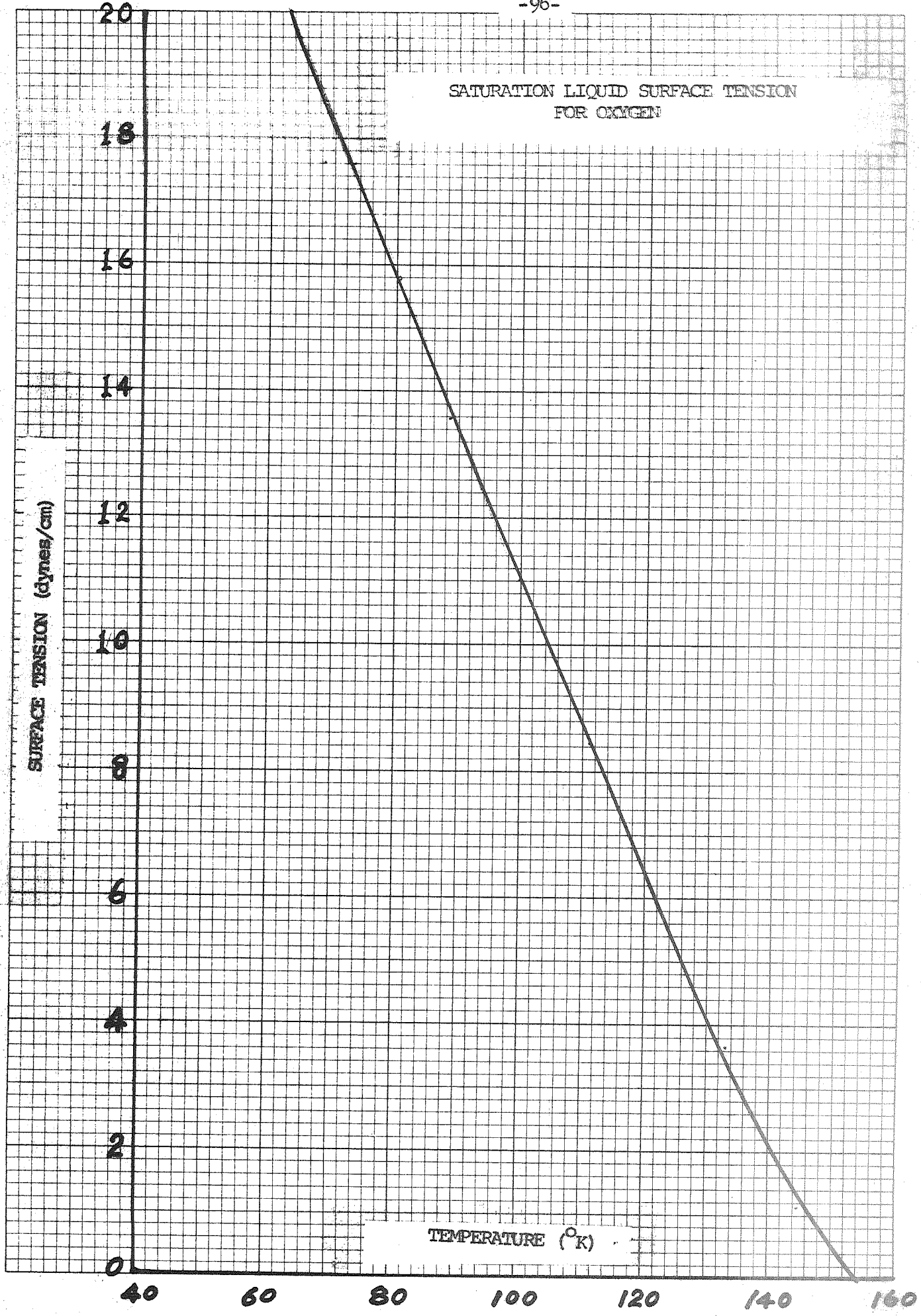

EUGENE DIETZGEN CO.
MADE IN U. S. A.
NO. 340-10 DIETZGEN GRAPH PAPER
10 X 10 PER INCH

Figure B7 (f)

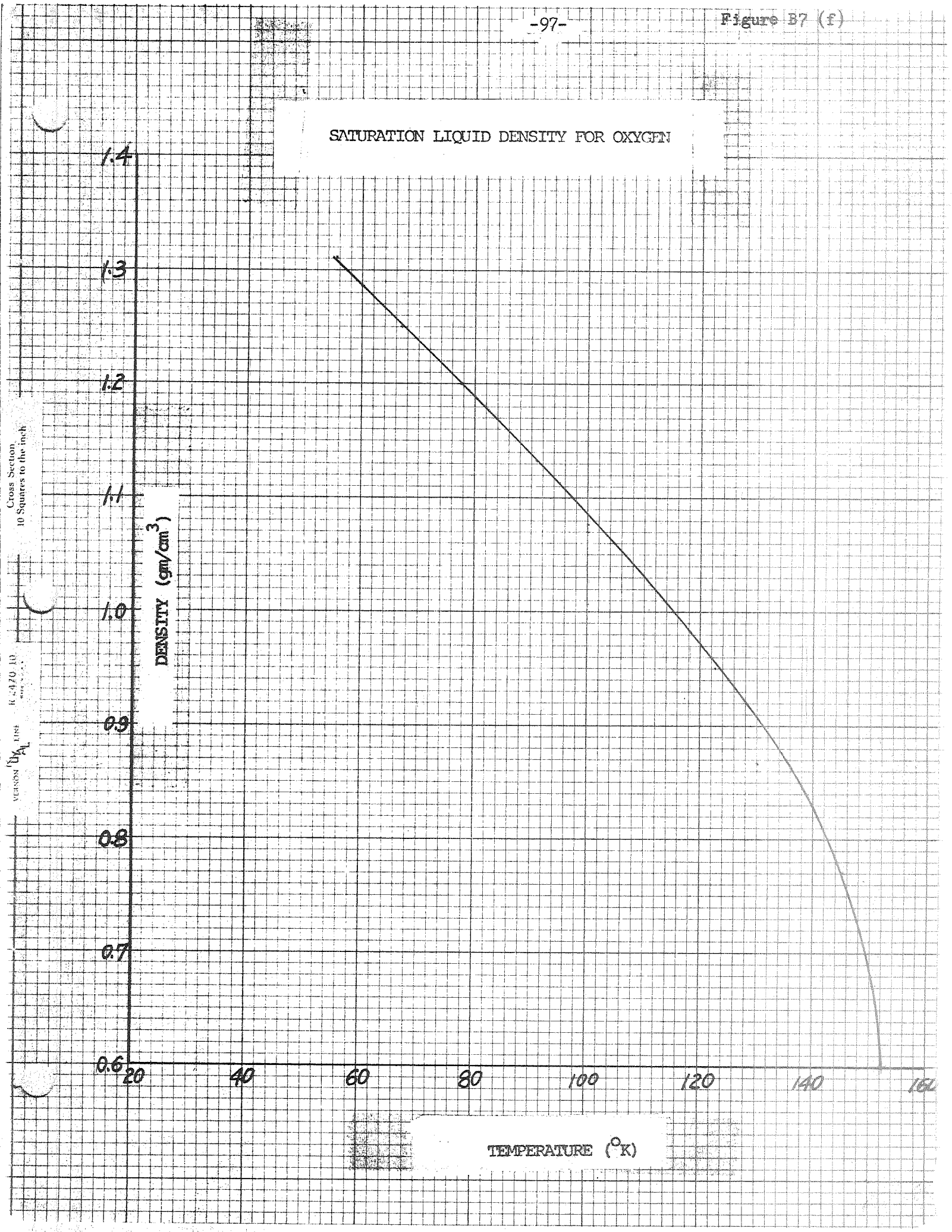
SATURATION LIQUID DENSITY FOR OXYGEN
1.4
1.3
1.2
1.1
1.0
0.9
0.8
0.7
0.6
DENSITY (gm/cm^3)
20
40
60
80
100
120
140
160
TEMPERATURE ($^{\circ}$K)

Figure B7 (g)

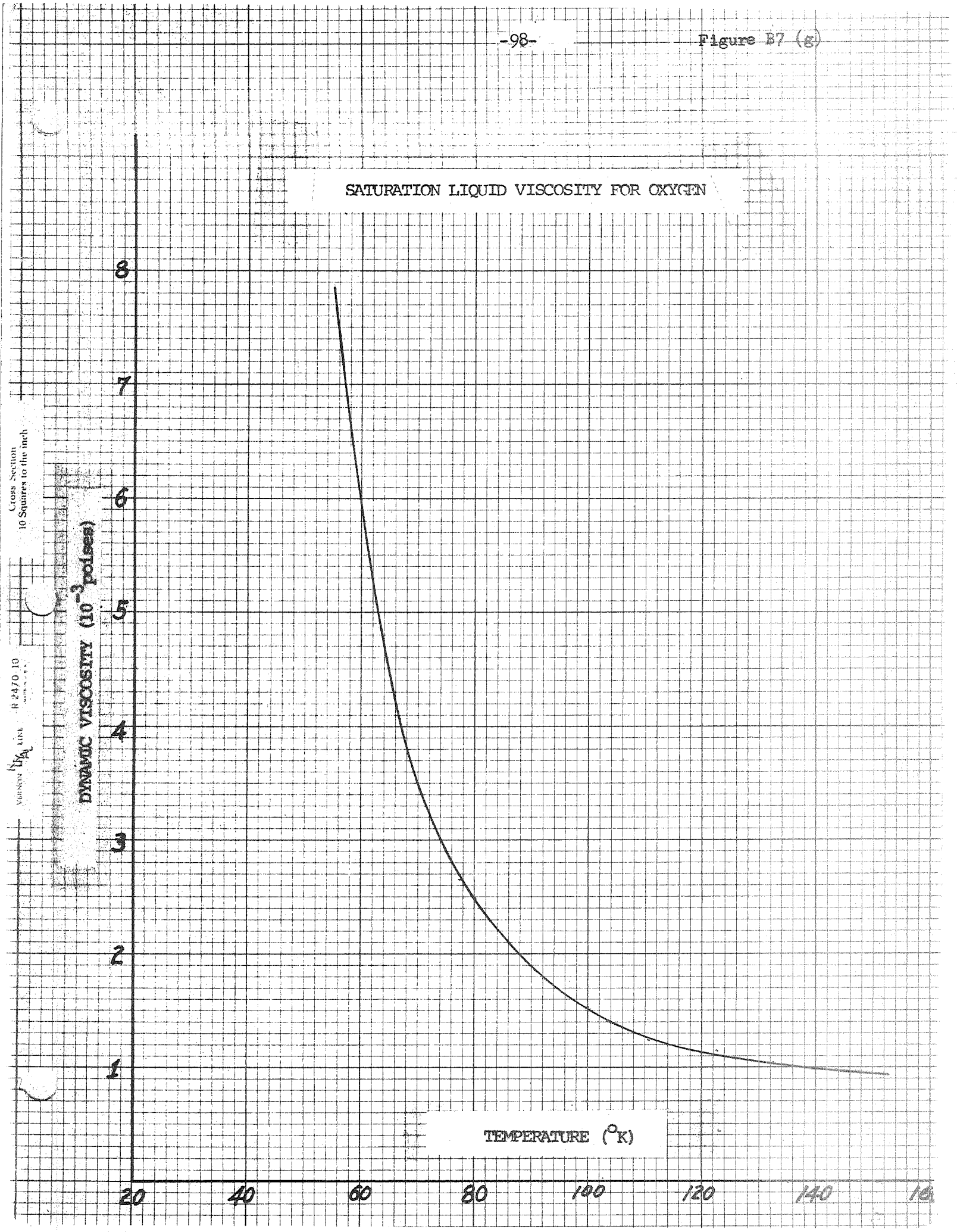
SATURATION LIQUID VISCOSITY FOR OXYGEN
DYNAMIC VISCOSITY (10^{-3} poises)
8
7
6
5
4
3
2
1
TEMPERATURE (^{o}K)
20
40
60
80
100
120
140

Figure B7 (h)

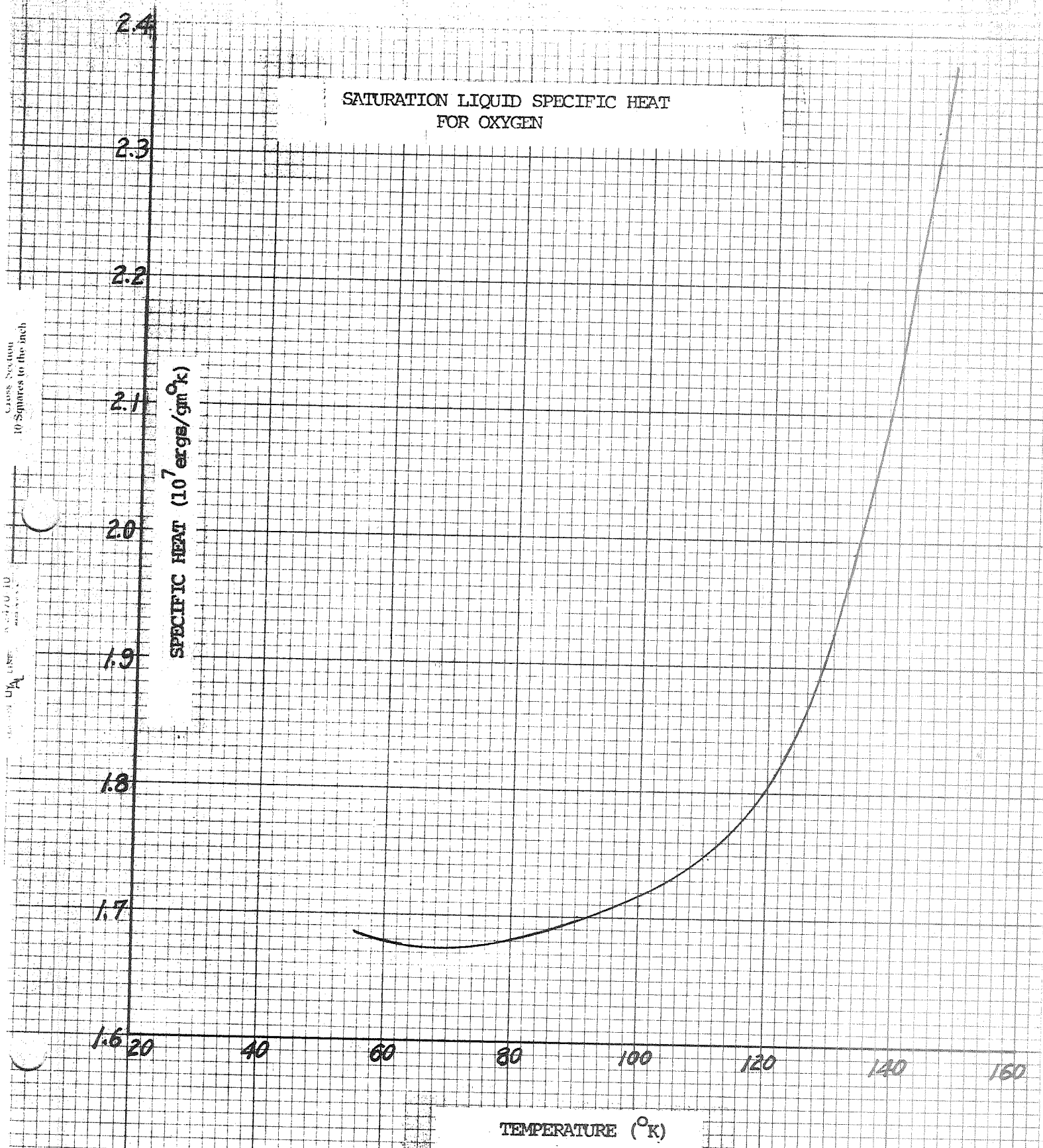
SATURATION LIQUID SPECIFIC HEAT
FOR OXYGEN
SPECIFIC HEAT (10^7 ergs/gm °K)
2.4
2.3
2.2
2.1
2.0
1.9
1.8
1.7
1.6
20
40
60
80
100
120
140
160
TEMPERATURE (°K)

Figure B7 (1)

SATURATION LIQUID THERMAL CONDUCTIVITY
FOR OXYGEN

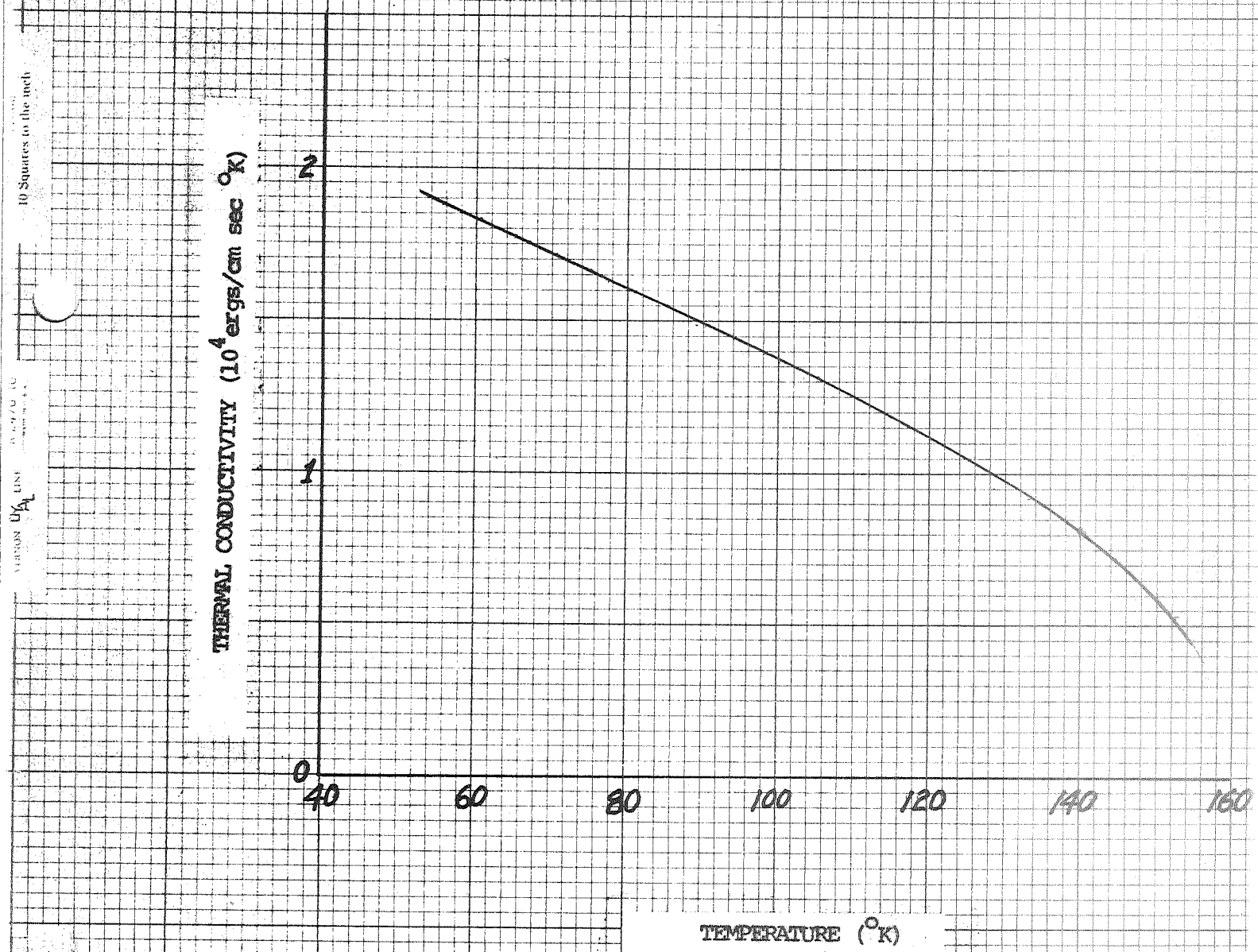

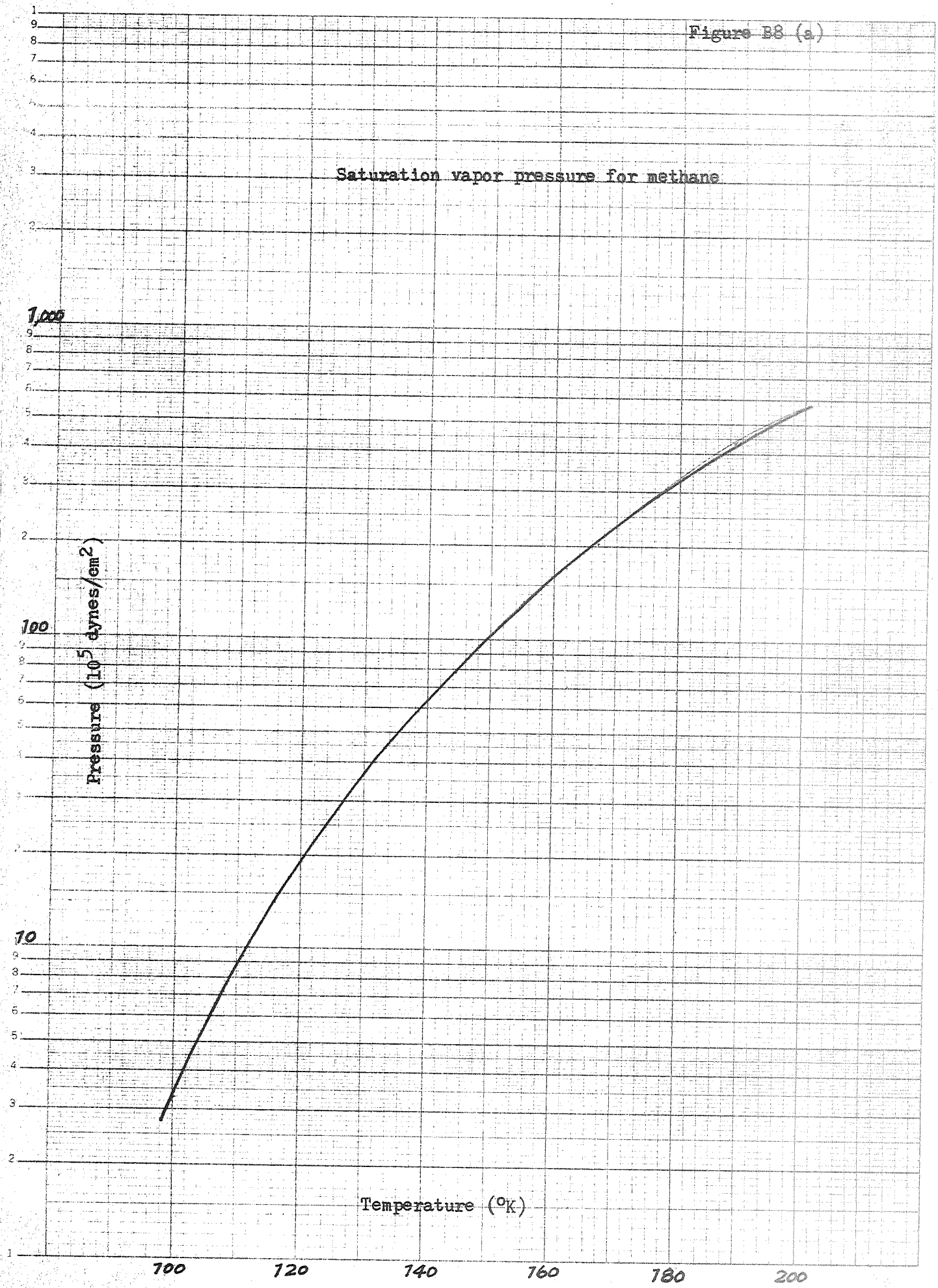
Figure B8 (a)
Saturation vapor pressure for methane
Pressure (10^5 dynes/cm^2)
1,000
100
10
Temperature (^oK)
100
120
140
160
180
200

Figure B8 (b)

SATURATION VAPOR DENSITY FOR METHANE

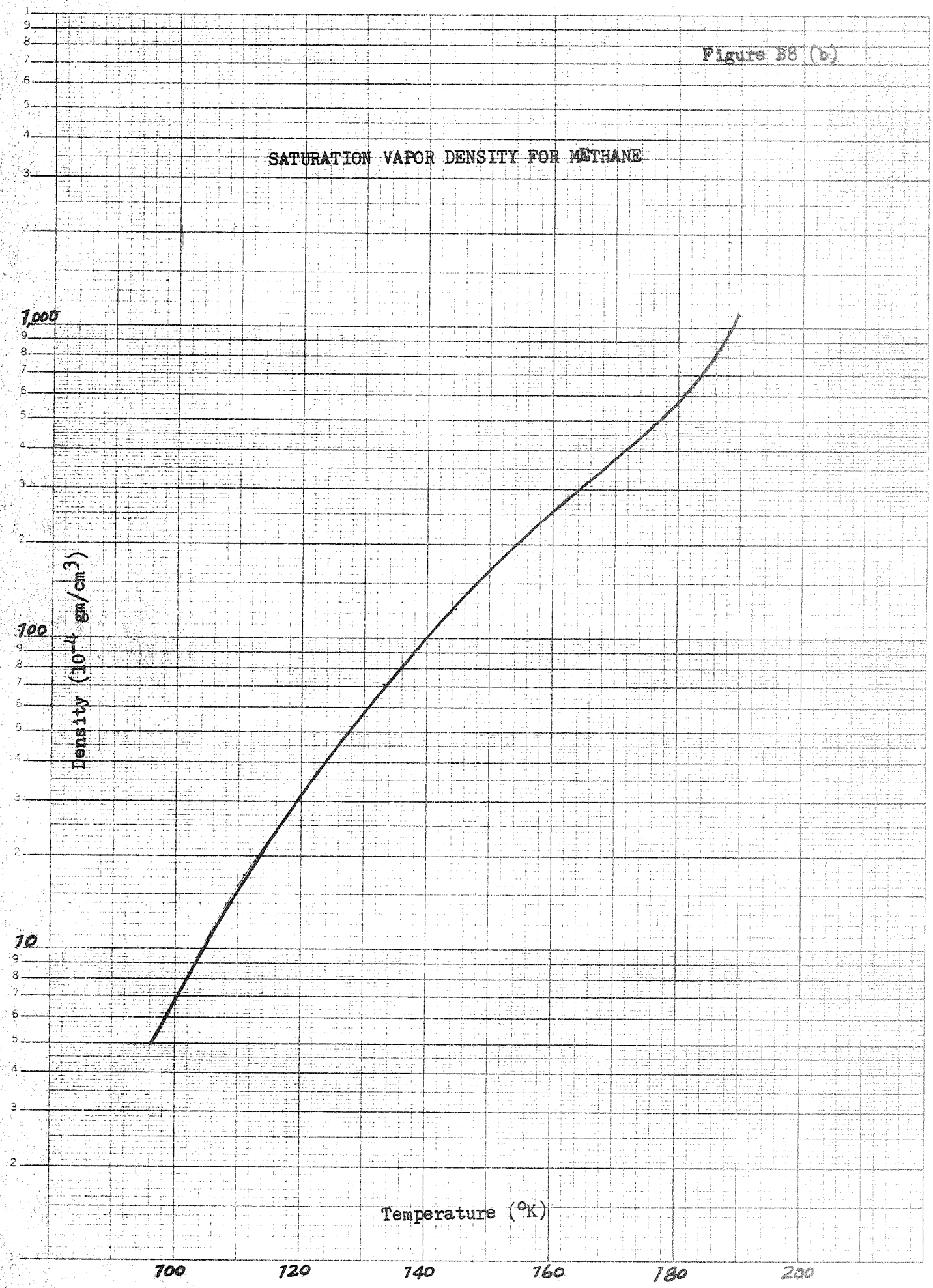

Figure B8 (c)

Saturation vapor density for methane

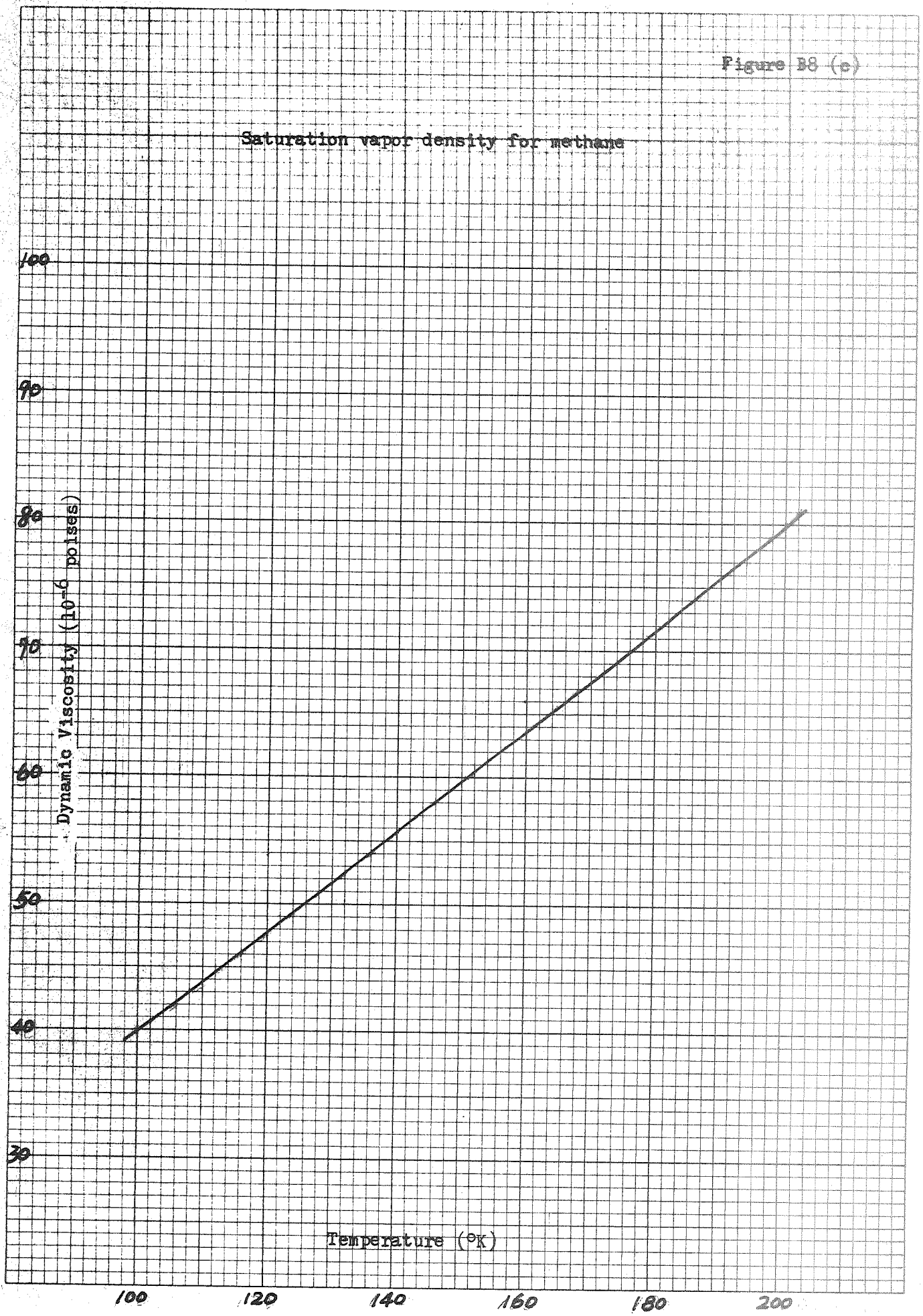

EUGENE DIETZGEN CO.
MADE IN U. S. A.
NO. 340-10 DIETZGEN GRAPH PAPER
10 X 10 PER INCH

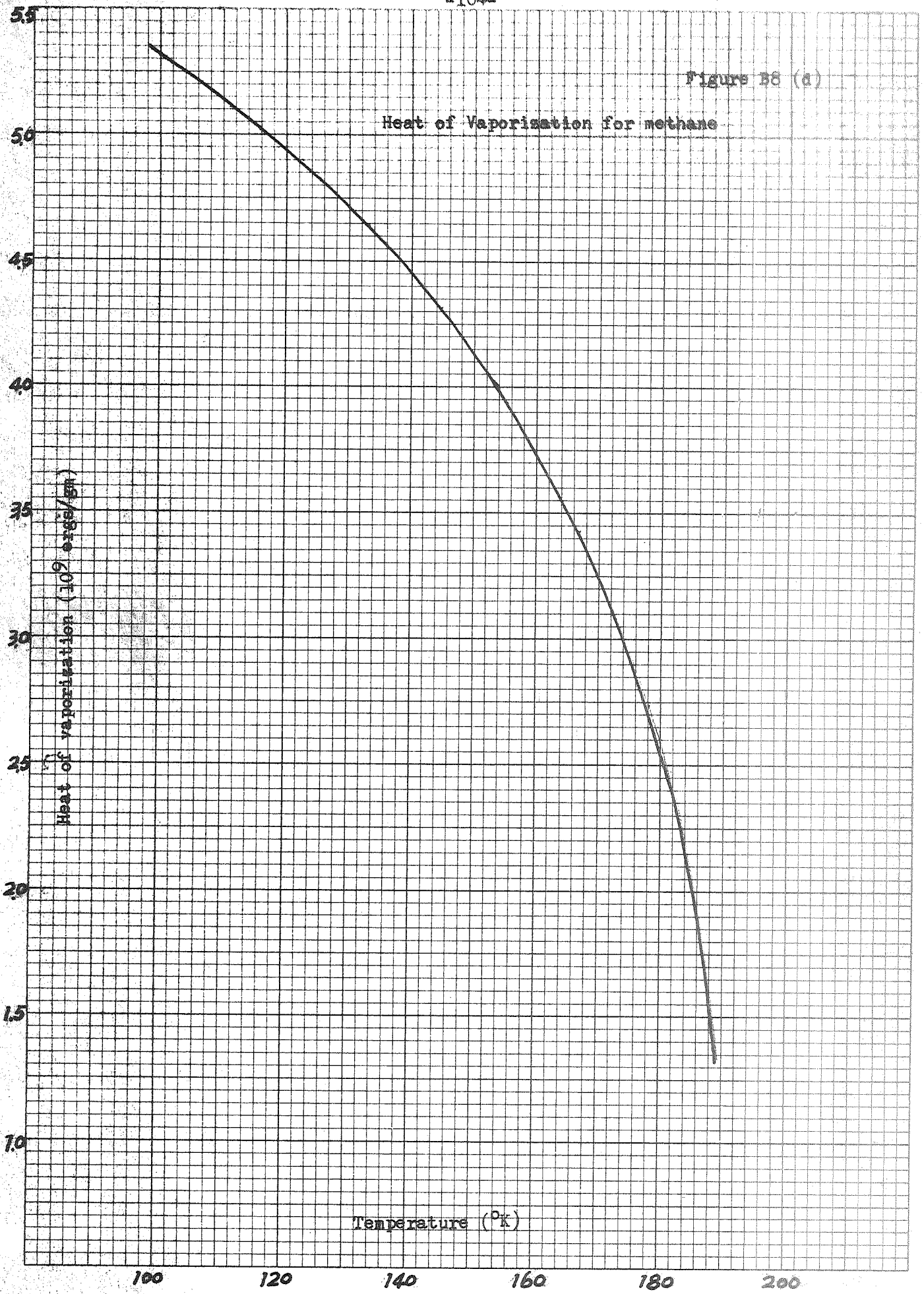

Figure 38 (d)

Heat of Vaporization for methane

EUGENE DIETZGEN CO.
MADE IN U. S. A.
NO. 340-10 DIETZGEN GRAPH PAPER
10 X 10 PER INCH

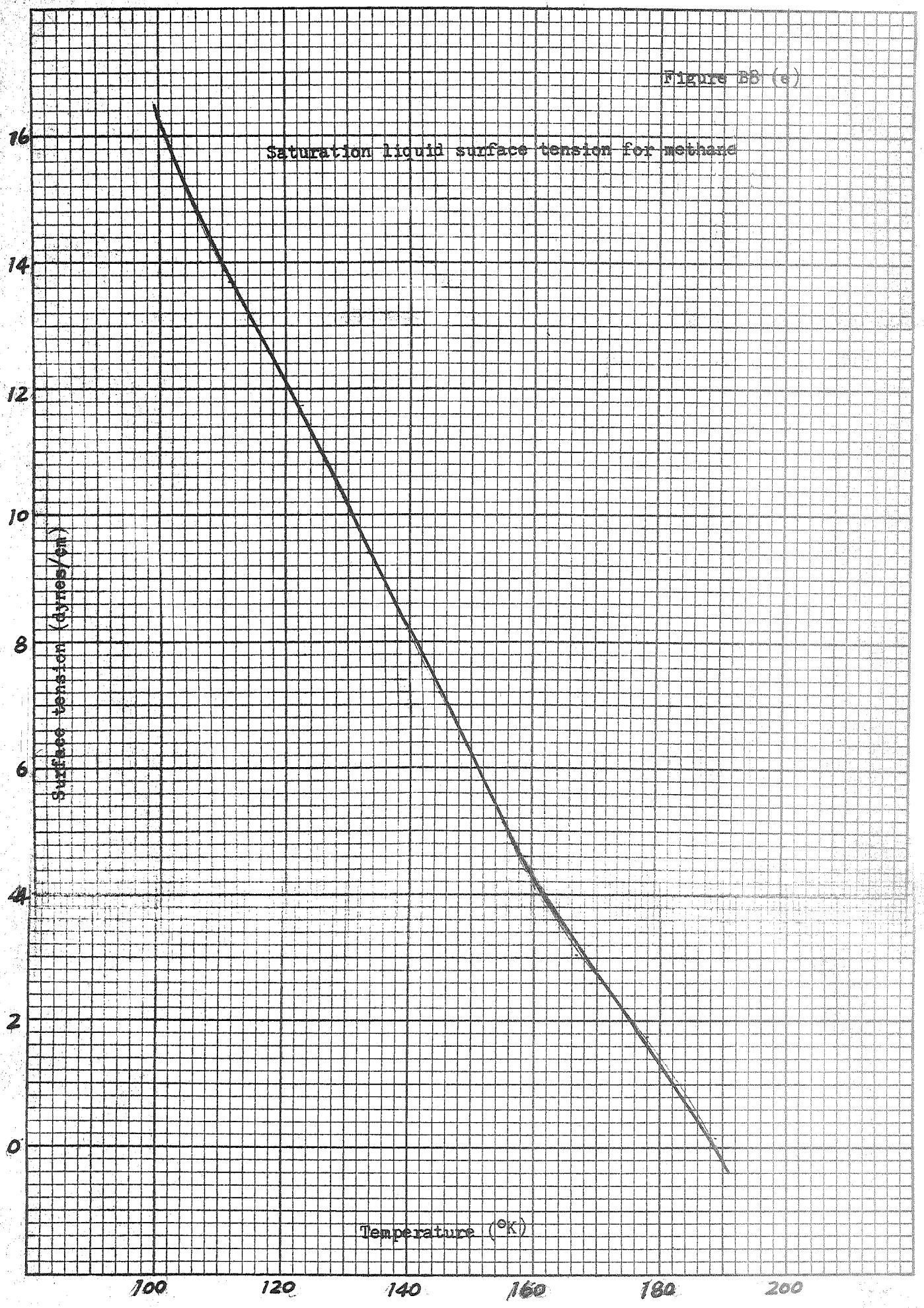

K+E 10 X 10 TO THE INCH 46 0782
7 X 10 INCHES MADE IN U.S.A.
KEUFFEL & ESSER CO.

Figure BB (f)

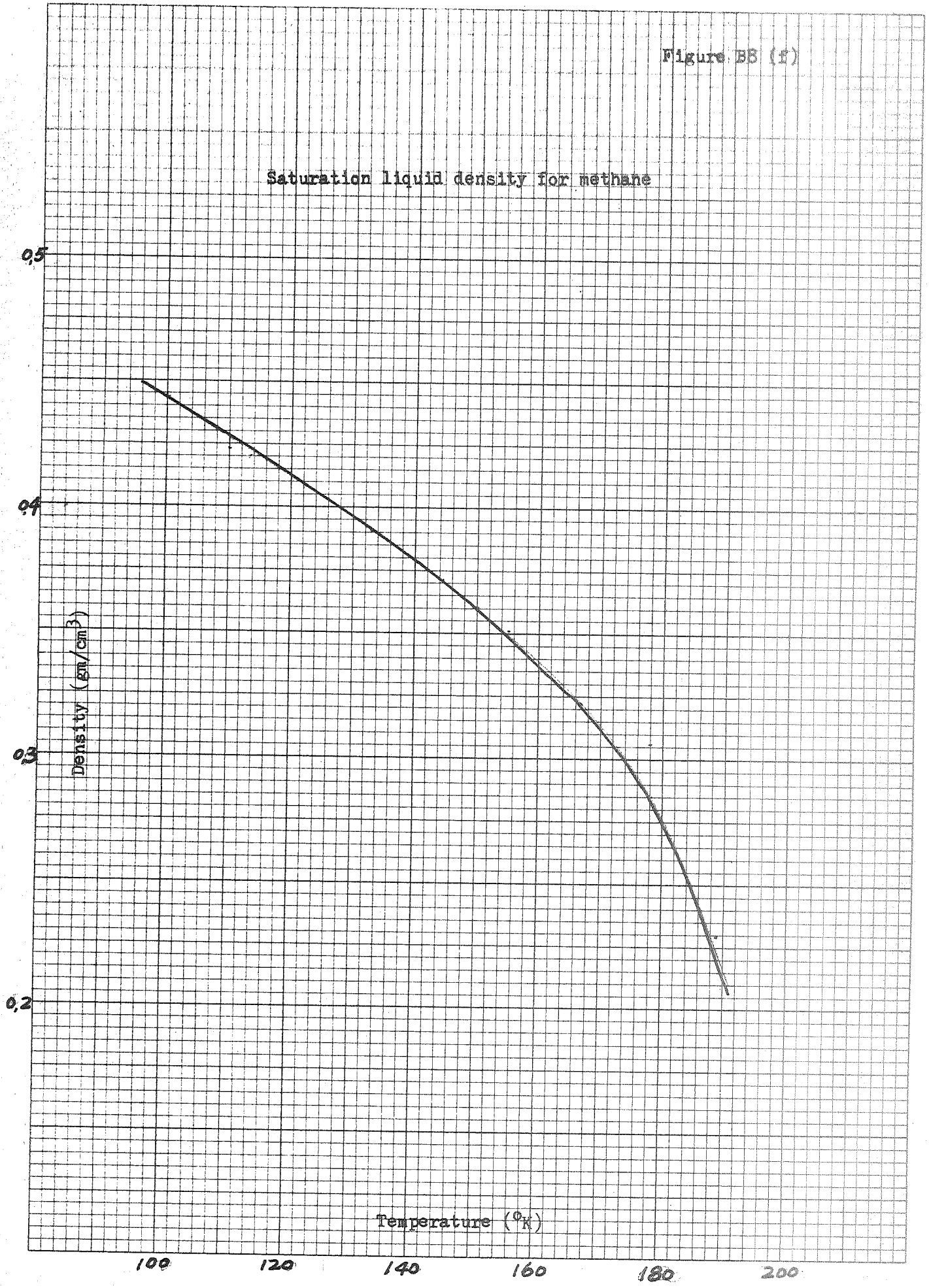

EUGENE DIETZGEN CO.
MADE IN U. S. A.
NO. 340-10 DIETZGEN GRAPH PAPER
10 X 10 PER INCH

Figure B8 (g)

Saturation liquid viscosity for methane

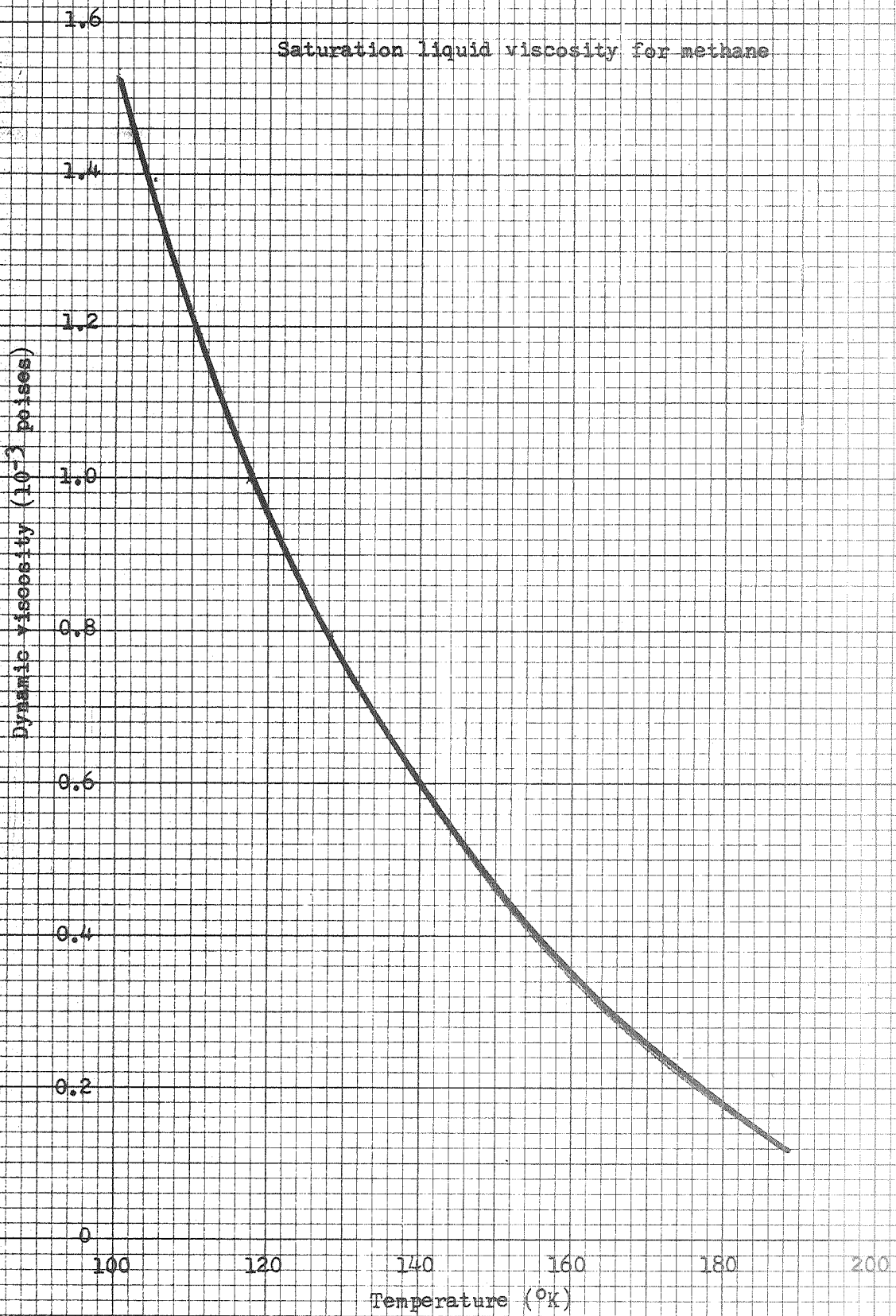

EUGENE DIETZGEN CO.
MADE IN U. S. A.
NO. 340-10 DIETZGEN GRAPH PAPER
10 X 10 PER INCH

Figure B8 (h)

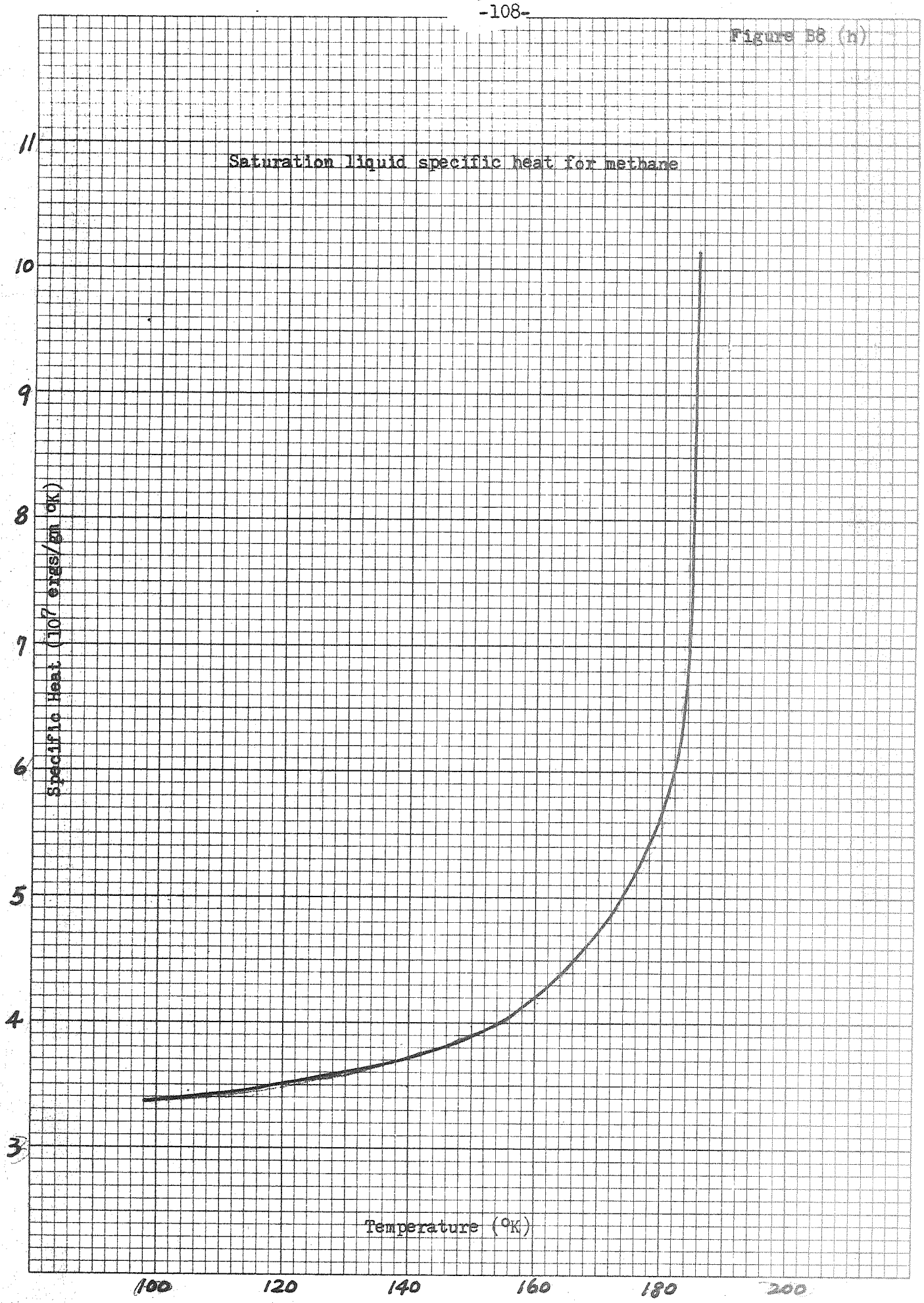

EUGENE DIETZGEN CO.
MADE IN U. S. A.
NO. 340-10 DIETZGEN GRAPH PAPER
10 X 10 PER INCH

Figure B8 (1)

Thermal conductivity of liquid methane

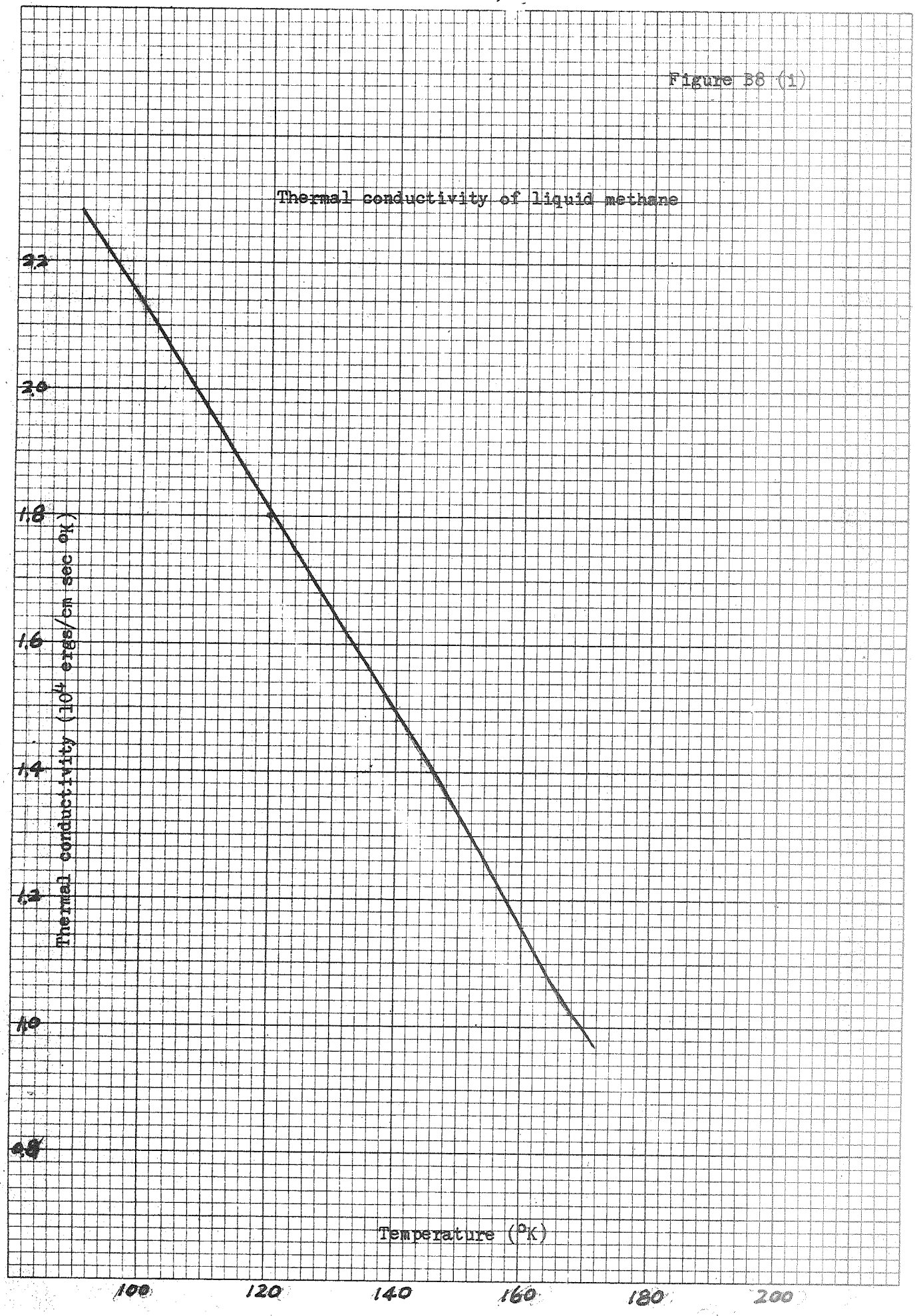

EUGENE DIETZGEN CO.
MADE IN U. S. A.
NO. 340-10 DIETZGEN GRAPH PAPER
10 X 10 PER INCH

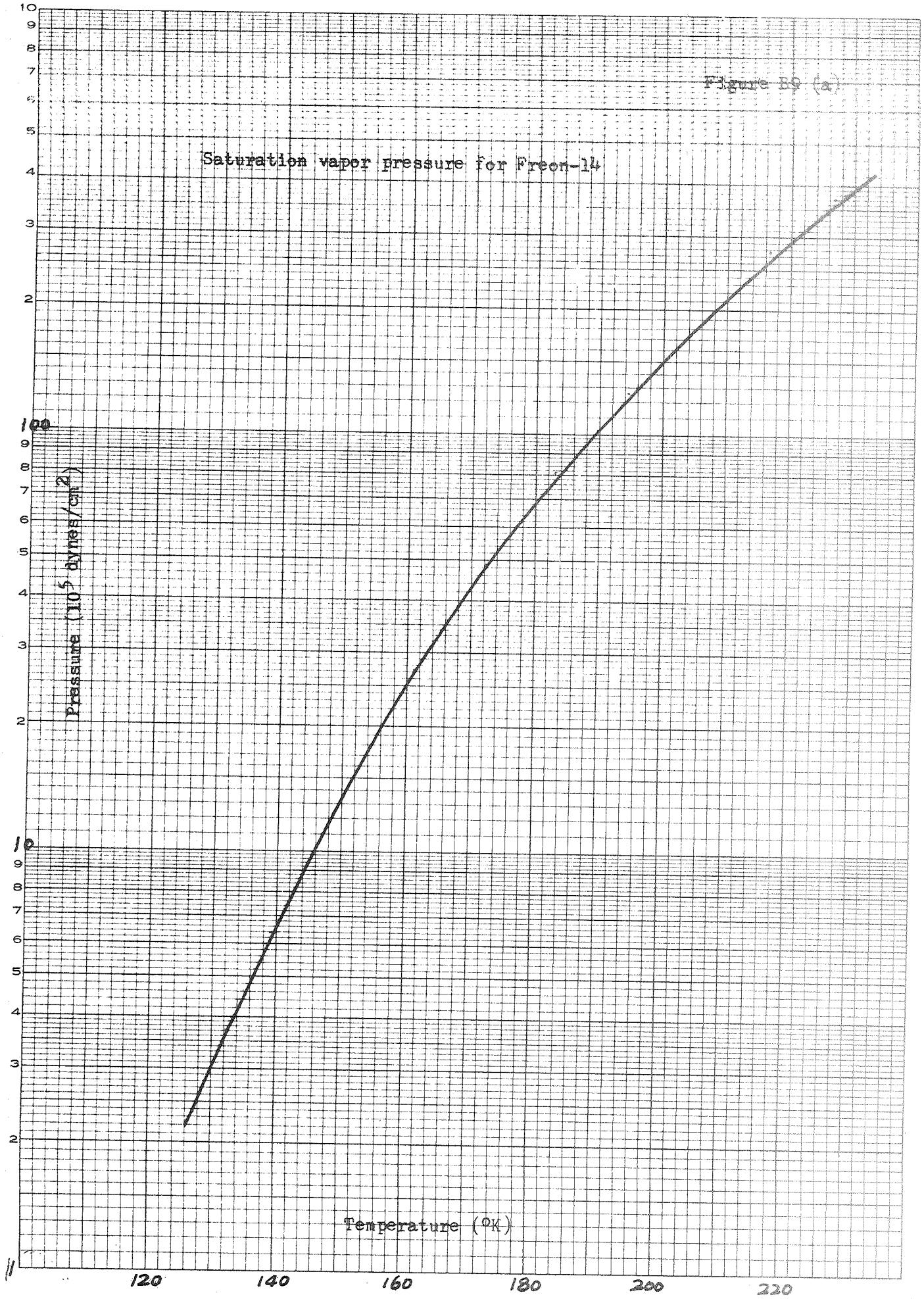

EUGENE DIETZGEN CO.
MADE IN U. S. A.
NO. 340-L310 DIETZGEN GRAPH PAPER
SEMI-LOGARITHMIC
3 CYCLES X 10 DIVISIONS PER INCH

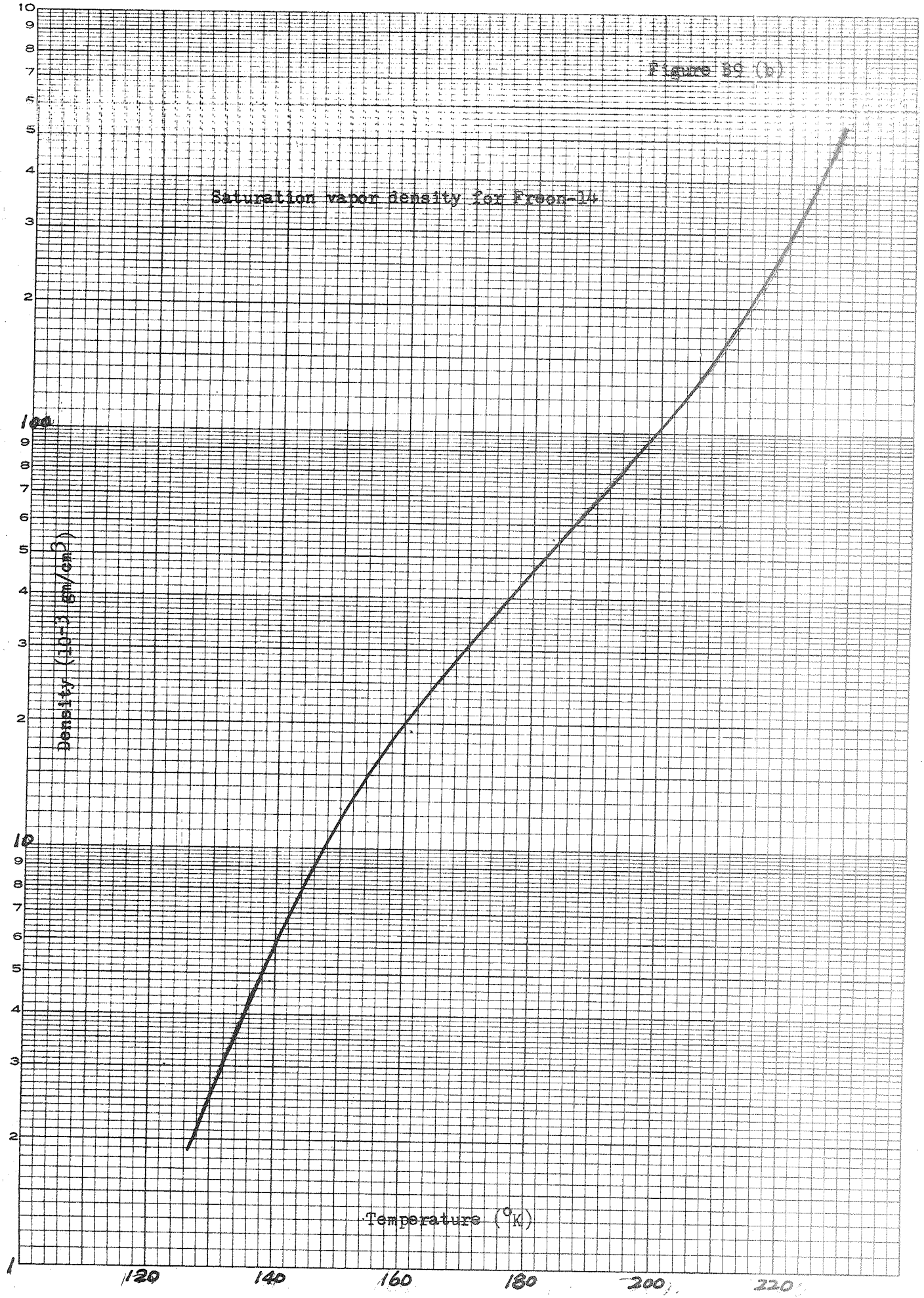

EUGENE DIETZGEN CO.
MADE IN U. S. A.
NO. 340-L310 DIETZGEN GRAPH PAPER
SEMI-LOGARITHMIC
3 CYCLES X 10 DIVISIONS PER INCH

Figure B9 (c)

Saturation vapor viscosity for Freon-14

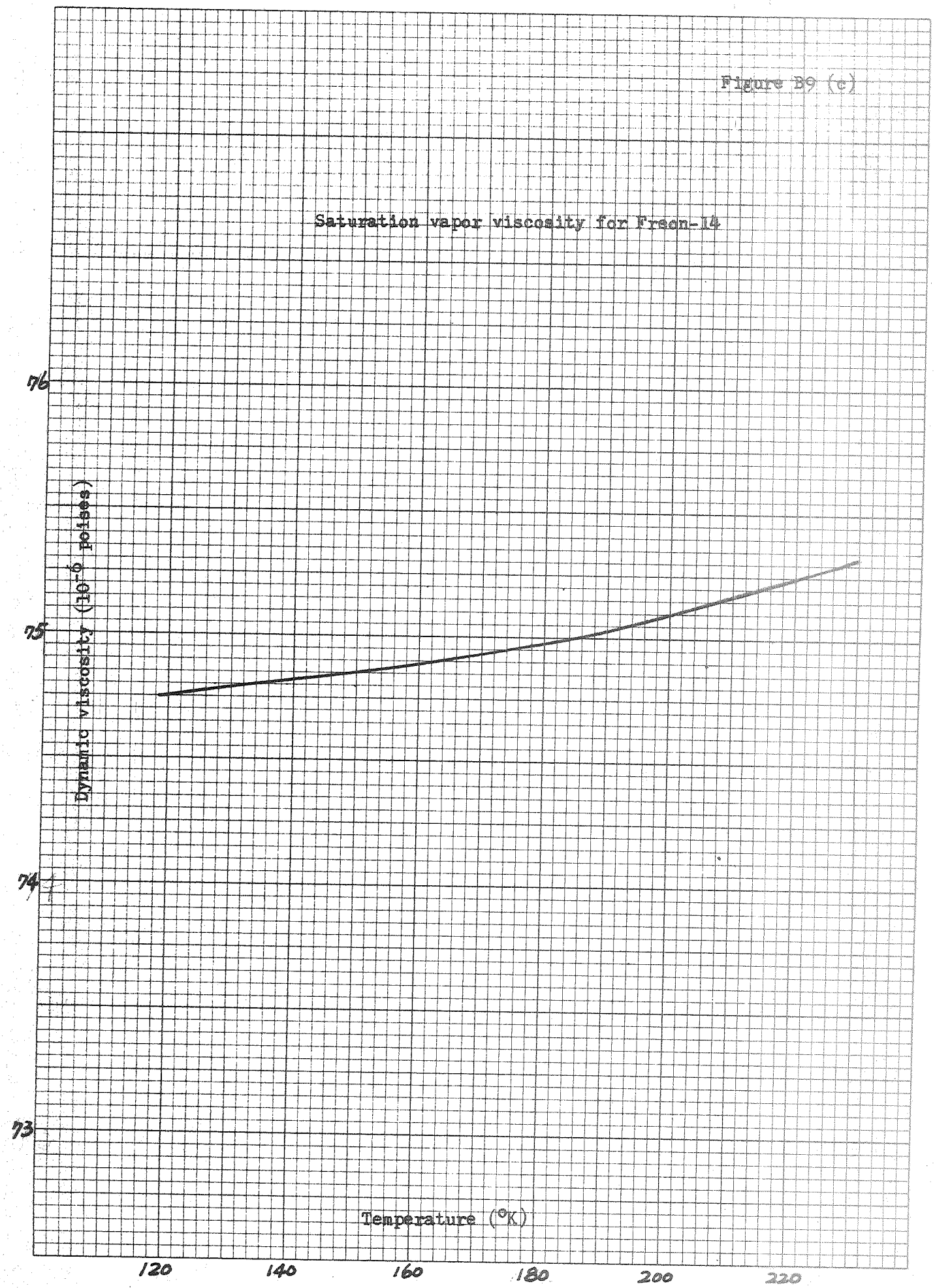

EUGENE DIETZGEN CO.
MADE IN U. S. A.
NO. 340-10 DIETZGEN GRAPH PAPER
10 X 10 PER INCH

Figure B9 (d)

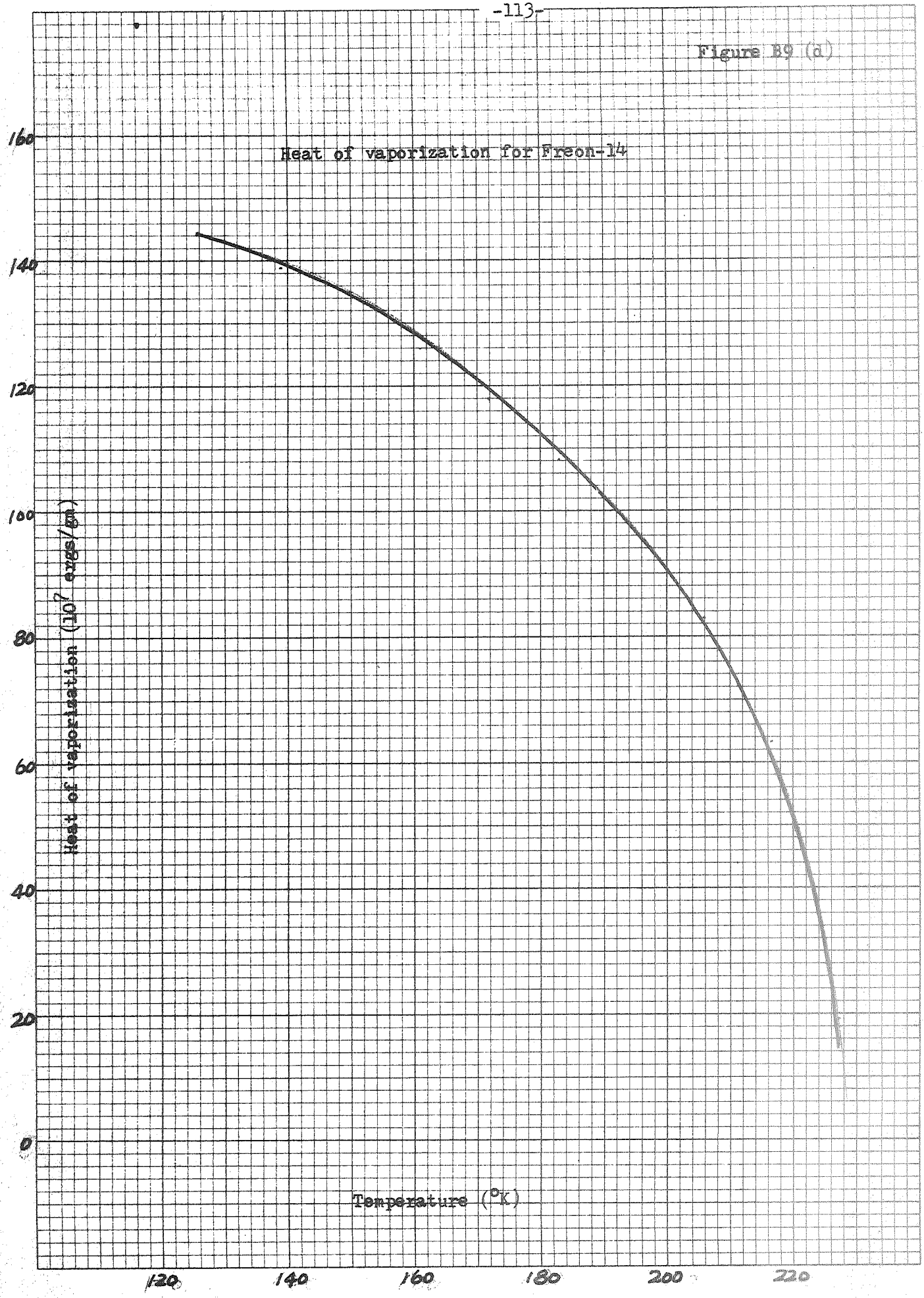

EUGENE DIETZGEN CO.
MADE IN U. S. A.
NO. 340-10 DIETZGEN GRAPH PAPER
10 X 10 PER INCH

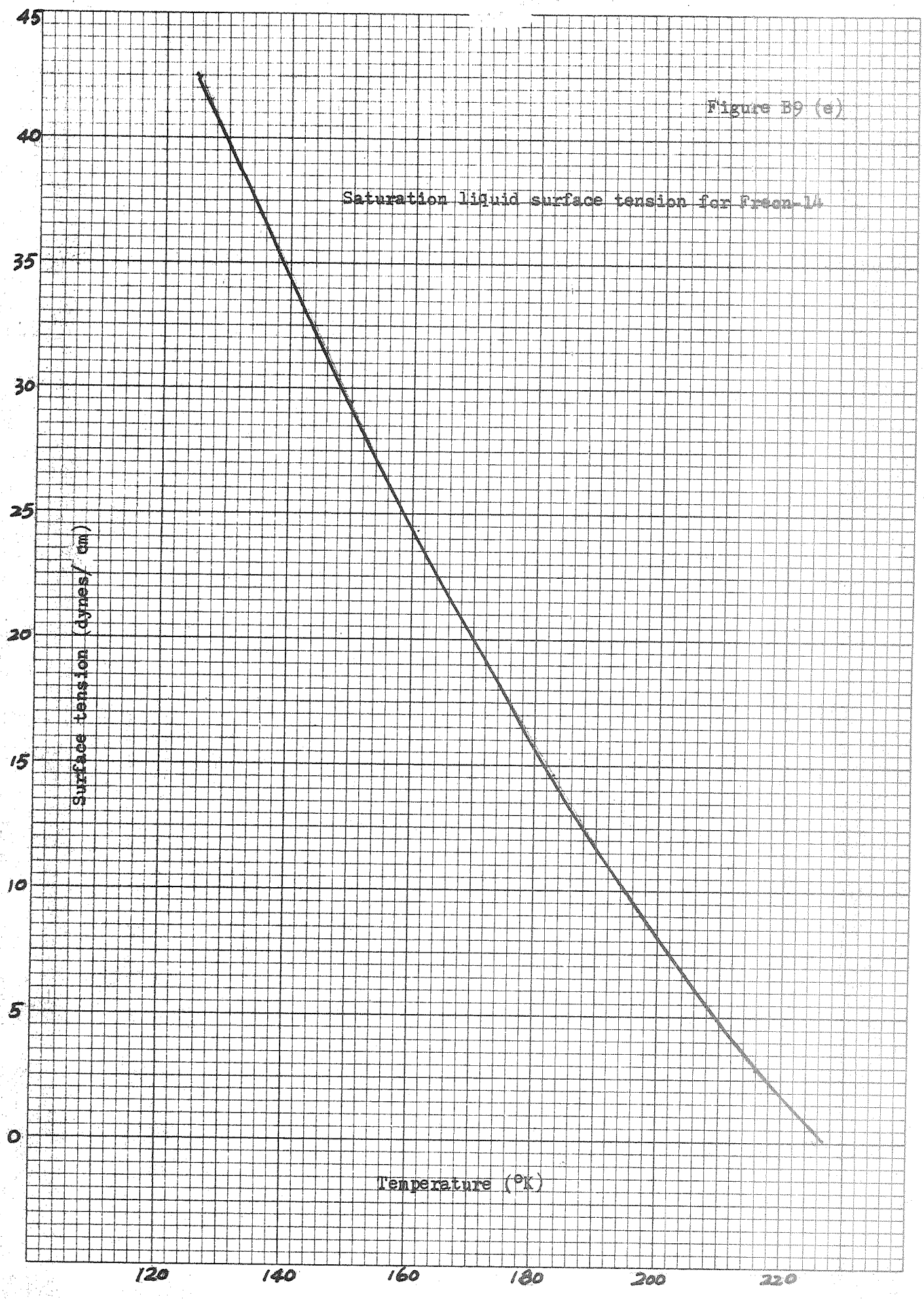

EUGENE DIETZGEN CO.
MADE IN U. S. A.
NO. 340-10 DIETZGEN GRAPH PAPER
10 X 10 PER INCH

Figure B9 (f)

Saturation liquid density for Freon-14

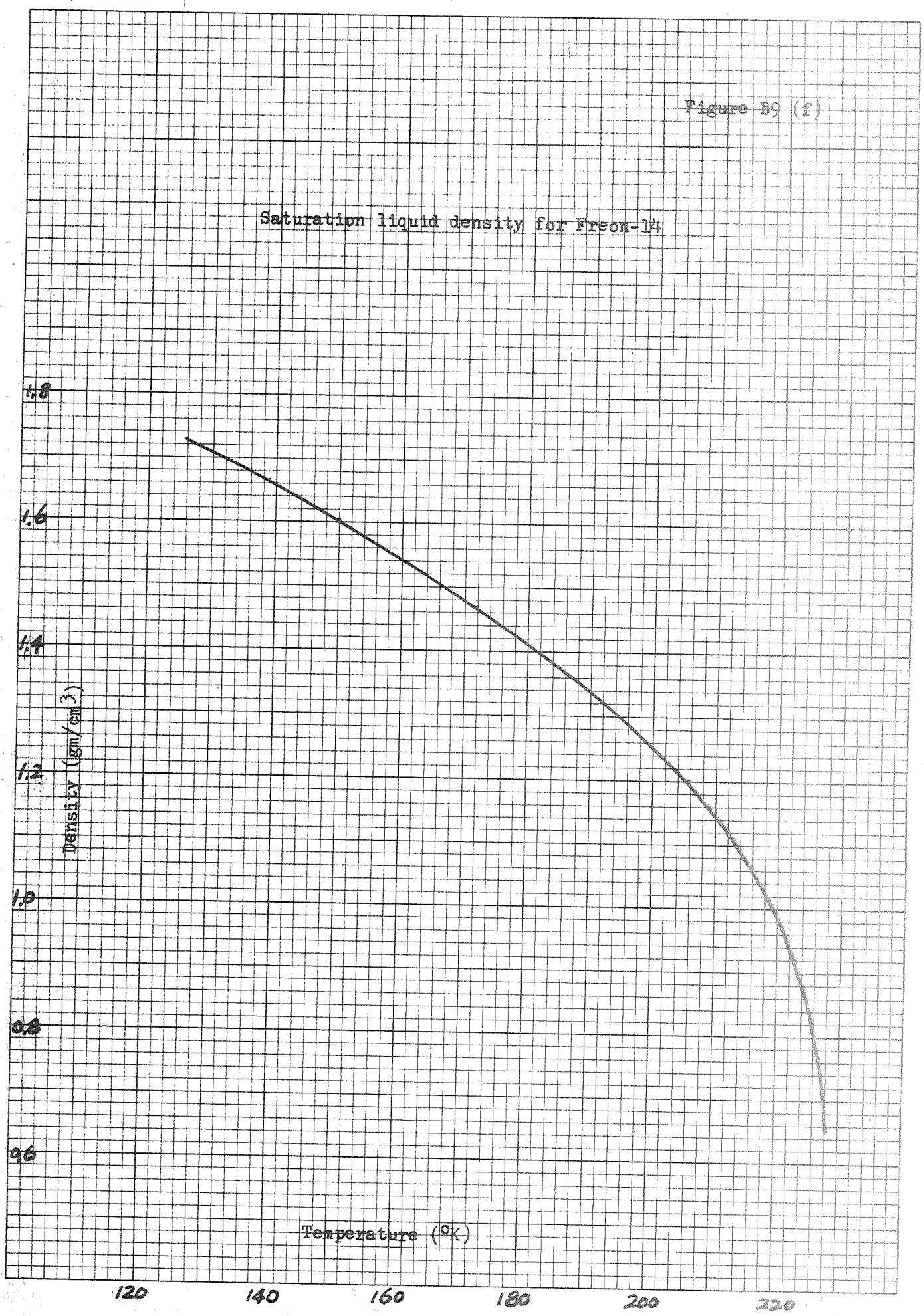

EUGENE DIETZGEN CO.
MADE IN U. S. A.
NO. 340-10 DIETZGEN GRAPH PAPER
10 X 10 PER INCH

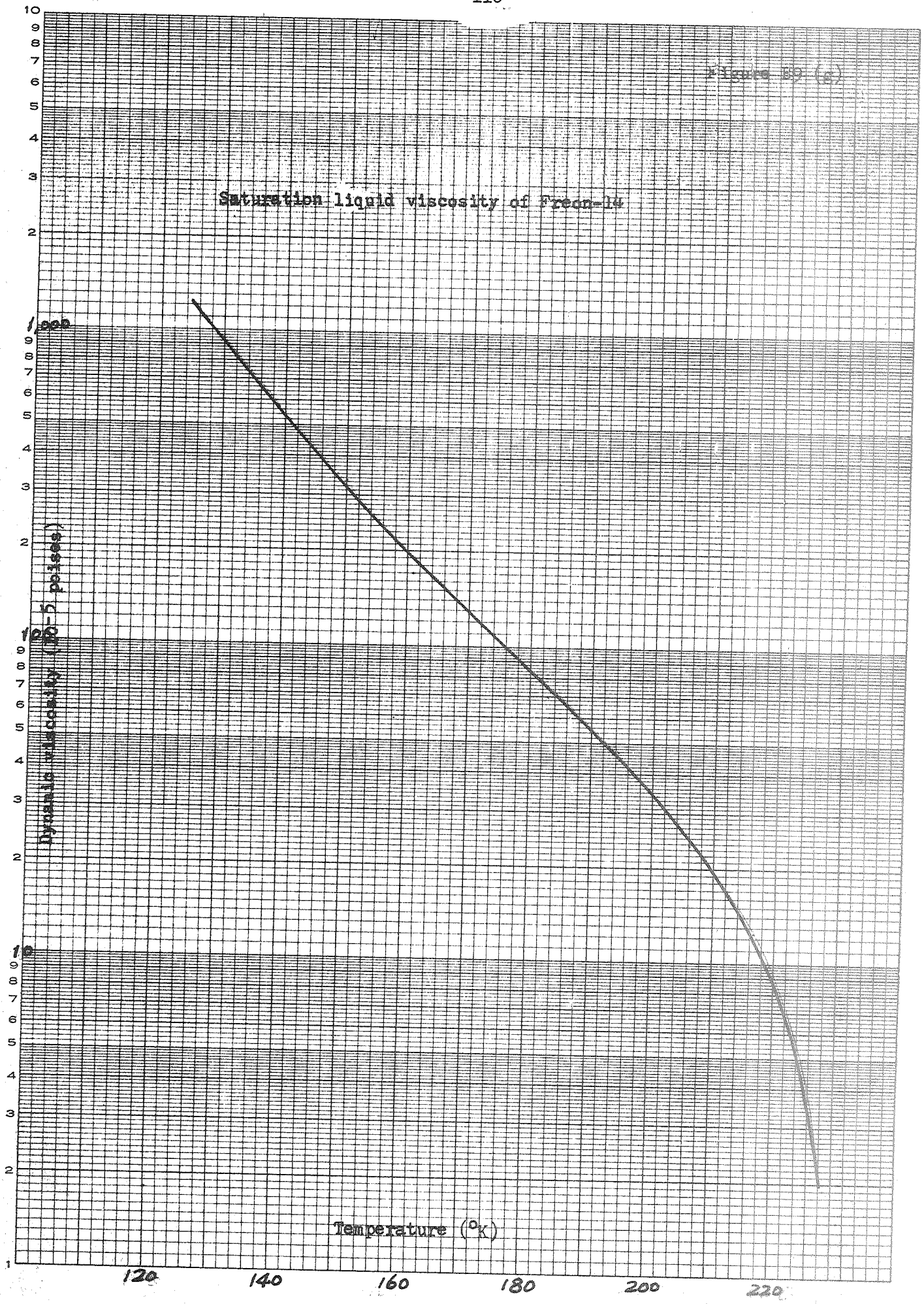

EUGENE DIETZGEN CO.
MADE IN U.S.A.
NO. 340-L410 DIETZGEN GRAPH PAPER
SEMI-LOGARITHMIC
4 CYCLES X 10 DIVISIONS PER INCH

Figure B9 (h)

Saturation liquid specific heat for Freon-14

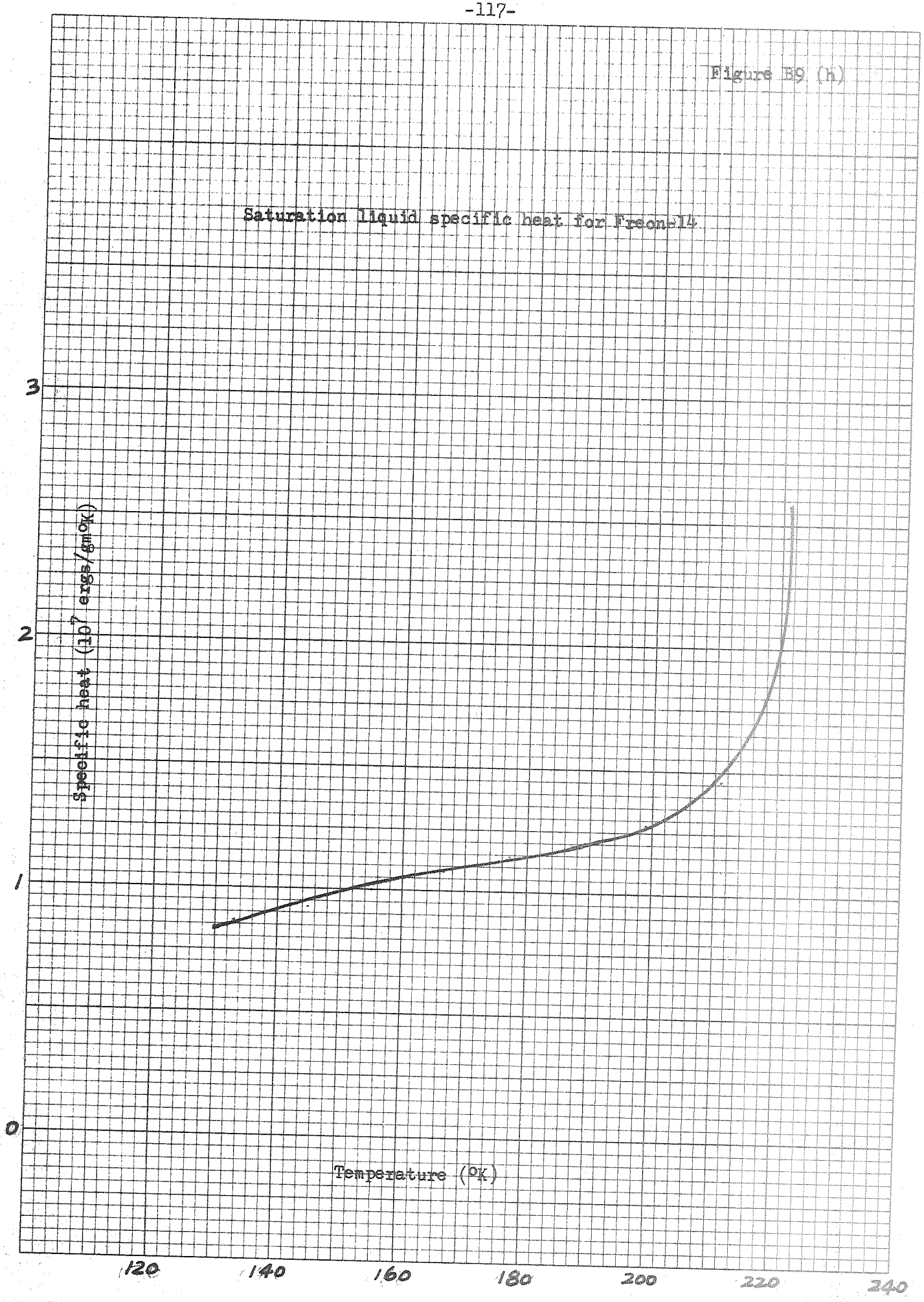

EUGENE DIETZGEN CO.
MADE IN U. S. A.
NO. 340-10 DIETZGEN GRAPH PAPER
10 X 10 PER INCH

Figure 39 (1)

Saturation liquid thermal conductivity for Freon-14

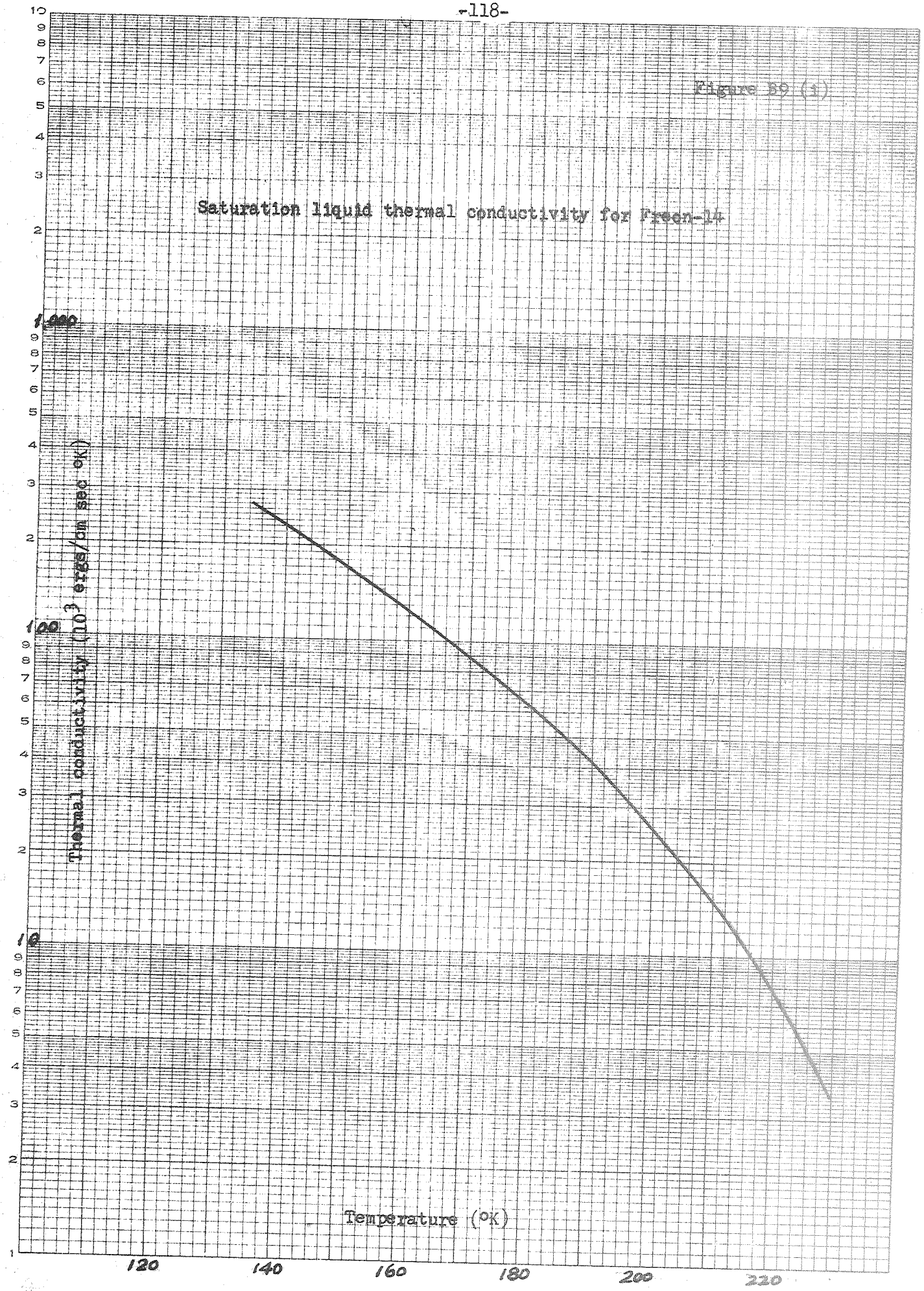

EUGENE DIETZGEN CO.
MADE IN U.S.A.
NO. 340-L410 DIETZGEN GRAPH PAPER
SEMI-LOGARITHMIC
4 CYCLES X 10 DIVISIONS PER INCH